
Regional Gravity Field Modeling with Adjusted Spherical Cap Harmonics in an Integrated Approach

Heft 39

Darmstadt, November 2013

Schriftenreihe der Fachrichtung Geodäsie
Fachbereich Bau- und Umweltingenieurwissenschaften
Technische Universität Darmstadt
ISBN 978-3-935631-28-0



TECHNISCHE
UNIVERSITÄT
DARMSTADT



Heft 39

Darmstadt, November 2013

Ghadi Younis

**Regional Gravity Field Modeling with Adjusted
Spherical Cap Harmonics in an Integrated Approach**

Schriftenreihe
Fachrichtung Geodäsie
Fachbereich Bau- und Umweltingenieurwissenschaften
Technische Universität Darmstadt

ISBN 978-3-935631-28-0

Schriftenreihe Fachrichtung Geodäsie der Technischen Universität Darmstadt
Zugl.: Darmstadt, Technischen Universität, Dissertation 2013.
D17

Online unter: <http://tuprints.ulb.tu-darmstadt.de>

Verantwortlich für die Herausgabe der Schriftenreihe:

Der Sprecher der Fachrichtung Geodäsie
im Fachbereich Bau- und Umweltingenieurwissenschaften
der Technischen Universität Darmstadt

Bezugsnachweis:
Technische Universität Darmstadt
Institut für Physikalische Geodäsie
Petersenstraße 13
64287 Darmstadt

ISBN: 978-3-935631-28-0

Regional Gravity Field Modeling with Adjusted Spherical Cap Harmonics in an Integrated Approach

Vom Fachbereich 13 Bau- und Umweltingenieurwissenschaften
der Technischen Universität Darmstadt
zur Erlangung des Akademischen Grades eines
Doktor-Ingenieurs (Dr.-Ing.) genehmigte Dissertation

Vorgelegt von

M.Sc. Ghadi K A Younis

aus Deir Ghazala , Palästina

Referent: **Prof. Dr.-Ing. Matthias Becker**
Korreferent: **Prof. Dr.-Ing. Reiner Jäger**
Korreferent: **Prof. Dr.-Ing. Carl Gerstenecker**

Tag der Einreichung: 26.11.2012

Tag der mündlichen Prüfung: 23.01.2013

Darmstadt, November 2013
D17

Regional Gravity Field Modeling with Adjusted Spherical Cap Harmonics in an Integrated Approach

Accepted by the Faculty of Civil and Environmental Engineering
in the Technische Universität Darmstadt
for the completion of the requirements of the Ph.D. degree.

Done by

MSc. Ghadi K A Younis

From Deir Ghazala, Palestine

First Supervisor:	Prof. Dr.-Ing. Matthias Becker
Second Supervisor:	Prof. Dr.-Ing. Reiner Jäger
Third Supervisor:	Prof. Dr.-Ing. Carl Gerstenecker

Date of Submission:	26.11.2012
Date of Oral Exam:	23.01.2013

Darmstadt, November 2013
D17

Summary

The main objective of this thesis is to develop an integrated approach for the computation of Height Reference Surfaces (HRS) in the context of GNSS positioning. For this purpose, the method of Digital Finite Element Height Reference Surface software (DFHRS) is extended, allowing the use of physical observations in addition to geometrical observation types. Particular emphasis is put on (i) using Adjusted Spherical Cap Harmonics to locally model the potential, (ii) developing a parameterization of coefficients for a least squares estimation, and (iii) optimizing the combination of data needed to calculate the coefficients. In particular, the selection of the terrestrial gravity measurements, height fitting points with known ellipsoidal and normal heights, and the use of the available global gravity models as additional observations are investigated. One of the main motivations is the need to compute a high precise local potential model with the ability to derive all components related to the potential W . These observation components are gravity g , quasigeoid height ζ , the geoid height N_G , deflections of the vertical in the east and north direction (η, ξ) , the fitting points $(\lambda, \phi, h/H)$ and the a priori information in terms of coefficients of a local potential model derived from the developed methods of a mapping of a global one.

This thesis provides a method for local and global gravity and geoid modelling. The Spherical Cap Harmonics (SCH) for modeling the Earth potential are introduced in detail, including their relationship to the normal Spherical Harmonics (SH). The different types of Spherical Cap Harmonics, such as Adjusted Spherical Cap Harmonics (ASCH), Translated-Origin Spherical Cap Harmonics (TOSCH) and the Revised Spherical Cap Harmonics (RSCH) are discussed. The ASCH method was chosen in further for modeling the local gravitational potential due to its simple principle, that the integer degree and order Legendre functions are preserved and lead to faster implementation algorithms. The ASCH are used in this thesis to transform the global gravity models like EGM2008 or EIGEN05c to local gravity models, guaranteeing a much smaller number of coefficients and making the calculations faster and easier.

Tests are applied to validate the use of ASCH for local gravity and potential modelling, with ASCH coefficients calculated in test areas. These coefficients were used to calculate the values of potential or the gravity for new points and then compared with the real measured values and reference values from global models. The tests include the transformation of global gravity models like EGM2008 and EIGEN05c to ASCH models and the integrated solution of heterogeneous groups of data including terrestrial gravity data, height fitting points and the locally mapped global gravity models.

The region of the federal state of Baden-Württemberg in Germany was used as a test area for this thesis to prove the concept. Nearly 15000 terrestrially measured gravity observations were used to implement an ASCH model in degree and order of 300 in order to achieve a resolution of 0.01 mGal^1 that corresponds to the measurement accuracy.

¹ $1 \text{ mGal} = 1 \times 10^{-5} \text{ ms}^{-2}$

Zusammenfassung

Die Zielsetzung dieser Thesis ist die Integration physikalischer Beobachtungen mit der geometrischer Beobachtungen und die Implementierung dieses Ansatzes in die DFHBF Software zur Berechnung einer Digitalen Finiten Höhenbezugsfläche, um die Berechnung von Höhenbezugsflächen zu ermöglichen. Die Schwerpunkte liegen insbesondere auf (i) der Verwendung von Adjusted Spherical Cap Harmonics (ASCH) zur Modellierung des lokalen Potentials, (ii) der Berechnung einer Kleinste-Quadrate-Ausgleichung zur Bestimmung der ASCH-Koeffizienten und (iii) einer zur Berechnung notwendigen, optimalen Datenfusion unterschiedlicher Beobachtungskomponenten, die sich aus terrestrischen Schweremessungen, Höhenpasspunkten mit bekannter, ellipsoidischer Höhe und Normalhöhe und der aus globalen Schwerefeldmodellen in die regionalen ASCH-Modelle abgebildeten apriori Information. Die Motivation zu dieser Arbeit besteht in der Notwendigkeit, ein integriertes Modell zu entwickeln und daraus alle Komponenten, die sich auf das Potenzial W beziehen abzuleiten. Diese sind u. a. die Gravitationsbeschleunigung g , Quasigeoidhöhen ξ , die Geoidhöhe N_G , und die Lotabweichungen in Nord und Ost (η, ζ) und die Höhenpasspunkte $(\lambda, \phi, h/H)$.

Die Thesis stellt einige der weit verbreiteten Methoden für lokale und globale Schwerefeld- und Geoidmodellierung vor. Im Anschluss werden Spherical Cap Harmonics (SCH) zur Modellierung des Schwerepotentials und ihre Beziehung zu normalen Spherical Harmonics im Detail präsentiert. Die verschiedenen Arten für Spherical Harmonics wie Adjusted Spherical Cap Harmonics (ASCH), Translated-Origin Spherical Cap Harmonics (TOSCH) und die Revised Spherical Cap Harmonics (RSCH) werden diskutiert. Die ASCH werden deshalb für die Modellierung des lokalen Schwerepotentials favorisiert, weil sie einem einfacheren Algorithmen und Design unterliegen und Legendre-Funktionen mit ganzzahliger Grad und Ordnung verwenden. Mithilfe der ASCH werden globale Schweremodelle wie EGM 2008 und EIGEN05c zu einem lokalen Schweremodell transformiert, sodass eine deutlich geringere Anzahl an Koeffizienten bestimmt werden muss und die Berechnung vereinfacht und beschleunigt werden kann.

Verschiedene Tests werden herangezogen, um die Verwendung von ASCH zur lokalen Schwerefeld- und Schwerepotentialmodellierung zu validieren. Dabei werden die ASCH-Koeffizienten in den Testbereichen berechnet. Diese Koeffizienten werden dazu verwendet, Potential- und Schwerewerte für neue Punkte zu generieren, die mit den realen gemessenen Werten als Referenzwerte und mit den globalen Modellen verglichen werden konnten. Die Tests beziehen sich auf einem neuen Ansatz zur Transformation globaler Schweremodelle, wie EGM2008 und EIGEN05c, in ASCH-Modelle zur Integration hybrider Datentypen wie terrestrische Schweredaten, Höhenpasspunkte und lokal transformierter globaler Schweremodelle.

Zur Verifizierung des Konzepts wurde in Rahmen dieser Arbeit das Bundesland Baden-Württemberg in Deutschland als Testgebiet ausgewählt, in dem nahezu 15000 terrestrisch gemessene Schwerebeobachtungen mit Grad und Ordnung von 300 parametrisiert wurden, um eine der Messgenauigkeit entsprechende Auflösung von 0.01 mGal zu erreichen.

Acknowledgements

This PhD thesis and the underlying research would not have been possible without the help of many people. First and foremost I want to thank my supervisors, Prof. Matthias Becker and Prof. Reiner Jäger, for their help and guidance during the four years of research. They were always available regardless of their busy schedule, and managed to keep me on track while giving me the freedom to pursue my own ideas. I also thank Prof. Carl Gerstenecker who was so kind to take responsibility for the supervision of the final thesis and gave most valued input.

Valuable input came from the Institute of Geodesy of TU-Darmstadt and the Faculty of Information Management and Media (IMM) in HS-Karlsruhe. In addition, a valuable help came from the Landesamt für Geobasisinformation und Landentwicklung (LGL) Baden-Württemberg, Karlsruhe by providing the required terrestrial gravity points and GNSS/Levelling fitting points for this research and the GFZ-Potsdam, who has given a valuable help by providing the EIGEN05c model with its full covariance matrix. A special support was offered from the Institute of Applied Research (IAF) in HS-Karlsruhe through providing a work place in the DFHBF-RaD project (www.dfhbf.de).

Also, special thanks for the German Academic Exchange Service (DAAD) (Deutscher Akademischer Austauschdienst) for giving me the chance to start this PhD study at the Technical University of Darmstadt. They always provided financial support for life and study as well administrative support for the travel to Germany, residence in Germany and helping supporting to bring my family to Germany.

My wife Tamara was always there with whatever support I needed - kind words to calm me down after a particular stressful day or the proverbial kick in the rear to keep me going. She, my parents, my brothers and my friends, motivated me by showing keen interest in my work and encouraging me to proceed with my work.

Table of Contents

Summary	i
Zusammenfassung	ii
Acknowledgements	iii
Table of Contents	iv
List of Figures	vi
List of Tables	viii
1. Introduction	1
2. Global and local gravity field modeling	4
2.1. The gravity field of the Earth	4
2.1.1. Laplace differential equation and Spherical Harmonics (SH)	5
2.1.2. The normalized SH	7
2.1.3. The normalized Legendre functions	8
2.1.4. Harmonic expansion of the Earth gravitational potential	8
2.1.5. Derivatives of the potential of the Earth	11
2.1.6. The spherical harmonic expansion of the Earth's gravity field	14
2.2. The local potential modeling	15
2.2.1. Stokes formula and remove-restore method	15
2.2.2. GNSS/Leveling	16
2.2.3. Digital finite elements height reference surface (DFHRS)	16
2.2.3.1 Principles of DFHRS	17
2.2.3.2 Extension of DFHRS to physical observations	19
2.2.4. Least Squares Collocation	21
2.3. Integrated Geodesy	22
2.4. State of the art in the gravity field modeling	23
3. Local potential modeling using Spherical Cap Harmonics	25
3.1. Spherical Cap Harmonics	25
3.1.1. Derivation of SCH	27
3.1.2. Legendre function of real degree and integer order	29
3.1.3. Roots of Legendre function	30
3.1.4. Spatial resolution of SCH model	31
3.1.5. Derivatives of the Potential in SCH	32
3.2. Adjusted Spherical Cap Harmonics	33
3.2.1. Derivation of the ASCH	34
3.3. Relationship between SCH and SH	35
3.4. Other modifications of SCH	36
3.4.1. Translated-Origin Spherical Cap Harmonics (TOSCH)	36
3.4.2. Revised Spherical Cap Harmonic (R-SCH)	38

3.5.	Other carrier functions for local potential modeling	39
3.5.1.	Spherical Radial Basis Functions (SRBF)	39
3.5.2.	Spherical Harmonic Splines	40
4.	Transformation of global SH gravity models to local ASCH	42
4.1.	Functional models	42
4.2.	Result of Transforming global SH to local ASCH	45
4.2.1.	The convergence of coefficients	45
4.2.2.	The boundary problem	46
4.2.3.	Design of the observations in the vertical direction	50
4.3.	Transformation of EGM2008 to a local ASCH	50
5.	Integrated Solution for ASCH modeling	57
5.1.	Solution introduction	57
5.2.	Observations	59
5.2.1.	Terrestrial gravity observation	59
5.2.2.	Height fitting points	63
5.2.3.	Deflections of the vertical	66
5.2.4.	Global gravity models	70
5.3.	Numerical Methods	71
5.3.1.	Storage Usage	71
5.3.2.	Cholesky block matrix decomposition	72
5.3.3.	Parallel processing	74
6.	Tests and Analysis of the Integrated Approach	75
6.1.	ASCH modeling using height fitting points	75
6.2.	The combination of height fitting points and global models	78
6.3.	Gravity prediction by means of ASCH	82
6.4.	ASCH modeling using terrestrial gravity observations in the integrated approach	86
6.5.	Combined solution	88
6.6.	Combined ASCH model of Baden-Württemberg	90
7.	Outlook and conclusions	98
	References	100
	List of Akronyms	106
	List of Symbols	107
	Eidesstattliche Erklärung	109
	The Author	110

List of Figures

Nr.	Description	Page
1.1	<i>The principle of GNSS-based height determination: $H = h - N$</i>	1
2.1	<i>Geographic coordinates (λ, ϕ, h) and the spherical coordinates $(r, \lambda, \bar{\phi})$</i>	6
2.2	<i>The gravitational and centrifugal accelerations of the Earth</i>	11
2.3	<i>Height anomaly ζ vs. geoid height N</i>	13
2.4	<i>The relation between orthometric height H, ellipsoidal heights h and geoid undulation N</i>	17
2.5	<i>DFHRS patches and meshes, where thick lines represent the patch boundary and thin lines represent the meshes.</i>	19
2.6	<i>The principle of harmonic coefficients calculation in EIGEN06c model.</i>	23
3.1	<i>Spherical cap area with its own pole located at the origin of the area of interest</i>	26
3.2	<i>The principle of Regula Falsi for determining the root of a function</i>	31
3.3	<i>The shift of the origin in the TOSCH</i>	37
4.1	<i>Distribution of a sample grid points over the cap area for the example of Baden-Württemberg state in Germany</i>	43
4.2	<i>Relation between the calculated parameters and the maximum degree and</i>	47
4.3	<i>The behavior of ASCH at the boundary of the cap area with opening angle $\theta_{\max} = 1.0^\circ$, the figure shows the residuals of the potential (V) in $m^2 s^{-2}$</i>	48
4.4	<i>The behavior of ASCH at the border of the cap area, the figure shows the residuals of the potential (V) in $m^2 s^{-2}$ with respect to the angle θ.</i>	49
4.5	<i>The residuals of the gravitational potential $(m^2 s^{-2})$ for the transformation of EGM2008 to a local ASCH model with cap opening angle of 1.5°.</i>	50
4.6	<i>The residuals of the gravitational potential $(m^2 s^{-2})$ for the transformation of EGM2008 to a local ASCH model with cap opening angle of 1.5°.</i>	52
4.7	<i>The standard deviations of the ASCH coefficients. The positive sign indicates C_{nm} and the negative sign indicates S_{nm}.</i>	53
4.8	<i>The ellipsoidal height in Baden-Württemberg above the GRS80 ellipsoid in meters</i>	55
4.9	<i>The height anomalies in Baden-Württemberg calculated by means of ASCH model with maximum degree and order of 80 in meters</i>	56
4.10	<i>The difference between the height anomalies calculated by EGM2008 with $N_{\max} = 2190$ and height anomalies calculated by means of ASCH with a maximum degree and order of 80</i>	57
5.1	<i>First order gravity network in the state of Baden-Württemberg (BW) and the neighboring states in Germany</i>	59
5.2	<i>The direction of the measured gravity vector</i>	60
5.3	<i>The gravity vector in the LGV-system and its radial component (after the reduction of the centrifugal acceleration part)</i>	62
5.4	<i>Definitions of Molodensky's Approach</i>	63
5.5	<i>The normal height H^* and the orthometric height H</i>	65
5.6	<i>Differences between the EVRF2007 and national reference tide gauges in cm</i>	66
5.7	<i>Flowchart for calculating ASCH parameters using parallel processing</i>	74
6.1	<i>The distribution of the height fitting points in the state of Baden-Württemberg</i>	76

6.2	<i>The calculated height anomaly over the state of Baden-Württemberg using ASCH with maximum degree and order of 10</i>	77
6.3	<i>Difference between the reference DFHRS-DB and the ASCH model using height fitting points only</i>	77
6.4	<i>The height anomalies in BW by ASCH using the combining height fitting points and the EIGEN05c</i>	79
6.5	<i>The height anomalies in BW by ASCH using the combining height fitting points and the EGM2008</i>	79
6.6	<i>The differences between DFHRS-DB and the combination of height fitting points and EIGEN05c</i>	80
6.7	<i>The differences between DFHRS-DB and the combination of height fitting points and EGM2008</i>	80
6.8	<i>The standard deviations and the degree variances of the ASCH coefficients for Baden-Württemberg using combination of EGM2008 an height fitting points</i>	81
6.9	<i>Gravity values differences between original EIGEN model predicted values and the ASCH model with maximum degree and order of 30</i>	82
6.10	<i>Gravity values differences between original EIGEN model predicted values and the ASCH model with maximum degree and order of 45</i>	83
6.11	<i>Gravity values differences between original EIGEN model predicted values and the ASCH model with maximum degree and order of 80</i>	83
6.12	<i>Height anomalies differences between original EIGEN model predicted values and the ASCH model with maximum degree and order of 80</i>	84
6.13	<i>Gravity value using ASCH model depending on height fitting points only with maximum degree and order of 10</i>	85
6.14	<i>Gravity value using ASCH model depending on height fitting points combined with EIGEN05c model with maximum degree and order of 80</i>	85
6.15	<i>Gravity value using ASCH model depending on height fitting points combined with EGM2008 model with maximum degree and order of 80</i>	86
6.16	<i>Residuals of ASCH adjustment using terrestrial gravity observations only</i>	87
6.17	<i>The comparison between the height anomalies by the DFHRS-DB and the ASCH model</i>	89
6.18	<i>The relative frequency histogram of the height fitting points residuals</i>	91
6.19	<i>The relative frequency histogram of the terrestrial gravity points residuals</i>	91
6.20	<i>The standard deviations and the degree variances of the ASCH coefficients using the combined solution of the state of Baden-Württemberg</i>	92
6.21	<i>The residuals of the terrestrial gravity points in Baden-Württemberg</i>	93
6.22	<i>The difference between height anomalies using ASCH combined model and the 1cm-DFHRS-DB</i>	95
6.23	<i>The difference between height anomalies using ASCH combined model and the GCG2011</i>	96
6.24	<i>The difference between height anomalies using DFHRS-DB combined model and the GCG2011</i>	97

List of Tables

Nr.	Description	Page
2.1	<i>Some of the common global gravity models with their data sources</i>	14
2.2	<i>The potential related observations and their linear operators $L(T)$</i>	21
2.3	<i>Examples of satellite only and combined geoid models. (GFZ-website, 2012)</i>	24
3.1	<i>Examples of Legendre coefficients</i>	39
4.1	<i>Tests of observations design in the vertical direction using the height anomalies</i>	50
4.2	<i>The defining parameters of the EGM2008</i>	51
4.3	<i>The defining parameters of the ASCH model in Baden-Württemberg with a cap size of 1.5°</i>	51
4.4	<i>The defining parameters of the ASCH model in Baden-Württemberg with a cap size of 1.7°</i>	51
6.1	<i>The results of ASCH modeling of height anomalies as compared to DFHRS-DB</i>	78
6.2	<i>The results of ASCH modeling related to real gravity measurements</i>	84
6.3	<i>The results of ASCH adjustment using terrestrial observations only</i>	87
6.4	<i>Results of ASCH modeling using combined solution</i>	88
6.5	<i>The detection of the blunders in the observations for Baden-Württemberg observations</i>	90
6.6	<i>The results of the final adjustment of the combined ASCH model in Baden-Württemberg with maximum degree of 300</i>	91
6.7	<i>The differences between the ASCH modeling and the DFHRS-DB in Baden-Württemberg</i>	94
6.8	<i>The differences between the ASCH modeling and the GCG2011 in Baden-Württemberg</i>	94
6.9	<i>The differences between the DFHRS-DB and the GCG2011 in Baden-Württemberg</i>	94

1. Introduction

The availability of GNSS related code- and phase-measurement, differential GNSS (DGNSS) RTCM correction messages, as well as precise point positioning (PPP), which are provided by different GNSS-positioning services worldwide lead to the replacement of classical terrestrial geodetic reference frames for the georeferencing of positions. E.g. in Germany, several millions of trigonometric plane and height positions have been replaced by different online GNSS services operating in the GNSS and International Terrestrial Reference Frame (ITRF) consistent frame ETRF89 (Jäger et al., 2006).

The station coordinates of these GNSS-online positioning services are given in the ITRF-frame or regional adoptions of it, like the time invariant ETRF89 for the stable part of Europe. Examples in Germany are the SAPOS (www.sapos.de), AXIONET (www.axio.net), VRSNow (www.trimble.com/positioning-services/vrs-now.aspx), and SMARTNET (de.smartnet-eu.com) services, with 150-250 stations nation-wide (Jäger, 2011). Further networks in European states and others round the world are available. Such services can provide the end user with highly accurate real time positions at a relatively low cost. In corresponding GNSS online processing, the positioning problem is divided into two parts: horizontal positioning and vertical positioning (Jäger, 2011). The horizontal position is transformed to the local coordinate systems through geometrical datum transformations and residuals interpolation followed by a specific map projection. In this way the horizontal positions can easily be merged with other traditional horizontal positioning techniques (Jäger et al., 2010).

For the vertical position (height), the situation is different, because the GNSS height is the geometric height measured along the normal above the ellipsoid's surface (ellipsoidal height h). The so-called physical heights H (or "sea-level heights"), which can also be measured with leveling instruments, refer to the Earth gravity field (Jekeli, 2007). They are based on potential differences to the reference potential W_0 and the zero level (geoid). The vertical datum is fixed in modern height reference systems by the geopotential number of one or more datum reference points.

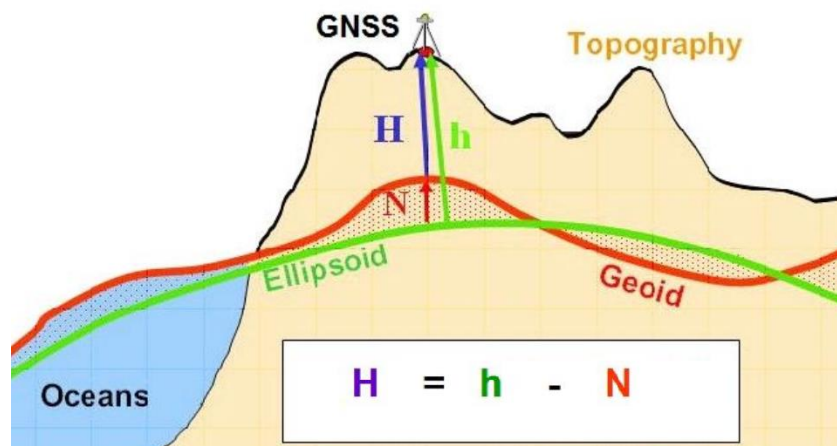


Figure (1.1): The principle of GNSS-based height determination: $H = h - N$ (Jäger et al., 2012).

In Europe, the Normaal Amsterdam's Peil (NAP) is the reference point for the European vertical reference system (EVRS2007). Depending on the detailed and slightly different physical definition of the basic height system types, these heights H are called orthometric heights, normal or spheroid normal heights (NN-heights). The respective height reference surface (HRS) is described with the symbol N in figure (1.1), and it is called the geoid, quasigeoid or NN-surface, depending on the kind of the above gravity field based height system (Schneid, 2006).

The aim of the DFHRS research project at the Institute of Applied Research (IAF) of the Hochschule Karlsruhe - University of Applied Sciences (HSKA) is the parametric modeling and computation of HRS from geometric and physical observation components in a hybrid adjustment approach (DFHRS). Access to the parametric HRS model is enabled by DFHRS databases (DFHRS-DB), which allow the direct conversion of GNSS-heights h into physical standard heights H . DFHRS databases are used for online GNSS-height determination in DGNSS-networks (SAPOS, AXIONET, etc.) directly on the GNSS controllers and via RTCM transformation messages in the real time GNSS positioning, and in GIS. The DFHRS databases have been computed for different states in Germany, as well as for several nations and regions in Europe, Africa and in USA. In most of these areas, the DFHRS-DB are used as the official vertical reference surface. The accuracy of the obtained results varies from 0.01-0.1 meter (Jäger et al., 2006). Recently, the terrestrial gravity measurements have been integrated in the DFHRS using the Spherical Cap Harmonics (SCH) to model the disturbing potential T and the related quantities like gravity anomalies, gravity disturbances, geoid heights and deflections of the vertical (Schneid, 2006).

The main objective of this thesis is to further develop the SCH-modeling, started by Schneid (2006), and to find more stable parameterizations, either by modifying the present Spherical Cap Harmonics or by using alternatives, for the physical observations.

Among the different types of SCH models, the Adjusted Spherical Cap Harmonics (ASCH) models have advantages over the other types of SCH (De Santis et al., 1997). ASCH do not require a search for the roots of Legendre function and its derivatives to satisfy the orthogonality requirements. The roots of the Legendre functions in the case of ASCH can be calculated easily using a direct formula with no need for complex and iterative solutions (De Santis et al., 1997). In addition, the Legendre functions of integer degree and order are used in the principle of ASCH. This enables the use of the well-known recursive and non-iterative formulas of Legendre functions similar to the ordinary Spherical Harmonics (SH) (De Franceschi et al., 1994). For these reasons, the ASCH have been chosen for modeling gravity and potential in regional areas.

One goal of this thesis is to find an optimal way for the combination of the geometric observations (e.g. fitting points with known ellipsoidal and normal heights and deflections of the) and physical observations (e.g. gravity data) for the HRS-representation using the Adjusted Spherical Cap Harmonics (ASCH). In the solution, the recent global gravity models presented by means of Spherical Harmonics (e.g. EIGEN05c and EGM2008) are transformed to local ASCH models and used as additional input in the adjustment of the combined ASCH solution. Another objective of this study is to compute a high precise height reference surface (1cm accuracy) for the state of Baden-Württemberg using the ASCH model for the combination of global gravity models, terrestrial gravity data and height fitting points.

In the following, Chapter (2) the general methods for global and local potential modeling using Spherical Harmonics, the Stokes formula, least squares collocation and the Finite elements methods are introduced. The principle of Integrated Geodesy is also introduced, and a general overview of the state-of-the-art of the latest global and local gravity and geoid models is provided.

Chapter (3) introduces the local gravity potential modeling using SCH and ASCH. The derivations of SCH and ASCH are explained in detail. Other modifications of SCH, as well as other carrier functions for local modeling of the potential are treated.

Chapter (4) describes the principles and results of the transformations of the global gravity models, presented by SH to local ASCH-models, and the results are discussed and validated. In addition, the design of the observations in the horizontal and vertical directions is discussed and tested.

The use of Integrated Geodesy for gravity potential modeling using ASCH is explained in chapter (5). Solution algorithms using direct least squares solutions are introduced. The required reductions and transformations of the different observation types are explained. The observation equations as well as stochastic models are discussed in detail. Additionally, numerical methods and aspects are discussed. The methods of Cholesky decomposition, block matrix Cholesky-decomposition and parallel processing are also presented.

Chapter (6) discusses the results and analysis of the Quasigeoid computations based on gravity data by the developed ASCH approach for the state of Baden-Württemberg. Different data types of geometric and physical observations combinations are introduced. The results of these different data combinations are presented.

Chapter (7) summarizes the thesis and its final results. In addition, conclusions and recommendations for further research are given.

2. Global and local gravity field modeling

This chapter introduces the potential of the Earth and its applications based on Newton's law of attraction, the relationship between the potential and the attraction force is explained. This chapter shows the solution of Laplace's equation using the SH model, which is applied to gravity field modeling of the Earth. The relationship between the actual gravity field and the normal gravity field of the Earth is also explained, whereby the anomalous gravity field is introduced.

The common way to represent the potential of the Earth is by SH, but the related methods require a global modeling. There is always a need to model the potential by other methods with local support for national and regional needs. Here, some of the common methods for local modeling of the potential of the Earth are discussed. Such suitable methods are the Stokes integral for gravimetric geoid modeling, the least squares collocation and the DFHRS developed at the Karlsruhe University of Applied Sciences.

The so called Integrated Geodesy principle, where combination of different data types of observations $l = l(\bar{x}, W(\bar{x}, p))$ are modeled in the gravity and geometry space, is also briefly discussed. In addition, the state-of-the-art of the latest global and local geoid and gravity models is presented.

2.1. The gravity field of the Earth

The attraction force F between two mass points m_1 and m_2 [kg], separated by a distance l [m], can be calculated according to Newton's law of attraction (equation 2-1) (Hofmann-Wellenhopf & Moritz, 2005). The attraction force F reads:

$$\bar{F} = G \frac{m_1 m_2}{l^2} \quad (2-1)$$

Here, G is Newton's gravitational constant with the value of $6.6742 \times 10^{-11} m^3 kg s^{-2}$. The attraction force F is symmetric. To study how a mass m attracts other masses, the attracted masses assumed to be a unit mass ($m_1 = 1$). The force attracting the unit mass at point $P(X, Y, Z)$ by the mass m at $P_0(X_0, Y_0, Z_0)$ separated by a distance l is (Heiskanen & Moritz, 1967):

$$F = G \frac{m}{l^2} \quad (2-2)$$

The force \bar{F} is represented by a vector from P_0 to P . The vector of the gravitational force \bar{F} can be defined by its magnitude F and 3D components of the unit vector (Fan, 2004). \bar{F} is given by

$$\bar{F} = \begin{bmatrix} F_x \\ F_y \\ F_z \end{bmatrix} = -F \begin{bmatrix} (X - X_0)/l \\ (Y - Y_0)/l \\ (Z - Z_0)/l \end{bmatrix} = -\frac{GM}{l^2} \begin{bmatrix} (X - X_0)/l \\ (Y - Y_0)/l \\ (Z - Z_0)/l \end{bmatrix} \quad (2-3)$$

The gravitational potential is a conservative, which satisfies the Laplace differential equation outside the Earth (see chapter 2.1.1). A scalar force generating potential exists. This function is called the gravitational potential $V(X, Y, Z)$ (Fan, 2004), where V reads:

$$V(X, Y, Z) = \frac{GM}{l} \quad (2-4)$$

The unit mass related force vector \vec{F} in equation (2-3) can be rewritten in terms of V as follows:

$$\vec{F} = \text{grad}(V) \quad (2-5a)$$

$$\vec{F} = \begin{bmatrix} F_x \\ F_y \\ F_z \end{bmatrix} = \begin{bmatrix} \frac{\partial V}{\partial X} \\ \frac{\partial V}{\partial Y} \\ \frac{\partial V}{\partial Z} \end{bmatrix} \quad (2-5b)$$

Assuming a system of point masses m_1, m_2, \dots, m_n are attracting the point P , and separated from the point P by distances l_1, l_2, \dots, l_n , then the gravitational potential V is the summation of all single potentials (Hofmann-Wellenhof & Moritz, 2005). The total gravitational potential is:

$$V(X, Y, Z) = \sum_{i=1}^n V_i = \sum_{i=1}^n \frac{Gm_i}{l_i} \quad (2-6)$$

If the point P is influenced by a solid body with a volume v and a density of $\rho(X, Y, Z)$, then the potential V is calculated by a superimposing infinite number of point masses dm . The point mass can be calculated by the volume of point mass dv and the density ρ , reading:

$$dm = \rho dv \quad (2-7)$$

The total gravitational potential by the solid body is calculated by the integration over the whole volume of the solid body (Torge, 2001). V is given by:

$$V = \int dV = G \iiint_V \frac{\rho(X, Y, Z) dv}{l} \quad (2-8)$$

2.1.1. Laplace differential equation and Spherical Harmonics (SH)

For a function $V(X, Y, Z)$, the Laplace equation for this function is the Laplace operator $\Delta(\cdot) = 0$ and reads (Fan, 2004):

$$\Delta(V) \equiv \frac{\partial^2 V}{\partial X^2} + \frac{\partial^2 V}{\partial Y^2} + \frac{\partial^2 V}{\partial Z^2} = 0 \quad (2-9)$$

Using spherical coordinates (r, ϕ, λ) as defined in fig (2.1), Laplace's equation can be transformed to:

$$r^2 \frac{\partial^2 V}{\partial r^2} + 2r \frac{\partial V}{\partial r} + \frac{\partial^2 V}{\partial \bar{\phi}^2} - \tan \bar{\phi} \frac{\partial V}{\partial \bar{\phi}} + \frac{\partial^2 V}{\cos^2 \bar{\phi} \partial \lambda^2} = 0 \quad (2-10)$$

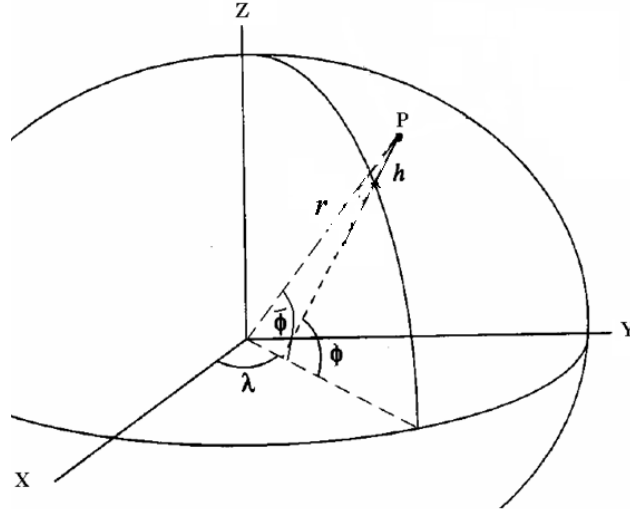


Figure (2.1): Geographic coordinates (λ, ϕ, h) and the spherical coordinates $(r, \lambda, \bar{\phi})$.

Assuming that the density ρ is constant (ρ is given the value of the average density of the Earth) and dv is the same for all elements, then only l is changing for each element. The Laplace operator for the gravitational potential in equation (2-8) is given by:

$$\Delta(V) = \Delta \left(G \iiint_v \frac{\rho dv}{l} \right) = G \iiint_v \Delta \left(\frac{1}{l} \right) \rho dv = 0 \quad (2-11)$$

As $\Delta \left(\frac{1}{l} \right) = 0$, V is a harmonic function. The solution of Laplace's equation is found by separating the variables r, λ , and $\bar{\phi}$ using the substitution in equation (2-12) (Fan, 2004), reading:

$$V(r, \bar{\phi}, \lambda) = f_1(r) f_2(\bar{\phi}) f_3(\lambda) \quad (2-12a)$$

$$f_1(r) = \frac{1}{r^{n+1}} \quad n = 0, 1, 2, \dots \quad (2-12b)$$

$$f_2(\bar{\phi}) = P_{nm}(\sin \bar{\phi}) \quad n=0, 1, 2, \dots \quad \text{and } m=0, 1, 2, \dots, n-1, n \quad (2-12c)$$

$$f_3(\lambda) = \cos m\lambda \quad \text{or} \quad \sin m\lambda \quad m=0, 1, 2, \dots, n-1, n \quad (2-12d)$$

In equation (2-12), $P_{nm}(\sin \bar{\phi})$ are the Legendre functions of degree n and order m . Assuming $\sin \bar{\phi} = t$, the Legendre function is generally defined by the differential formula in equation (2-13) (Hofmann-Wellenhof & Moritz, 2005):

$$P_{nm}(t) = \frac{1}{2^n n!} (1-t)^{m/2} \frac{d^m P_n(t)}{dt^m} (t^2-1)^n \quad (2-13)$$

As the differential equation (2-10) is linear, for each integer n there is a solution. The summation of all solutions is also a solution for Laplace's equation $\Delta V = 0$. The potential V can be written in terms of surface Spherical Harmonics (SH) in equation (2-15) (Hofmann-Wellenhof & Moritz, 2005).

$$V(r, \bar{\phi}, \lambda) = \sum_{n=0}^{\infty} \frac{1}{r^{n+1}} \sum_{m=-n}^n A_{nm} Y_{nm}(\bar{\phi}, \lambda) \quad (2-14)$$

$$Y_{nm}(\bar{\phi}, \lambda) = \begin{cases} \cos m\lambda P_{|m|}(\sin \bar{\phi}) & , m \leq 0 \\ \sin m\lambda P_{nm}(\sin \bar{\phi}) & , m > 0 \end{cases} \quad (2-15a)$$

$$A_{nm} = \begin{cases} a_{nm} & , m \leq 0 \\ b_{nm} & , m > 0 \end{cases} \quad (2-15b)$$

Equation (2-14) can be reformulated as double summation. In this case V reads:

$$V(r, \bar{\phi}, \lambda) = \sum_{n=0}^{\infty} \frac{1}{r^{n+1}} \sum_{m=0}^n (a_{nm} \cos m\lambda + b_{nm} \sin m\lambda) P_{nm}(\sin \bar{\phi}) \quad (2-16)$$

2.1.2. The normalized SH

As shown above, the gravitational potential V satisfies the Laplace equation. In equation (2-14), V was modeled to solve the Laplace equation in terms of SH. When higher degrees and orders Legendre functions $P_{nm}(t)$ are calculated, instability problems appear in the calculations (Fan, 2004). To avoid these issues, a normalized form of equation (2-14) is introduced in equation (2-17) using the normalized Legendre functions $\bar{P}_{nm}(t)$ (Sneeuw, 2006).

$$V(r, \bar{\phi}, \lambda) = \sum_{n=0}^{\infty} \frac{1}{r^{n+1}} \sum_{m=-n}^n \bar{A}_{nm} \bar{Y}_{nm}(\bar{\phi}, \lambda) \quad (2-17a)$$

$$\bar{Y}_{nm}(\bar{\phi}, \lambda) = f_{nm} Y_{nm}(\bar{\phi}, \lambda) \quad (2-17b)$$

$$\bar{P}_{nm}(t) = f_{nm} P_{nm}(t) \quad (2-17c)$$

$$\bar{A}_{nm} = \frac{A_{nm}}{f_{nm}} \quad (2-17d)$$

Finally, the potential V reads:

$$V(r, \bar{\phi}, \lambda) = \sum_{n=0}^{\infty} \frac{1}{r^{n+1}} \sum_{m=0}^n (\bar{a}_{nm} \cos m\lambda + \bar{b}_{nm} \sin m\lambda) \bar{P}_{nm}(\sin \bar{\phi}) \quad (2-18)$$

The normalizing function f_{nm} in equation (2-17) reads (Torge, 2001):

$$f_{nm} = \begin{cases} \sqrt{2n+1} & , m = 0 \\ \sqrt{2(2n+1) \frac{(n-m)!}{(n+m)!}} & , m \neq 0 \end{cases} \quad (2-19)$$

The coefficients \bar{a}_{nm} and \bar{b}_{nm} are constants, which have to be determined. They are generally called the spherical harmonic coefficients.

2.1.3. The normalized Legendre functions

Substituting the normalizing function f_{nm} in equation (2-19) in the recursive formula of Legendre function P_{nm} in equation (2-13), the fully normalized Legendre function in equation (2-20) is realized. $\bar{P}_{nm}(\sin \bar{\phi})$ is the fully normalized associated Legendre function. $\bar{P}_{nm}(\sin \bar{\phi})$ can be calculated by the recursive formulas (2-20), with the abbreviations $t = \sin \bar{\phi}$ and $u = \cos \bar{\phi}$ (Holmes & Featherstone, 2002) as follows:

$$\bar{P}_{n,m} = a_{nm} t \bar{P}_{n-1,m} - b_{nm} \bar{P}_{n-2,m} \quad (2-20a)$$

$$a_{nm} = \sqrt{\frac{(2n-1)(2n+1)}{(n-m)(n+m)}} \quad (2-20b)$$

$$b_{nm} = \sqrt{\frac{(2n+1)(n+m-1)(n-m-1)}{(n-m)(n+m)(2n-3)}} \quad (2-20c)$$

$$\bar{P}_{0,0} = 1, \quad \bar{P}_{1,0} = \sqrt{3}t, \quad \bar{P}_{1,1} = \sqrt{3}u \quad (2-20d)$$

If $n=m$, then $\bar{P}_{n,m}$ reads:

$$\bar{P}_{m,m} = u \sqrt{\frac{2m+1}{2m}} \bar{P}_{m-1,m-1} \quad (2-20e)$$

The first derivative of the fully normalized Legendre polynomial $\frac{\partial \bar{P}_{n,m}}{\partial \bar{\phi}}$ can be calculated using the calculated values of the recursive formulas in equations (2-20). There is no need for new recursive formulas to calculate the derivatives of the Legendre functions; the calculated value of the Legendre polynomial $\bar{P}_{n,m}$ can be applied directly to calculate the derivatives of the Legendre polynomial (Tscherning et al., 1983), reading:

$$\frac{\partial \bar{P}_{n,m}}{\partial \bar{\phi}} = \frac{1}{u} (n t \bar{P}_{n,m} - \sqrt{\frac{(n^2 - m^2)(2n+1)}{2n-1}} \bar{P}_{n-1,m}) \quad \text{for } n > m \quad (2-21a)$$

$$\frac{\partial \bar{P}_{n,m}}{\partial \bar{\phi}} = \frac{1}{u} n t \bar{P}_{n,m} \quad \text{for } n = m \quad (2-21b)$$

2.1.4. Harmonic expansion of the Earth gravitational potential

Equations (2-17) and (2-18) are used to evaluate the gravitational potential V at a point $P(r, \bar{\phi}, \lambda)$ attracted by the solid body of the Earth. Equations (2-20a) to (2-20e) are used to calculate the Legendre functions. The coefficients (a_{nm} , b_{nm}) in equation (2-18) can be used to evaluate the gravitational potential V at the point P created by the mass of the Earth (Hofmann-

Wellenhof & Moritz, 2005). Depending on the orthogonality conditions, the coefficients \bar{a}_{nm} and \bar{b}_{nm} are given by (Fan, 2004):

$$\bar{a}_{nm} = \frac{G}{2n+1} \iiint_V (r')^n \cos m\lambda' \bar{P}_{nm}(\sin \bar{\phi}') \rho dv \quad (2-22a)$$

$$\bar{b}_{nm} = \frac{G}{2n+1} \iiint_V (r')^n \sin m\lambda' \bar{P}_{nm}(\sin \bar{\phi}') \rho dv \quad (2-22b)$$

By substituting $m=0$ and $n=0$, we find $\bar{b}_{00}=0$, and \bar{a}_{00} is given by (Fan, 2004):

$$\bar{a}_{00} = G \iiint_V \rho dv = GM \quad (2-23)$$

Substituting \bar{a}_{00} in equation (2-18) results in:

$$V_{00} = \frac{GM}{r} \quad (2-24)$$

To find \bar{a}_{10} , \bar{a}_{11} , and \bar{b}_{11} , we have:

$$\bar{a}_{10} = \frac{G}{3} \iiint_V r' \sqrt{3} \sin \bar{\phi}' dm \quad (2-25a)$$

$$\bar{a}_{11} = \frac{G}{3} \iiint_V r' \cos \lambda' \sqrt{3} \cos \bar{\phi}' dm \quad (2-25b)$$

$$\bar{b}_{11} = \frac{G}{3} \iiint_V r' \sin \lambda' \sqrt{3} \cos \bar{\phi}' dm \quad (2-25c)$$

Geographic coordinates of the point element can be transformed to the Cartesian coordinates using equations (2-26a) to (2-26c).

$$r' \sin \phi' = z' \quad (2-26a)$$

$$r' \cos \phi' \cos \lambda' = x' \quad (2-26b)$$

$$r' \cos \phi' \sin \lambda' = y' \quad (2-26c)$$

Then \bar{a}_{10} , \bar{a}_{11} , and \bar{b}_{11} read:

$$\bar{a}_{10} = \frac{G}{\sqrt{3}} \iiint_V z' dm \quad (2-27a)$$

$$\bar{a}_{11} = \frac{G}{\sqrt{3}} \iiint_V x' dm \quad (2-27b)$$

$$\bar{b}_{11} = \frac{G}{\sqrt{3}} \iiint_V y' dm \quad (2-27c)$$

In mechanics, the coordinates of the center of mass of a rigid body are (Torge, 2001):

$$x_0 = \frac{1}{M} \iiint_V x' dm \quad (2-28a)$$

$$y_0 = \frac{1}{M} \iiint_V y' dm \quad (2-28b)$$

$$z_0 = \frac{1}{M} \iiint_V z' dm \quad (2-28c)$$

Inserting equations (2-28a) to (2-29c) in equations (2-27a) to (2-28c) results in:

$$\bar{a}_{10} = \frac{GM}{\sqrt{3}} z_0 \quad (2-29a)$$

$$\bar{a}_{11} = \frac{GM}{\sqrt{3}} x_0 \quad (2-29b)$$

$$\bar{b}_{11} = \frac{GM}{\sqrt{3}} y_0 \quad (2-29c)$$

For a properly chosen reference frame, the origin of the coordinate system coincides with the center of mass of the Earth. Therefore, x_0 , y_0 and z_0 are equal to zero, meaning that the related coefficients are zero as well.

$$\bar{a}_{10} = \bar{a}_{11} = \bar{b}_{10} = \bar{b}_{11} = 0 \quad (2-30)$$

Inserting equation (2-24) and (2-30) in equation (2-25) results in:

$$V(r, \bar{\phi}, \lambda) = \frac{GM}{r} + \sum_{n=2}^{\infty} \frac{1}{r^{n+1}} \sum_{m=0}^n (\bar{a}_{nm} \cos m\lambda + \bar{b}_{nm} \sin m\lambda) \bar{P}_{nm}(\sin \bar{\phi}) \quad (2-31)$$

The spherical harmonic coefficients \bar{a}_{nm} and \bar{b}_{nm} in equation (2-31) can be normalized using the gravitational constant GM and the semimajor axis of the reference ellipsoid a as shown in equations (2-32a) and (2-32b) to get new normalized coefficients \bar{C}_{nm} and \bar{S}_{nm} (Fan, 2004).

$$\bar{C}_{nm} = \frac{1}{a^n GM} \bar{a}_{nm} \quad (2-32a)$$

$$\bar{S}_{nm} = \frac{1}{a^n GM} \bar{b}_{nm} \quad (2-32b)$$

Inserting (2-32) in equation (2-31) results in equation (2-33a) or equivalently (2-33b).

$$V(r, \bar{\phi}, \lambda) = \frac{GM}{r} + \frac{GM}{a} \sum_{n=2}^{\infty} \left(\frac{a}{r}\right)^{n+1} \sum_{m=0}^n (\bar{C}_{nm} \cos m\lambda + \bar{S}_{nm} \sin m\lambda) \bar{P}_{nm}(\sin \bar{\phi}) \quad (2-33a)$$

$$V(r, \bar{\phi}, \lambda) = \frac{GM}{r} + \frac{GM}{r} \sum_{n=2}^{\infty} \left(\frac{a}{r}\right)^n \sum_{m=0}^n (\bar{C}_{nm} \cos m\lambda + \bar{S}_{nm} \sin m\lambda) \bar{P}_{nm}(\sin \bar{\phi}) \quad (2-33b)$$

2.1.5. Derivatives of the potential of the Earth

A point P on the Earth's surface is subjected to two types of acceleration (see figure 3.1). The first type is the gravitational acceleration part \bar{g}_1 due to the Earth's mass M. The second type \bar{z} is the centrifugal acceleration due to the Earth's rotation. The total acceleration \bar{g} is the vector summation of both gravitational and centrifugal accelerations (Fan, 2004), which represent the actual gravity vector:

$$\bar{g} = \bar{g}_1 + \bar{z} \quad (2-34)$$

The relationship between the accelerations in equation (2-34) and their related potential is given in equation (2-35). The total gravity potential W, created by the total acceleration, \bar{g} , is the summation of the gravitational potential V and the centrifugal potential Ω . This total gravity potential is given by:

$$W = V + \Omega \quad (2-35)$$

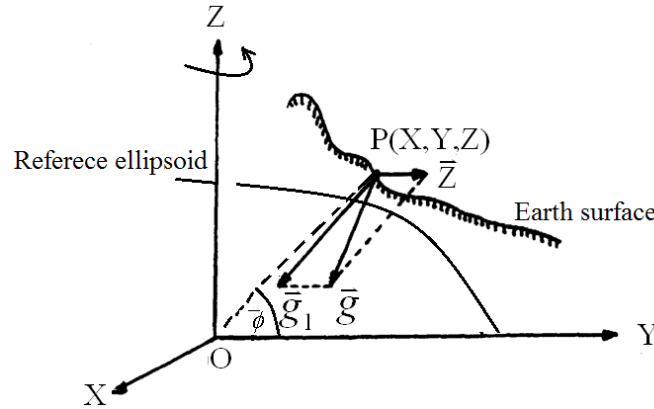


Figure (2.2): The gravitational and centrifugal accelerations of the Earth (Fan, 2004).

The centrifugal potential is caused by rotation of the Earth around its minor axis. The centrifugal acceleration vector will therefore have only two components in the X and Y directions. As the angular velocity ω of the Earth around its minor axis is $0.7292115 \times 10^{-4} s^{-1}$ as defined by the GRS80 (Torge, 2001), the centrifugal potential reads:

$$\Omega = 0.5 \omega^2 r^2 \cos \bar{\phi} = \frac{1}{2} \omega^2 (X^2 + Y^2) \quad (2-36)$$

Its related centrifugal acceleration vector and magnitude are:

$$\bar{z} = \text{grad}(\Omega) = \begin{bmatrix} \omega^2 X \\ \omega^2 Y \\ 0 \end{bmatrix} = \begin{bmatrix} \omega^2 r \cos \bar{\phi} \cos \lambda \\ \omega^2 r \cos \bar{\phi} \sin \lambda \\ 0 \end{bmatrix} \quad (2-37a)$$

$$z = |\bar{z}| = \sqrt{\left(\frac{\partial \Omega}{\partial X}\right)^2 + \left(\frac{\partial \Omega}{\partial Y}\right)^2 + \left(\frac{\partial \Omega}{\partial Z}\right)^2} = \omega^2 \sqrt{X^2 + Y^2} = \omega^2 r \cos \bar{\phi} \quad (2-37b)$$

The total gravity vector is the gradient of the gravity potential W ($\bar{\mathbf{g}} = \text{grad } W$). This can be formulated in equation (2-38) in 3D-cartesian coordinates (Torge, 2001).

$$\bar{\mathbf{g}} = \begin{bmatrix} \frac{\partial W}{\partial X} & \frac{\partial W}{\partial Y} & \frac{\partial W}{\partial Z} \end{bmatrix} \quad (2-38)$$

In spherical coordinates, equation (2-38) reads:

$$\bar{\mathbf{g}} = \begin{bmatrix} \frac{\partial W}{\partial r} & \frac{\partial W}{r \cos \bar{\phi} \partial \lambda} & \frac{\partial W}{r \partial \bar{\phi}} \end{bmatrix} \quad (2-39)$$

Substituting equation (2-35) in equation (2-39) results in:

$$\bar{\mathbf{g}} = \begin{bmatrix} \frac{\partial(V + \Omega)}{\partial r} & \frac{\partial(V + \Omega)}{r \cos \bar{\phi} \partial \lambda} & \frac{\partial(V + \Omega)}{r \partial \bar{\phi}} \end{bmatrix} \quad (2-40)$$

The derivatives of the gravitational potential V in equation (2-40) are given by:

$$\frac{\partial V}{\partial r} = -\frac{GM}{r^2} - \frac{GM}{r^2} \sum_{n=2}^{\max-n} \left(\frac{a}{r}\right)^n (n+1) \sum_{m=0}^n (\bar{C}_{n,m} \cos(m\lambda) + \bar{S}_{n,m} \sin(m\lambda)) \bar{P}_{n,m}(\sin \bar{\phi}) \quad (2-41a)$$

$$\frac{\partial V}{\partial \lambda} = \frac{GM}{r} \sum_{n=2}^{\max-n} \left(\frac{a}{r}\right)^n \sum_{m=0}^n m (\bar{S}_{n,m} \cos(m\lambda) - \bar{C}_{n,m} \sin(m\lambda)) \bar{P}_{n,m}(\sin \bar{\phi}) \quad (2-41b)$$

$$\frac{\partial V}{\partial \bar{\phi}} = \frac{GM}{r} \sum_{n=2}^{\max-n} \left(\frac{a}{r}\right)^n \sum_{m=0}^n (\bar{C}_{n,m} \cos(m\lambda) + \bar{S}_{n,m} \sin(m\lambda)) \frac{\partial \bar{P}_{n,m}}{\partial \bar{\phi}} \quad (2-41c)$$

The derivatives of the centrifugal potential read:

$$\frac{\partial \Omega}{\partial r} = \omega^2 \cos^2 \bar{\phi} \quad (2-42a)$$

$$\frac{\partial \Omega}{\partial \lambda} = 0 \quad (2-42b)$$

$$\frac{\partial \Omega}{\partial \bar{\phi}} = -\omega^2 r^2 \cos \bar{\phi} \sin \bar{\phi} \quad (2-42c)$$

The magnitude of gravity reads:

$$g = |\bar{\mathbf{g}}| = \sqrt{\left(\frac{\partial(V + \Omega)}{\partial r}\right)^2 + \left(\frac{\partial(V + \Omega)}{r \cos \bar{\phi} \partial \lambda}\right)^2 + \left(\frac{\partial(V + \Omega)}{r \partial \bar{\phi}}\right)^2} \quad (2-43)$$

By using the SH formulas, it is easy to derive any other functional quantities related to the potential (Heiskanen & Moritz, 1967). The most referred functional quantities in equation (2-44) are the gravity vector $\bar{\mathbf{g}}_{LGV_Sphere}$ in spherical-LGV, $\bar{\mathbf{g}}_{LGV}$ in LGV, quasigeoid heights (height anomalies) ζ , the geoid height N , and deflections of the vertical in the east and north directions (η, ξ) (Fan, 2004).

$$\mathbf{g}^{\text{LGV_Sphere}} = \left[\frac{\partial W}{\partial r} \quad \frac{\partial W}{r \cos \bar{\varphi} \partial \lambda} \quad \frac{\partial W}{r \partial \bar{\varphi}} \right] \text{ and } \mathbf{g}^{\text{LGV_Ellipsoid}} = \mathbf{R}(\lambda, \varphi)_e^n \cdot \begin{bmatrix} W_x \\ W_y \\ W_y \end{bmatrix}, \quad (2-44a)$$

where the absolute value g at a position $P(x,y,z)$ is both the same. The following quantities (2-44b) to (2-44e) are referring to the ellipsoid, a modern ellipsoidal georeferencing, and the respective reference gravity field (at present GRS80):

$$\zeta = \frac{T}{\gamma_Q} \quad (2-44b)$$

$$N = \frac{T}{\gamma_Q} + \frac{\bar{g} - \bar{\gamma}}{\bar{\gamma}} H_p = \zeta + \frac{\bar{g} - \bar{\gamma}}{\bar{\gamma}} H_p \quad (2-44c)$$

$$\xi = -\frac{\partial N}{\partial s_{\text{North}}} = -\frac{1}{\gamma_Q(M+h)} \frac{\partial T}{\partial \phi} \quad (2-44d)$$

$$\eta = -\frac{\partial N}{\partial s_{\text{East}}} = -\frac{1}{\gamma_Q(N+h) \cos \phi} \frac{\partial T}{\partial \lambda} \quad (2-44e)$$

With $\bar{\gamma}$ and \bar{g} the integrated quantities of the reference and the true gravity field (2-44a), respectively, along the plumb line (practically and without loss of validity computed along the ellipsoidal normal) are introduced. T is the disturbing potential, defined as the difference between the gravity potential W and the ellipsoidal normal potential U (see chapter 5.2.2). γ_Q is the ellipsoidal normal gravity for a point Q on the so-called telluroid with the same latitude and longitude as the calculation point and an ellipsoidal height of $h_Q = H^*_P = h_P - \zeta$. The telluroid is defined as the surface whose normal potential U_Q is equal to the actual potential at point W_P (Hofmann-Wellenhof & Moritz, 2005) (see figure 2.3). The telluroid is not an equipotential surface. s_{North} and s_{East} are the differential distance elements towards North and East, respectively. M and N are the ellipsoidal radii of curvature in the directions of longitude and latitude, respectively. The geoid (N) coincides with the mean sea level and was earlier used height reference surface by measuring the tide gauges at the coast of a country. The difference in the definitions between the geoid (N) and the quasigeoid (ζ) is discussed in details in chapter (5.2.2).

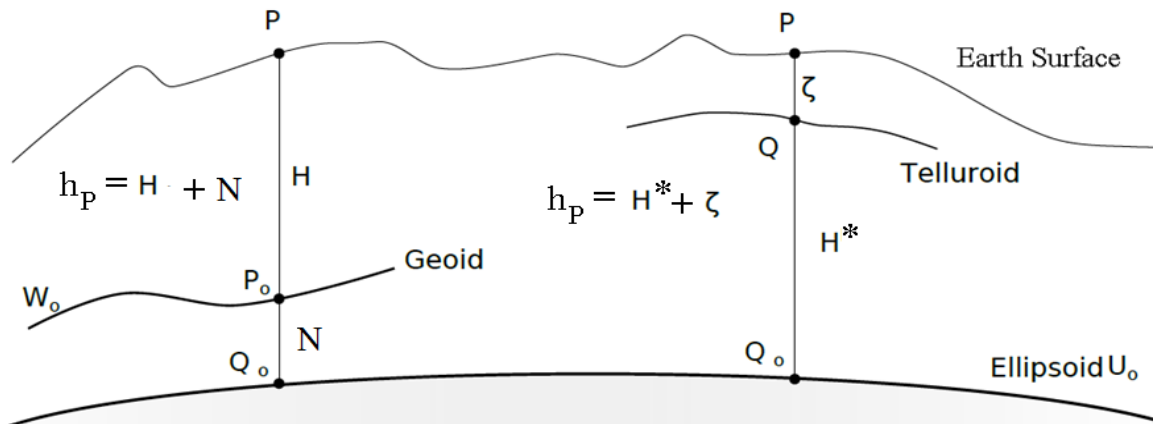


Figure (2.3): Height anomaly ζ vs. geoid height N .

2.1.6. The spherical harmonic expansion of the Earth's gravity field

The common way for representing the gravitational potential V in a global model is to use the SH (Hofmann-Wellenhof & Moritz, 2005). Presently, there are many global gravity potential field models available from various sources and with different spatial resolutions. The International Center for Global Gravity Models (ICGEM) provides access to the various satellite only or combined models on behalf of the International Association of Geodesy (<http://icgem.gfz-potsdam.de/ICGEM/ICGEM.html>) (ICGEM, 2012). Examples of these models are shown in table (2.1).

Table (2.1): Some of the common global gravity models with their data sources.

Model	Year	Degree	Data
<i>EIGEN06c</i>	2011	1420	S(GOCE,GRACE,LAGEOS),G,A
<i>EIGEN051c</i>	2010	359	S(GRACE, CHAMP),G,A
<i>EIGEN05c</i>	2008	360	S(GRACE,LAGEOS),G,A
<i>EGM2008</i>	2008	2190	S(GRACE),G,A
<i>EIGEN-GL04c</i>	2006	360	S(GRACE,LAGEOS),G,A
<i>GGM02c</i>	2004	200	S(GRACE),G,A
<i>EIGEN-CG01c</i>	2004	360	S(CHAMP,GRACE),G,A
<i>PGM2000A</i>	2000	360	S,G,A
<i>EGM96</i>	1996	360	S,G,A

Data: S=Satellite gravity data, G = Gravity data, A = Altimetry data

The calculation of the SH coefficients can only be solved by means of global data coverage. This could only be achieved after the first geodetic satellite missions (like the LAGEOS, GRACE, GOCE and CHAMP missions). The satellite missions are utilizing different types of measurement principles. The LAGEOS satellites apply the principle of Satellite Laser Ranging (SLR), while the CHAMP mission uses the principle of Satellite-to-Satellite tracking in high-low mode, where the residual gravity accelerations are additionally measured by means of an accelerometer. The GRACE Satellite mission uses the principle of Satellite-to-Satellite tracking in low-low mode, where the gravity differences between two satellites separated by hundreds of kilometers are observed. The most modern GOCE mission uses the principle of gravity gradiometry using a group of accelerometers fixed on the three axes of the satellite. The combination of satellite observations with terrestrial measurements led to the combined gravity models (e.g. EGM98A, EGM96, EIGEN06c and EGM2008). The SH can be calculated by two methods: the first is the integration method that keeps the orthogonality conditions of the SH, and second is the least squares estimation (Fan, 2004).

The integration methods have several problems. One is that the data have to be downward continued to the zero level (geoid) resulting in the so-called surface SH; the other is that weighting of observations of different sources is not possible. The integration formulas to calculate the spherical harmonic coefficients using the gravity anomalies Δg and the geoid heights N are given by Torge (2001):

$$\left\{ \begin{array}{l} \bar{C}_{nm} \\ \bar{S}_{nm} \end{array} \right\} = \frac{1}{4\pi GM} \iint_{\sigma} r\gamma \left(\frac{r}{a}\right)^n N \bar{P}_{nm} \left\{ \begin{array}{l} \cos m\lambda \\ \sin m\lambda \end{array} \right\} d\sigma \quad (2-45a)$$

$$\left\{ \begin{array}{l} \bar{C}_{nm} \\ \bar{S}_{nm} \end{array} \right\} = \frac{1}{4\pi GM} \iint_{\sigma} \frac{r^2}{n-1} \left(\frac{r}{a}\right)^n \Delta g \bar{P}_{nm} \left\{ \begin{array}{l} \cos m\lambda \\ \sin m\lambda \end{array} \right\} d\sigma \quad (2-45b)$$

In the least squares solution, the introduction of the variance and covariance matrices is possible for each group of data or for any single observation (Hofmann-Wellenhof & Moritz, 2005).

The solutions have always been applied in two modes: the satellite-only models and the combined models. The advantage of satellite-only methods is that they use direct gravity or a potential function as input without the need for any reductions or corrections. On the other hand, there is always mixing related to the terrestrial gravity data in the combined methods. Sometimes the terrestrial gravity data are free air gravity and sometimes Bouguer anomalies. The geoid/quasigeoid heights at the height fitting points may also be related to different vertical datums. They can also be in different types of heights like the orthometric, normal or dynamic heights. For these reasons, it is more desirable to have the satellite-only models alone without the combination with terrestrial data (Tscherning, 2001).

The satellite-only models use data measured over long time periods. This provides information about time dependent changes of the Earth like plate tectonics, ocean circulation, ice mass variations, tides, etc. Each of these time dependent effects will affect the measured gravity values. For these reasons they are suitable to be used in defining the global physical reference surface (Hofmann-Wellenhof & Moritz, 2005)

The satellite-only methods have a limited resolution which leads to lower degree and order of the SH model. In addition, there are always some gaps in the data, especially near the poles, but the representation of the quasigeoid requires high degrees and orders with global coverage of data (Tscherning, 2001). For these reasons terrestrial data are required to achieve higher accuracy in the combined models.

2.2. The local potential modeling

Here, different principles of local potential and gravity modeling are introduced. The methods discussed in this chapter are the Stokes formula including the remove-restore method, GNSS/Leveling, the Finite Elements Methods and the Least Squares Collocation. Other functional principles like SCH and its different modifications, Spherical Radial Basis Function and Spherical Harmonic Splines are introduced in chapter (3). There are many other principles available, like the astrogeodetic methods, ..., etc.

2.2.1. Stokes formula and remove-restore method

The Stokes formula (Stokes Integral), derived by Stokes (1849), is one of the most commonly used methods for the computation of highly accurate geoid models by means of a grid of surface gravity anomalies Δg . Here, Δg is the difference between the real gravity on the geoid surface g_p observation and the ellipsoidal normal gravity on the ellipsoid surface γ_Q . The gravity anomaly Δg reduced to geoid level to get Δg_0 to calculate the geoid using free correction and terrain corrections. Where Δg and Δg_0 read:

$$\Delta g = g_p - \gamma_Q \quad (2-46a)$$

$$\Delta g_0 = g_{p0} - \gamma_{Q0} \quad (2-46b)$$

The point P, P₀, Q and Q₀ are explained in fig (2.3). The Stokes formula reads:

$$N = \frac{a}{4\pi\gamma_m} \iint_{\sigma} S(\psi) \Delta g \, d\sigma \quad (2-47)$$

Here, a is the semimajor axis of the reference ellipsoid, The Stokes function $S(\psi)$ is given by:

$$S(\psi) = \sum_{n=2}^{\infty} \frac{2n+1}{n-1} P_n(\psi) \quad (2-48)$$

In equation (2-47), ψ is the spherical distance between the point of interest and a grid point with given gravity anomaly Δg . $P_n(\psi)$ is the zero order Legendre function related to ψ . For the implementation of Stokes integral, the scattered gravity anomalies gravity points have to be gridded over the complete Earth's surface to enable calculation of the geoid heights.

As the Stokes formula has to be applied globally in principle, an enhancement to this formula has commonly been used to model the geoid height locally using the long-wavelength effect, which is introduced by the available global gravity models. In addition, the combination of the global models with dense gravity data and high resolution Digital Terrain Models (DTM) leads to the so-called remove-restore technique.

In the remove-restore technique, the gravity anomaly grid points Δg are reduced by the gravity anomalies computed from a global gravity model Δg_{global} . The effect of the terrain then has to be reduced Δg_{DTM} . The resultant gravity anomalies (residual anomalies) $\Delta g_{\text{residual}}$ are applied in the Stokes formula to obtain the residual geoid heights $\Delta N_{\text{residual}}$ (Torge, 2001). The final geoid height is given by:

$$N = N_{\text{global}} + \Delta N_{\text{residual}} + \Delta N_{\text{DTM}} \quad (2-49)$$

The use of remove-restore method enables the application of Stokes formulas over smaller areas. This makes it possible to work with planar approximations, enabling application of the FFT. The use of the Stokes formula is not possible by combination of different data types with different accuracy measures. Furthermore, a grid of gravity anomalies must always be used. In this way, the single gravity observations cannot be statistically weighted and tested according to the measurement accuracy (Torge, 2012).

2.2.2. GNSS/Leveling

The GNSS/GPS leveling can be directly used in the defining the height reference surface (HRS) by measuring the ellipsoidal heights (h) of points with known orthometric height (H) or normal height (H^*). The ellipsoidal heights are measured directly by means of GPS/GNSS. The height anomaly ($\zeta=h-H^*$) or the geoid height ($N=h-H$) at a given point is directly determined (Fan, 2004).

2.2.3. Digital finite elements height reference surface (DFHRS)

The finite-element method has been used for modeling the height reference surface (HRS) in the Digital Finite Element Height Reference Surface (DFHRS) project (www.dfhbf.de). The DFHRS research project at IAF of the Hochschule Karlsruhe - University of Applied Sciences

aims to implement a parametric modeling and computation of height reference surfaces for the geometric and the physical observation components in a hybrid adjustment approach (DFHRS). Access to the parametric HRS model is enabled by DFHRS databases (DFHRS-DB), which allow the direct conversion of GNSS-heights (h) into physical heights (H). DFHRS data-bases are used for online GNSS-height measurements in DGNSS-networks (SAPOS, AXIONET etc.) and in the Geographic Information Systems (GIS). The DFHRS-DB have been computed for different states in Germany as well as several nations and regions in Europe, Africa and the USA. The accuracy of the obtained results varies from 0.01-0.1 meter (Jäger et al., 2006).

The direct conversion of the ellipsoidal GNSS height h (Ellipsoidal height), determined at the Earth surface, into the physical Earth gravity field based physical height H , is necessary for GNSS-based height measurements in modern GNSS-positioning services (Ghilani & Wolf, 2008). The basic relation between the GNSS-based height h and the standard height (orthometric height H) in figure (2.4) reads:

$$H = h - N \quad (2-50)$$

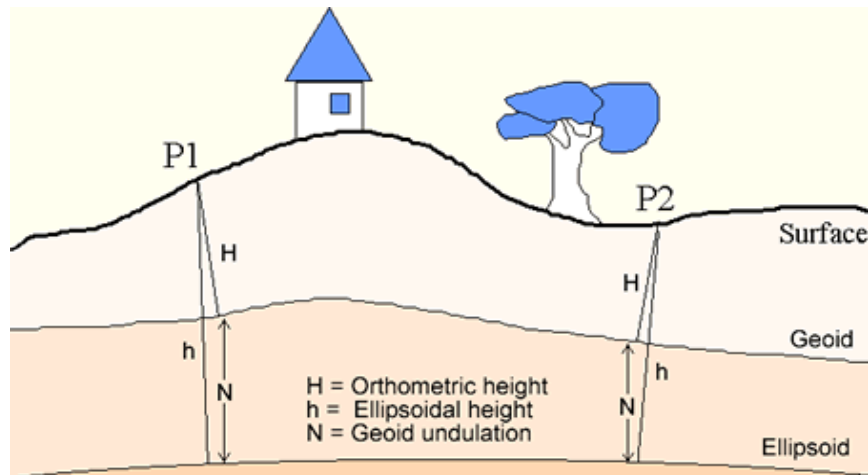


Figure (2.4): The relation between orthometric height H , ellipsoidal heights h and geoid undulation N .

2.2.3.1 Principles of DFHRS

The geoid is represented by its height above the Ellipsoid or the so-called geoid undulation (N). In DFHRS, N is represented by the Finite Element Method (FEM) with polynomial parameters \mathbf{p} . These describe a finite element HRS called NFEM($\mathbf{p} | \lambda, \phi, h$). If a scale difference Δm is considered for old reference systems, then the HRS is represented by NFEM($\mathbf{p}, \Delta m | \lambda, \phi, h$) (Jäger & Schneid, 2002). Equation (2-50) can therefore be written as:

$$H = h - DFHRS(\mathbf{p}, \Delta m | \lambda, \phi, h) \quad (2-51)$$

Or equivalently,

$$H = h - NFEM(\mathbf{p}, \Delta m | \lambda, \phi, h) \quad (2-52)$$

The finite element representation NFEM($p|x,y$) is carried out by bivariate polynomials of degree n , which are set up in regular or irregular meshes (Jäger & Kälber, 2000). If we describe with \mathbf{p}^i the polynomial coefficients ($a_{00}, a_{10}, a_{01}, a_{20}, a_{11}, a_{02}, \dots$) of the i -th mesh of n meshes in total, the height NFEM($\mathbf{p}^i|x,y$) of the HRS over the ellipsoid is:

$$NFEM(\mathbf{p}^i | x, y) = \mathbf{f}(x, y)^T \mathbf{p}^i \quad (2-53)$$

$$\mathbf{p}^i = [p_{jk}^i]^T; j = 0, n; k = 0, n \text{ and } \mathbf{f}(x, y)^T = (1, x, y, x^2, xy, y^2, \dots) \quad (2-54)$$

The principle of the DFHRS is to divide an area or region of a continuous HRS into a number of patches, with each patch further divided into a number of meshes as shown in figure (2.5). Each patch has a datum and associated transformation parameters (\mathbf{d}) and each mesh has HRS parameters (\mathbf{p}). Continuity condition must also be considered. The NFEM for a point in the boundary between two meshes should be the same depending on the two meshes (the so-called C_0 -continuity), as should the slope at the boundary for both meshes (so-called C_1 -continuity) so that the meshes represent the whole area. The DFHRS parameters (\mathbf{p}) and the mesh information are stored in the DFHRS-DB.

The DFHRS geometrical observations include points with ellipsoidal (h) and normal or orthometric heights (H) as identical points, geoid heights from global or regional geoid models, astronomical deflections of the vertical (ξ, η) from geoid models and the points with observed ellipsoidal heights (h) or orthometric heights (H).

The parameters stored in the DFHRS-DB are ($\mathbf{p}, \Delta m$) and are related to the projected coordinates (x, y). The polynomial representation of the DFHRS is written in terms of design matrix \mathbf{f} and parameters vector \mathbf{p} :

$$NFEM(\mathbf{p} | x, y) = \mathbf{f}(x, y)^T \mathbf{p} \quad (2-55)$$

The observation equation for an ellipsoidal normal height in the i -th mesh with covariance matrix \mathbf{C}_h has the following observation equation:

$$h + v = H + h\Delta m + \mathbf{f}(x, y)^T \mathbf{p}^i \quad (2-56a)$$

The observation equation of a global potential model (GPM) geoid height in the i -th mesh and the j -th patch is:

$$N_{GPM} + v = \mathbf{f}(x, y)^T \mathbf{p}^i + \partial N(\mathbf{d}^j) \quad (2-56b)$$

The deflections of the vertical in the i -th mesh and j -th patch observation equations are:

$$\zeta + v = \frac{-\mathbf{f}_\phi^T}{M(\phi) + h} \mathbf{p}^i + \partial \zeta(\mathbf{d}_{\eta, \zeta}^j) \quad (2-56c)$$

$$\eta + v = \frac{-\mathbf{f}_L^T}{N(\phi) \cos(\phi) + h} \mathbf{p}^i + \partial \eta(\mathbf{d}_{\eta, \xi}^j) \quad (2-56d)$$

The observation equation for the physical (orthometric or normal) heights reads:

$$H + v = H \quad (2-56e)$$

The continuity conditions between different neighbour meshes are considered as additional observation equations:

$$C + v = C(\mathbf{p}) \quad (2-56f)$$

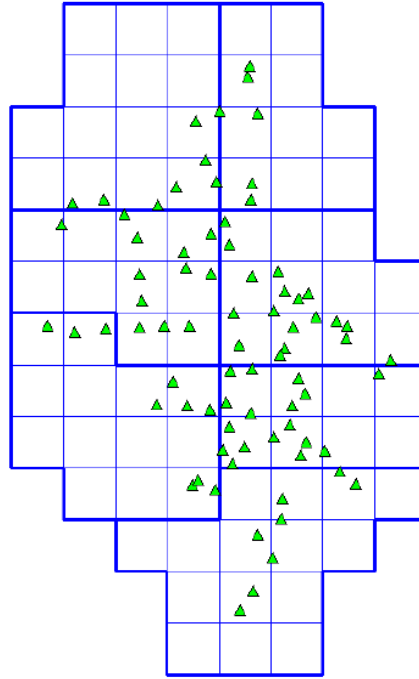


Figure (2.5): DFHRS patches and meshes, where thick lines represent the patch boundary and thin lines represent the meshes.

In the equations (2-56a) to (2-56f), $\partial N(\mathbf{d})$ is the datum parameterization of the GPM quasigeoid or geoid grid heights in the patch. $\partial \zeta(\mathbf{d})$ and $\partial \eta(\mathbf{d})$ are datum parameterizations of the deflections of the vertical. f_ϕ is the partial derivative of $f(x,y)$ with respect to the latitude. And finally, f_λ is the partial derivative of $f(x,y)$ with respect to the longitude.

To reduce the effect of medium- or long-wave length systematic shape deflections, specifically the natural and stochastic “weak shapes” (Schneid, 2006), in the observations N and (ζ, η) from geoid or GPM models, these observations are subdivided into a number of patches; see the thick blue in figure(2.5).

2.2.3.2 Extension of DFHRS to physical observations

The DFHRS physical observations include terrestrial, airborne and space borne gravity measurements. In addition, physical observations from a global or regional geopotential model (GPM) of the Earth gravitational potential V for limited size cap area and cap pole, represented

by the so-called SCH (S'_{nm}, C'_{nm}) (see figure3.1) may be integrated by use of Spherical Cap Harmonic (SCH) approach developed by Schneid (2006).

The advantage of SCH is that the number of parameters for the local cap area is significantly less than that needed in an ordinary global SH model. The disturbing potential using SCH in a cap coordinates system, as defined in chapter (3.1), can be written as (Schneid, 2006):

$$T(r, \alpha, \theta) = \sum_{k=0}^{k_{\max}} \left(\frac{R}{r} \right)^{n(k)+1} \sum_{m=0}^k (C'_{n(k),m} \cos m\alpha + S'_{n(k),m} \sin m\alpha) P_{n(k),m}(\cos \theta) \quad (2-57)$$

The DFHRS model can be used in SCH as a condition so that NFEM=N(SCH).

$$v_{\Delta N} = N(C'_{n(k),m}, S'_{n(k),m}) - \mathbf{f}^T \mathbf{p} \quad (2-58)$$

The gravity observation g_p at the Earth surface, taken with a gravity meter, refers to the local astronomical vertical system (LAV). The respective observed three-dimensional gravity vector in total is given by:

$$\mathbf{g}^{LAV} = [0, 0, -g_p]^T \quad (2-59a)$$

The related gravity anomaly is $\Delta g = g_p - \gamma_Q$. The gravity vector can be rotated using the deflections of the vertical (ξ, η) or equivalently by the astronomical latitude and longitude ($\Phi = \phi + \xi$, $\Lambda = \lambda + \eta / \cos(\phi)$) to the Earth-centered Earth-fixed system (ECEF) using (Φ, Λ), (see chapter 5.2.1). Following this rotation, the centrifugal parts are removed, and the original observation in equation (2-59a) is strictly reduced with respect to deflections of the vertical and the centrifugal acceleration. After a further rotation to the local geodetic vertical system (LGV) related to the cap sphere, the reduced observation (2-59a) is:

$$\Delta \mathbf{g}_{red}^{LGV} = [\Delta g_N, \Delta g_E, \Delta g_r]^T \quad (2-59b)$$

In the SCH frame (2-59b) using the transformation equations (5-10) to (5-17) is written as:

$$\Delta \mathbf{g}_{grav}^{SCH} = \left[\frac{1}{r} \frac{\partial T}{\partial \theta}, \frac{1}{r \sin \theta} \frac{\partial T}{\partial \alpha}, \frac{\partial T}{\partial r} \right]^T \quad (2-59c)$$

The harmonic expansion of the radial component of equation (2-59c) is:

$$\Delta g_{grav_r}^{SCH} = \sum_{k=0}^{\infty} \left(\frac{R}{r} \right)^{n(k)+1} \frac{(n(k)+1)}{r} \left(\sum_{m=0}^k (C'_{n(k),m} \cos m\alpha + S'_{n(k),m} \sin m\alpha) P_{n(k),m}(\cos \theta) \right) + dg(\mathbf{d}_g) \quad (2-59d)$$

The SCH have an integer order m and a real degree n_k . The real degree n_k satisfies the property of orthogonality of the function in the cap area (Haines, 1985a). These represent the roots of Legendre function and its derivatives according to the following conditions:

$$P_{n(k),m}(\cos \theta) = 0 \quad \text{for } k-m=\text{odd} \quad (2-60a)$$

$$\frac{dP_{nk(m)}(\cos \theta)}{d\theta} = 0 \quad \text{for } k-m=\text{even} \quad (2-60b)$$

This principle has disadvantages, because of the need to search for the real degrees n_k according to the conditions in equations (2-60a) and (2-60b). The different algorithms for calculating the roots of Legendre functions introduce additional errors, because they are mostly iterative with certain approximations or complicated algorithms (see chapter 3.1.2). Furthermore, the computation of the real degree n_k is time consuming (De Santis, 1997). The calculations of Legendre functions and their derivatives with non-integer degrees, where no recursive formulas are given in the literature, is also a time consuming process making use of approximations (Haines, 1985b). More detailed information about SCH and their different modification of SCH are given in chapter (3).

2.2.4. Least Squares Collocation

The basic principle of the Least Squares Collocation (LSC) is that the disturbing potential T satisfies Laplace's equation. It is represented by a group of suitable harmonic base functions φ_k at given positions with their related coefficients b_k . In this case, the disturbing potential reads:

$$T(P) = f(P) = \sum_{k=1}^q b_k \varphi_k \quad (2-61)$$

The measurements are assumed to be linear functionals $L(T)$ of the disturbing potential T . The linear operators of deflections of the vertical, gravity anomalies and gravity disturbances related to the disturbing potential are given in table (2.2) (Hofmann-Wellenhof & Moritz, 2005).

Table (2.2): The potential related observations and their linear operators $L(T)$.

Variable	Relation to the potential	$L(T)$
Deflection of vertical east-west	$-\frac{1}{\gamma_Q(N+h)\cos\phi} \frac{\partial T}{\partial \lambda}$	$-\frac{1}{\gamma_Q(N+h)\cos\phi} \frac{\partial}{\partial \lambda}$
Deflection of vertical north-south	$-\frac{1}{\gamma_Q(M+h)} \frac{\partial T}{\partial \phi}$	$-\frac{1}{\gamma_Q(M+h)} \frac{\partial}{\partial \phi}$
Gravity anomalies	$-\frac{\partial T}{\partial z} - \frac{2}{R} T$	$-\frac{\partial}{\partial z} - \frac{2}{R}$
Gravity disturbance	$-\frac{\partial T}{\partial z}$	$-\frac{\partial}{\partial z}$

For a given observation I , we have:

$$\sum_{i=1}^q B_{ik} b_k = l_i \quad (2-62)$$

The coefficients B_{ik} read:

$$B_{ik} = L_i(\varphi_k) \quad (2-63)$$

In equation (2-62), we can solve for q coefficients by using q observations. This method is called collocation. If we consider a harmonic covariance propagation function (K) that is symmetric with respect the point P and the reference point Q , the base function φ_k related to the observation type of Q is :

$$\varphi_k = L_k^Q K(P, Q) = C_{Pk} \quad (2-64)$$

Substituting (2-64) in (2-63) results in:

$$B_{ik} = L_i^P L_k^Q K(P, Q) = C_{ik} \quad (2-65)$$

Solving (2-62) for b_k and substituting in (2-61) results in:

$$f(P) = [C_{P1} \quad C_{P2} \quad \cdots \quad C_{Pq}] \begin{bmatrix} C_{11} & C_{12} & \cdots & C_{1q} \\ C_{21} & C_{22} & \cdots & \vdots \\ \vdots & \vdots & \ddots & \vdots \\ C_{q1} & C_{q2} & \cdots & C_{qq} \end{bmatrix}^{-1} \begin{bmatrix} l_1 \\ l_2 \\ \vdots \\ l_q \end{bmatrix} \quad (2-66)$$

The covariance propagation function K as given by Torge (2001) reads:

$$K(P, Q) = \sum_{n=2}^{\infty} \sigma_n^2 \left(\frac{R^2}{r_P r_Q} \right)^{n+1} P_n(\psi_{PQ}) \quad (2-67)$$

In equation (2-67), σ_n^2 is the n -th degree variance that can be theoretically calculated by the Tscherning & Rapp method or from the global gravity models. ψ_{PQ} is the spherical distance between the points P and Q (Hofmann-Wellenhof & Moritz, 2005).

The greatest advantage of LSC is the flexibility in estimating any kind of the potential related quantities using a combination of all available geodetic physical and geometrical observations, in addition to its proper use for local and global implementation. The primary problem, however, is that for huge areas a large amount of data would be required. This requires extended computation time of the new points.

2.3. Integrated Geodesy

High speed computers allowed the processing of large amounts of data of different types to solve a large system of equations. The integrated data processing for a unified model for three dimensional geodesy is called “Integrated Geodesy”. In the classical geodesy, only one type of observation is used for gravity field modeling. An example of the classical geodesy is the Stokes formula for geoid modeling, where only the gravity anomalies are used to compute the disturbing potential T (Hein, 1986).

The principle of Integrated Geodesy is that any time independent observation l can be expressed as a function with parameters vector p depending on the position (Geometry) $\bar{x}(X, Y, Z)$ and the Earth potential W (Heck et al., 1995):

$$l = l(\bar{x}, W(\bar{x}, p)) \quad (2-68)$$

In most cases, the position (geometry) is assumed to be fixed. The parameterization is to model the potential and its related quantities. The quantities introduced in chapter (2.1.5) are all functions of the potential that apply to equation (2-68). Examples of Integrated Geodesy are each of the modeling principles introduced in chapter (3). The DFHRS described in chapter (2.2.2) also qualifies as Integrated Geodesy.

2.4. State of the art in the gravity field modeling

There currently exist many published global, regional and local geoids. In the global models, they are mostly modeled by means of SH as described in chapter (2.1). EGM2008 is the global combined gravity model with the highest degree and order presently available, with a maximum degree and order of 2190. The EGM2008 would satisfy a 5cm geoid height accuracy, in case it would be free of “weakshapes” (Pavlis et al., 2008). Other combined global gravity models were calculated and introduced by GFZ-Potsdam (EIGEN models). The most recent of these is the EIGEN06c, which has a maximum degree and order of 1420. In the geoid heights, the accuracy of the EIGEN06c is comparable to the EGM2008. Other combined models with less degree and order (EIGEN01-05c) are up to degree and order of 360.

The estimation of high degree and order models like EGM2008 and EIGEN06c have introduced new calculation methods. In these methods, the parameters are calculated using a combination of integrals and least squares (Shako et al., 2010). Figure (2.6) shows the use of different data types, and how they contribute to finding the harmonic coefficients of the EIGEN06c model.

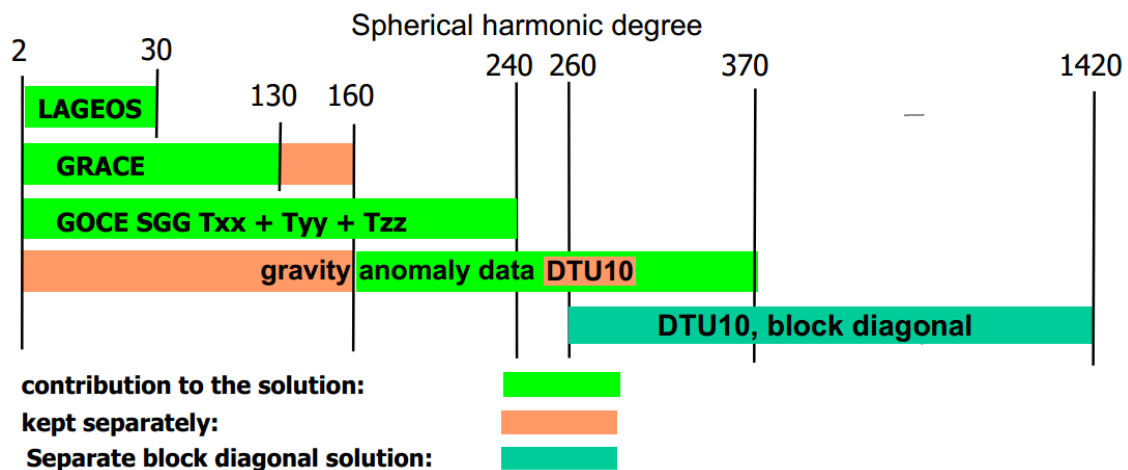


Figure (2.6): The principle of harmonic coefficients calculation in EIGEN06c model. (Förste et al., 2011)

For modeling the satellite-only gravity data, which are free of datum and zero level, satellite-only models are always introduced. One of the most common applications is the satellite orbit determination. These models, however, suffer from problems associated with ground geoid determination. This is because of low degrees and orders due to the loss of data, especially in pole areas. Table (2.3) shows selected combined and satellite-only models and their related maximum degree and order with the accuracy of the model.

Table (2.3): Examples of satellite only and combined global geoid models. (GFZ-website, 2012)

Model	Publishing date	N-max	Data	geoid accuracy in Europe (m)
EGM2008	2008	2190	S(GRACE),G,A	0.208 m
EIGEN06c	2011	1420	S(GOCE,GRACE,LAGEOS),G,A	0.214 m
EIGEN06s	2011	240	S(GOCE,GRACE,LAGEOS)	0.449 m
GGM03c	2009	360	S(GRACE),G,A	0.515 m
GGM03s	2008	150	S(GRACE)	1.416 m

S= Satellite data, G=Terrestrial gravity, A=height fitting points

The EGG07, computed by IfE-Hannover, is one of the latest regional gravity models in Europe, and has supplanted the European quasigeoid EGG97 (Torge & Denker, 1999). The EGG07 was calculated by the remove-restore method with updated terrestrial gravity, marine gravity and airborne gravity data. When compared to GPS/leveling heights the EGG07 has a RMSE of 0.01-0.06 m. The worst results were in high mountains in Austria and France (Denker et al., 2008). Another regional geoid model was calculated by the DFHRS software for the Baltic countries (Latvia, Estonia, and Lithuania). The achieved accuracy of the Baltic geoid was 1-3cm (Jäger et al., 2012). For Europe, a geoid model using DFHRS software was calculated in 2004 with an accuracy of better than 10 cm.

In terms of local geoid models, the USGG09 and GEOID09 were introduced in 2010 for the United States of America by the NGS (National Geodetic Survey). The USGG09 is an absolute gravimetric geoid model using the remove-restore method using millions of land and ocean gravity data points with EGM96 support for long wave geoid heights. The combined geoid model (GEOID09) is applied by combining the USGG09 with nearly 20000 GPS/leveling points using Multi-Matrix Least Squares collocation (MMLSC). In the GEOID09 six LSC matrices were applied to achieve 2km geoid resolution with RMSE of 1.5cm (Roman et al., 2010).

In Germany, the German Combined Quasi geoid 2011(GCG2011) was introduced by the Bundesamt für Kartographie und Geodäsie (BKG) and IfE-Hannover. The GCG2011 was calculated by the remove-restore method combined with point mass method using terrestrial gravity, GOCE gravity and GPS/leveling points. The GCG2011 accuracy is 1-2 cm in flat and hilly areas, but is reduced to approximately 3-4 cm in the high mountains. In ocean areas, the accuracy of the GCG2011 geoid is in the range of 4-10cm (BKG, 2011).

In 2010, the DFHRS software was used to calculate the Height Reference Surface (Quasigeoid) for the State of Moldova. The solution was applied using a mesh design of 5x5km. In Moldova, there are two height systems in use. One system is for urban areas, while the other is for rural areas. For this reason the solution was done twice by preparing two DFHRS-DBs. Field tests have shown an average accuracy of 1-2 cm over the entire country (Jäger et al., 2010).

3. Local potential modeling using Spherical Cap Harmonics

In this chapter, the modeling of the Earth's gravitational potential using Spherical Cap Harmonics (SCH) is presented. The derivations and applications to the potential modeling of SCH are explained, as well as different modifications to the model, including the ASCH model, Translated Origin Spherical Cap Harmonics (TOSCH) and Revised Spherical Cap Harmonics (R-SCH) are discussed. Other methods to represent the potential with local support are introduced as well. The Spherical Radial Basis Functions (SRBF) and the harmonic Spline functions are briefly explained.

The ASCH have many advantages over standard SCH models and are discussed in this chapter. The derivation of the ASCH and their principles are explained. The application of ASCH for modeling the gravitational potential and the calculations of the derived functional quantities including gravity, geoid/quasigeoid and deflections of the vertical are introduced.

A special case of application of SCH or ASCH is to represent the gravitational potential V of the Earth. In this case, the ordinary SH are used. The SH representation is only valid for a global modeling. The relationships between SH, SCH and ASCH are explained in this chapter.

3.1. Spherical Cap Harmonics

A method for modeling the gravity potential was introduced by G. Haines (1985a). This method is to be used in a local area for modeling the gravitational potential V using the so-called SCH (S'_{nm}, C'_{nm}). These SCH are suitable for the area of a local cap covering a region of interest on the sphere instead of the whole sphere (see figure 3.1). The cap position is described by the vector to the cap center with spherical coordinates $(\lambda_0, \bar{\phi}_0, R)$. The position of points in the cap region is described by a spherical coordinates (α, θ, r) related to the cap pole. Here, α is the azimuth of the spherical line from the cap pole to point. θ is the spherical distance from the cap pole $(\lambda_0, \bar{\phi}_0, R)$ to point P. Finally, r is the radial distance from the Earth center to the point P. The relationship between global coordinates and local coordinates reads:

$$\tan \alpha = \frac{\cos \bar{\phi} \sin(\lambda - \lambda_0)}{\sin \bar{\phi} \cos \bar{\phi}_0 - \cos \bar{\phi} \sin \bar{\phi}_0 \cos(\lambda - \lambda_0)} \quad (3-1a)$$

$$\cos \theta = \sin \bar{\phi} \sin \bar{\phi}_0 - \cos \bar{\phi} \cos \bar{\phi}_0 \cos(\lambda - \lambda_0) \quad (3-1b)$$

In equation (3-1), $(\lambda, \bar{\phi})$ are the spherical longitude and latitude of the point. $(\lambda_0, \bar{\phi}_0)$ are the spherical longitude and latitude of the cap pole. R is the radius of the reference sphere. The gravitational potential V in terms of SCH for a point $P(r, \alpha, \theta)$ within the cap reads (Haines, 1988):

$$V(r, \alpha, \theta) = \frac{GM}{r} \sum_{k=0}^{k_{\max}} \left(\frac{R}{r} \right)^{n(k)} \sum_{m=0}^k \left(C'_{nm} \cos m\alpha + S'_{nm} \sin m\alpha \right) \bar{P}_{n(k),m}(\cos \theta) \quad (3-2)$$

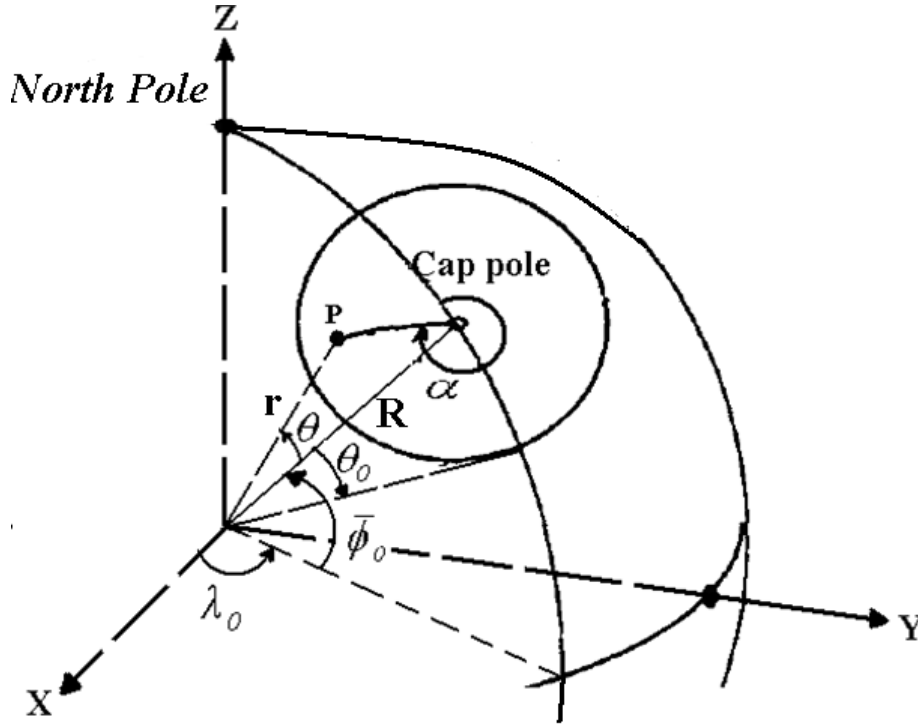


Figure (3.1): Spherical cap area with its own pole located at the origin of the area of interest.

The SCH equation (3-2) looks similar the SH equation (2-33). The difference is the use of α instead of λ , θ instead of $\bar{\phi}$, and power of $n(k)$ instead of n . The advantage of SCH in equation (3-2) is that the number of coefficients (C'_{nm}, S'_{nm}) necessary for a particular resolution for the local cap area is much smaller than that (C_{nm}, S_{nm}) needed in ordinary global SH for the same resolution (Haines, 1988).

The SCH have an integer order m and a real degree $n(k)$, where the real degree $n(k)$ are the root of the Legendre functions. Legendre functions and their derivatives have to satisfy the orthogonality conditions in the cap area according to equations (3-3a) and (3-3b) (Haines, 1985). In equation (3-3), k is the integer degree, and m is the order. θ_0 is the angular spherical distance from the pole of the cap area to the boundary of the area of interest.

$$\left. \frac{dP_{n(k),m}(\cos \theta)}{d\theta} \right|_{\theta_0} = 0 \quad \text{for } k-m=\text{even} \quad (3-3a)$$

$$P_{n(k),m}(\cos \theta) \Big|_{\theta_0} = 0 \quad \text{for } k-m=\text{odd} \quad (3-3b)$$

The Legendre function with the real degree $n(k)$ and the integer m cannot be done by direct and recursive formulas, as it is in the case of integer degree and order (see chapter 3.1.2). It is instead defined by an infinite power series (Haines, 1988), which must be elaborated iteratively introducing certain approximations; these will introduce additional errors, otherwise, complex algorithms must be used (Oliver & Smith, 1983).

When applying SCH, certain issues must be considered. First, a search for the real degrees $n(k)$ according to the conditions in equation (3-3) must be performed. The algorithms to search for the roots of the Legendre functions are non-direct or iterative resulting on additional errors. These algorithms are also time consuming (De Santis et al., 1999). Furthermore, the calculations of Legendre functions and their derivatives with non-integer degrees are again a time consuming iterative process (Schneid, 2006). Such algorithms introduce errors due to certain approximations used (Haines, 1985b). Another difficulty in SCH is the use of Legendre functions of real degree and integer order, which are not so commonly used given their limited availability in the geodetic literature in comparison to easily found Legendre functions with integer degree and order.

In addition to the proper use for local modeling of the gravity field, an advantage of SCH over the other methods is their ability to model the potential itself instead of the disturbing potential. Furthermore, there is no need to interpolate a grid of data to calculate the Spherical Cap Harmonic coefficients; the directly observed data can be used to set up observation equations in a least squares solution.

3.1.1. Derivation of SCH

Haines (1985a) has developed a method to use the Spherical Harmonics principle in a local cap area through a basis carrier function, referred to previously as SCH. Here, the coordinate system is defined by a local pole and the opening angle of the cap area in figure (3.1). This principle has been widely applied in geomagnetic as well as gravity potential field modeling (Haines, 1985b). The SCH model given in equation (2-2) is equivalently written as:

$$V(r, \alpha, \theta) = \sum_{k=0}^{k_{\max}} \sum_{m=0}^k V_{k,m}(r, \alpha, \theta) \quad (3-4)$$

Where

$$V_{k,m} = \frac{GM}{r} \left(\frac{R}{r} \right)^{n(k)} \left(C'_{km} \cos m\alpha + S'_{km} \sin m\alpha \right) \bar{P}_{n(k),m}(\cos \theta) \quad (3-5)$$

The gravitational potential V representations (3-4) and (3-5) satisfy Laplace's equation. The values $n(k)$ and m are the single eigenvalues of equation (3-5) calculated using the boundary conditions of equation (3-5) given in (3-6a, b) and (3-7a-d) for α , θ and r (Schneid, 2006).

As α can reach any numerical value between α and $\alpha + 2\pi$, the boundary conditions for α are:

$$V_{k,m}(r, \alpha, \theta) = V_{k,m}(r, \alpha + 2\pi, \theta) \quad (3-6a)$$

$$\frac{\partial V_{k,m}(r, \alpha, \theta)}{\partial \alpha} = \frac{\partial V_{k,m}(r, \alpha + 2\pi, \theta)}{\partial \alpha} \quad (3-6b)$$

These conditions force m to be real and integer valued and the value of $S'_{k,0}$ to be zero (Korte, 1999). The boundary condition for θ are at the cap pole $\theta=0$ and the cap boundary $\theta=\theta_0$. The boundary values for θ are:

$$V_{k,m}(r, \alpha, \theta_0 = 0) = 0 \quad (3-7a)$$

$$\frac{\partial V_{k,m}(r, \alpha, \theta_0 = 0)}{\partial \theta} = 0 \quad (3-7b)$$

$$V_{k,m}(r, \alpha, \theta_0) = f(r, \alpha) \quad (3-7c)$$

$$\frac{\partial V_{k,m}(r, \alpha, \theta_0)}{\partial \theta} = g(r, \alpha) \quad (3-7d)$$

The boundary conditions (3-7a) and (3-7b) permit an arbitrary potential that is independent of α . The functions $f(r, \alpha)$ and $g(r, \alpha)$ are arbitrary functions, that are independent of θ . Haines (1985) has shown that the conditions (3-7c) and (3-7d) can be satisfied in the conditions given in equations (3-8a) and (3-8b) by taking all values of m in the boundary condition in equations (3-6a) and (3-6b) (Haines, 1985a).

$$V_{k,m}(r, \alpha, \theta_0) = 0 \quad (3-8a)$$

$$\frac{\partial V_{k,m}(r, \alpha, \theta_0)}{\partial \theta} = 0 \quad (3-8b)$$

These conditions can be satisfied using a Legendre function of the first kind. The roots $n(k)$ are real values and m are integer values. The conditions (3-8a) and (3-8b), however, cannot be simultaneously satisfied. Haines (1985a) has shown that the conditions (3-8a) and (3-8b) can be satisfied if the Legendre function and its derivative apply for the condition separately (Schneid, 2006). The Legendre function of first kind and its derivative apply for the conditions (3-8a) and (3-8b), when the conditions (3-9a) and (3-9b) are satisfied, respectively:

$$P_{n(k),m}(\cos \theta_0) = 0 \quad , k-m=\text{odd} \quad (3-9a)$$

$$\frac{dP_{n(k),m}(\cos \theta_0)}{d\theta} = 0 \quad , k-m=\text{even} \quad (3-9b)$$

The boundary condition in the direction of r reads:

$$\lim_{r \rightarrow \infty} V_{k,m}(r, \alpha, \theta) = 0 \quad (3-10)$$

The boundary condition (3-10) can be satisfied as $n(k) \geq 0$. Also, Haines (1985a) has shown that the boundary condition can be satisfied when k is not less than (-1) (Haines, 1985a). It can therefore be generalized that the SCH functions are orthogonal (Haines, 1985a).

To find roots $n(k)$ (roots of first kind Legendre function), the condition equations (3-9a) and (3-9b) have to be fulfilled. Chapter (3.1.3) introduces different methods to find the roots of functions. An approximate formula for the roots of Legendre function reads (Haines, 1988):

$$n_k(m) = \frac{90}{\theta_0} (k + 0.5) - 0.5 \quad (3-11)$$

3.1.2. Legendre function of real degree and integer order

The calculation of the Legendre function of real degree n and integer order m can be calculated in terms of heterogeneous functions (Oliver & Smith, 1983). The general formula for calculating the Legendre function reads:

$$P_{n,m}(\cos \theta) = K_{n,m} \sin^m \theta F\left(m-n, n+m, 1+m, \frac{1-\cos \theta}{2}\right) \quad (3-12a)$$

Where F is a heterogeneous function which reads:

$$F(\alpha, \beta, \gamma, x) = 1 + \frac{\alpha\beta}{1\gamma}x + \frac{\alpha(\alpha+1)\beta(\beta+1)}{1(2)\gamma(\gamma+1)}x^2 + \dots \quad (3-12b)$$

The factor $K_{n,m}$ is the normalizing factor. When the so-called Schmidt normalizing principle is used (Haines, 1985a), then $K_{n,m}$ reads:

$$K_{n,m} = \begin{cases} 1 & m = 0 \\ \frac{\sqrt{2}}{2^m m!} \sqrt{\frac{(n+m)!}{(n-m)!}} & m \neq 0 \end{cases} \quad (3-14)$$

For $n > m > 0$ an approximate formula of $K_{n,m}$ can be used by applying the so called Stirlings-formula. Here, $K_{n,m}$ is defined as:

$$K_{n,m} = \frac{2^{-m}}{(m\pi)^{0.5}} \left(\frac{n+m}{n-m}\right)^{0.5n+0.25} p^{0.5m} \exp(e_1 + e_2 + \dots) \quad (3-15a)$$

$$p = \left(\frac{n}{m}\right)^2 - 1 \quad (3-15b)$$

$$e_1 = -\frac{1}{12m} \left(1 + \frac{1}{p}\right) \quad (3-15c)$$

$$e_2 = -\frac{1}{360m^3} \left(1 + \frac{3}{p^2} + \frac{4}{p^3}\right) \quad (3-15d)$$

The heterogeneous function F in equation (3-13a) can be calculated by a recursive method depending on the normalizing factor $K_{n,m}$ (Haines, 1988). Then $P_{n,m}(\cos \theta)$ reads:

$$P_{n,m} = \sum_{j=0}^J A_j(m, n) \left(\frac{1-\cos \theta}{2}\right)^j \quad (3-16a)$$

$$A_j(m, n) = \begin{cases} K_{n,m} \sin^m \theta & j = 0 \\ \frac{(j+m-1)(j+m) - n(n+1)}{j(j+m)} A_{j-1}(m, n) & j > 0 \end{cases} \quad (3-16b)$$

The derivative of the Legendre function in equation (3-16) reads:

$$\frac{dP_{n,m}}{d\theta} = \begin{cases} \frac{\sin \theta}{2} \sum_{j=1}^J k A_j(m, n) \sin^{2(j-1)}(\theta/2) & m = 0 \\ \left[\frac{\sin \theta}{2} \sum_{j=1}^J k A_j(m, n) \sin^{2(j-1)}(\theta/2) \right] + \cos \theta \left[\frac{m}{\sin \theta} P_{n,m} \right] & m > 0 \end{cases} \quad (3-17)$$

The value of the upper limit of the power series (J) is not constant in all calculations, but it can be limited when the required rounding accuracy is achieved. The term J is also called the truncation factor. The incurred relative error introduced by the truncation approximately reads (Oliver & Smith, 1983):

$$e_{truncation} = \frac{2^{J-3}}{\pi J} \quad (3-18)$$

3.1.3. Roots of Legendre function

To calculate the gravitational potential V in equation (3-2), the roots $n_k(m)$ of the Legendre function are required. These roots are calculated by satisfying the conditions (3-9a) and (3-9b). As equations (3-16) and (3-17) are used to calculate the Legendre function and its derivative, it would be difficult to calculate the roots $n_k(m)$ with direct formulas.

An iterative method is normally used to find the roots $n_k(m)$. In this way, an approximate value of $n_k(m)$ is used to calculate the function in an iterative process. A small increment is then added or subtracted to $n_k(m)$. $n_k(m)$ is changed until the function is sufficiently close to zero (Press et al., 2002). To limit the iterations a good approximation for the initial value of $n_k(m)$ is needed; this is given by equation (3-19) (Haines, 1988), reading:

$$n_k(m) = n_k(0) = \frac{90^\circ}{\theta_0} (k + 0.5) - 0.5 \quad (3-19)$$

Another method to find $n_k(m)$ is to use the so-called Regula-Falsi procedure. The root of a function $f(x)$ is \tilde{x} . \tilde{x} is in the interval $(a < \tilde{x} < b)$ and $(f(a) < 0, f(b) > 0)$. The root is found initially by linear interpolation (Lang & Pucker, 2005); \tilde{x} reads:

$$\tilde{x} = \frac{a f(b) - b f(a)}{f(b) - f(a)} \quad (3-20)$$

Using the \tilde{x} calculated by equation (3-20), (see figure3.2), $f(\tilde{x})$ is calculated. If $f(\tilde{x})$ is negative and larger than a , then $a = f(\tilde{x})$. Otherwise, the result is $b = f(\tilde{x})$. In this way, the interval will be reduced each time. Even if this method converges better than the previously described methods, it is still for many functions slowly converging (Lang & Pucker, 2005).

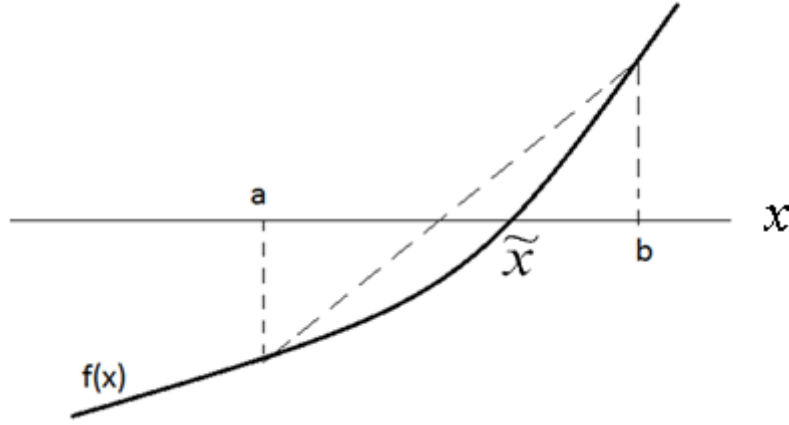


Figure (3.2): The principle of Regula Falsi for determining the root of a function.

Most often, Newton's method using the derivative of the function $f'(\tilde{x})$ converges faster than many other methods. In this method, the intersection of the tangent at the initial value \tilde{x} with x-axis gets closer to root of the function (Lang & Pucker, 2005). The recursive formula for calculating \tilde{x} is given by:

$$\tilde{x}_{i+1} = \tilde{x}_i - \frac{f(\tilde{x}_i)}{f'(\tilde{x}_i)} \quad (3-21)$$

3.1.4. Spatial resolution of SCH model

The spatial resolution of a spherical harmonic model is a function of the maximum degree used in the model. For the global modeling, the minimum wavelength represented by SCH is a function of n_{max} . The minimum wavelength w_{min} (in radians) reads (De Santis & Torta, 1997):

$$w_{min} = \frac{2\theta_0}{n_{max}} \quad (3-22)$$

The minimum spatial distance L_{min} , i.e. the sampling interval in space domain or simply the resolution in this case is

$$L_{min} = \frac{w_{min}R}{2} \quad (3-23)$$

In the case of SCH, the system is modified. When $m=0$, the root $n_k(m)$ is used to calculate the maximum degree K to get the required spatial resolution. Inserting (3-22) in (3-23) produces (Haines, 1988):

$$K = \frac{\theta_0}{90^\circ} \left(\frac{2\pi}{w_{min}} + 0.5 \right) - 0.5 \quad (3-24)$$

The spatial resolution of the SCH model is given as:

$$L_{\min} = \frac{2\theta_0 R}{K} \quad (3-25)$$

In comparison with global gravity models, the SCH model can have the same spatial resolution if a proper number of coefficients are chosen. The required number of coefficients in the SCH model reads (De Santis & Torta, 1997):

$$N_{SCH} \approx \frac{S_{cap}}{S_{Earth}} N_{SH} = \sin^2\left(\frac{\theta_0}{2}\right) N_{SH} \quad (3-26)$$

Here, N_{SH} is the number of spherical harmonic coefficients ($\bar{C}_{nm}, \bar{S}_{nm}$) that represent the Global model $N_{SH} = (n_{\max} + 1)^2$. N_{SCH} is the number of SCH coefficients (C'_{nm}, S'_{nm}). S_{Earth} is the spherical surface area of the Earth ($S_{Earth} = 4\pi R^2$). S_{cap} is the spherical surface area of the cap ($S_{cap} = 2\pi R^2 (1 - \cos \theta_0)$). Then maximum degree K to get a SCH model with same resolution of the global model reads:

$$K = \sqrt{N_{SCH}} - 1 \quad (3-27)$$

3.1.5. Derivatives of the Potential in SCH

Similar to the representation of ordinary SH, the gravitational acceleration is the gradient of the gravitational potential ($\bar{g}' = grad V$). To formulate the gravity in terms of SCH, we define a 3D-cartesian coordinate system (cap_e-frame), see fig (3.1). The origin of the system is the center of the mass of the Earth. The Z-axis coincides with the line passing the zenith from the center of the mass of the Earth and the cap's pole, the X-axis is defined in the direction of the meridian of the cap's pole and finally the Y-axis is perpendicular to the XZ-plane. The gravity vector in terms of the potential then reads (Hofmann-Wellenhof & Moritz, 2005):

$$\bar{g}'_{cap} = \left[\frac{\partial V}{\partial X} \quad \frac{\partial V}{\partial Y} \quad \frac{\partial V}{\partial Z} \right]_{cap_e-frame} \quad (3-28)$$

In spherical cap coordinates, equation (3-28) for the gravity vector related to the cap local spherical Local Geodetic Vertical (cap_LGV) following the transformation formulas in chapter (5.2.1) reads:

$$\bar{g}'_{cap} = \left[\frac{\partial V}{r \partial \theta} \quad \frac{\partial V}{r \sin \theta \partial \alpha} \quad \frac{\partial V}{\partial r} \right]_{cap_LGV} \quad (3-29)$$

The derivatives of the gravitational potential V in equation (3-29) are (Korte, 1999):

$$\frac{\partial V}{\partial r} = -\frac{GM}{r^2} \sum_{k=0}^K \left(\frac{R}{r}\right)^{n_k(m)+1} (n_k(m)+1) \sum_{m=0}^k (\bar{C}'_{n,m} \cos(m\alpha) + \bar{S}'_{n,m} \sin(m\alpha)) \bar{P}_{nk,m}(\cos \theta) \quad (3-30a)$$

$$\frac{\partial V}{\partial \alpha} = \frac{GM}{r} \sum_{k=0}^K \left(\frac{R}{r}\right)^{n_k(m)} \sum_{m=0}^k m (\bar{S}'_{k,m} \cos(m\alpha) - \bar{C}'_{k,m} \sin(m\alpha)) \bar{P}_{nk,m}(\cos \theta) \quad (3-30b)$$

$$\frac{\partial V}{\partial \theta} = \frac{GM}{r} \sum_{k=0}^K \left(\frac{R}{r}\right)^{n_k(m)} \sum_{m=0}^k (\bar{C}'_{n,m} \cos(m\alpha) + \bar{S}'_{n,m} \sin(m\alpha)) \frac{\partial \bar{P}_{nk,m}}{\partial \phi} \quad (3-30c)$$

The magnitude of the gravity acceleration reads:

$$g = |\bar{\mathbf{g}}| \quad (3-31)$$

To calculate the quasigeoid (ξ) and the geoid height (N), the disturbing potential at the point P must also be calculated ($T=W-U$ or $T=V-V'$). The gravitational potential V is calculated using equation (3-11). The normal gravitational potential V' is calculated through the reference ellipsoid coefficients. The quasigeoid and geoid height respectively read (Torge, 2001):

$$\xi = \frac{T}{\gamma_Q} = \frac{V_{SCH} - V_{normal}}{\gamma_Q} \quad (3-32a)$$

$$N = \frac{T}{\gamma_Q} + \frac{\bar{g} - \bar{\gamma}}{\bar{\gamma}} H_p \quad (3-32b)$$

The deflections of the vertical can be calculated in the cap coordinate system with spherical approximations in two components: the direction of the cap pole (η'), and the direction of the azimuth (ζ'). The quantities η' and ζ' are (De Santis & Torta, 1997):

$$\eta' = -\frac{1}{\gamma_Q r \sin \theta} \frac{\partial T}{\partial \alpha} \quad (3-33)$$

$$\zeta' = -\frac{1}{\gamma_Q r} \frac{\partial T}{\partial \theta} \quad (3-34)$$

The deflections of the vertical explained in equations (3-33) and (3-34) are with spherical approximation in the spherical cap system. The relationship to the ellipsoidal deflections of the vertical η and ζ are explained in chapter (5.2.3) in detail.

3.2. Adjusted Spherical Cap Harmonics

As previously discussed, the SCH use the Legendre functions of real degrees $n(k)$ and integer order m . The calculations of these functions and their derivatives are time consuming processes due the iterative and approximate algorithms implemented (Schneid, 2006). In addition, the roots of the Legendre functions $n(k)$ must be calculated according the conditions in equations (3-9a) and (3-9b).

To avoid the iterative and approximate methods, a modified approach of SCH was introduced by De Santis (1992), referred previously as ASCH. This approach uses the well-known integer

order and degree Legendre functions. The principle enlarges the cap area in figure (3.1) to a hemisphere using equations (3-35a) to (3-35d), where the pole of the hemisphere is also the pole of the cap itself (Franceschi & De Santis, 1994).

$$s = \frac{0.5\pi}{\theta_0} \quad (3-35a)$$

$$\mathcal{G} = s \theta \quad (3-35b)$$

$$\alpha' = \alpha \quad (3-35c)$$

$$r' = r \quad (3-35d)$$

According to the ASCH definition (3-35), equation (3-5) is modified, resulting in the formula in equation (3-36). The new formula is similar to the conventional SH model, but there is now no need to calculate the Legendre functions with real degree and integer order:

$$V(r, \alpha, \mathcal{G}) = \frac{GM}{r} \sum_{k=0}^{k_{\max}} \left(\frac{R}{r}\right)^{n(k)} \sum_{m=0}^k (C'_{km} \cos m\alpha + S'_{km} \sin m\alpha) \bar{P}_{km}(\cos \mathcal{G}) \quad (3-36)$$

3.2.1. Derivation of the ASCH

Equation (3-36) is similar to equation (3-2). The only difference is that the angle $\mathcal{G} = s\theta$ contains the scaling factor s . Therefore it is only needed to proof, that the part of \mathcal{G} is harmonic by applying it in the Laplace equation. The most common form for the part of θ in Laplace's equation is (Hofmann-Wellenhof & Moritz, 2005):

$$\frac{1}{\sin \theta} \frac{d}{d\theta} \left(\sin \theta \frac{dP}{d\theta} \right) + \left[n(n+1) - \frac{m^2}{\sin^2 \theta} \right] P = 0 \quad (3-37)$$

Here, P is the solution of equation (3-37), the Legendre function of degree n and order m ($P = P_{nm}(\theta)$). To avoid the complication of transforming $\sin \theta$ to $\sin \mathcal{G}$, it is assumed that $\sin \theta = \theta$. This assumption is valid as $\theta_0 < 20^\circ$ (De Santis, 1992). Equation (3-37) then reads:

$$\frac{1}{\theta} \frac{d}{d\theta} \left(\theta \frac{dP}{d\theta} \right) + \left[n(n+1) - \frac{m^2}{\theta^2} \right] P = 0 \quad (3-38a)$$

This can simply be rewritten as:

$$\frac{d^2 P}{d\theta^2} + \frac{1}{\theta} \frac{dP}{d\theta} + \left[n(n+1) - \frac{m^2}{\theta^2} \right] P = 0 \quad (3-38b)$$

As $\mathcal{G} = s \cdot \theta$ the following relationships are valid:

$$\frac{dP(\theta)}{d\theta} = s \frac{dP(\mathcal{G})}{d\mathcal{G}} \quad (3-39a)$$

$$\frac{dP^2(\theta)}{d\theta^2} = s \frac{dP^2(\vartheta)}{d\vartheta^2} \quad (3-39b)$$

$$\frac{d\vartheta}{d\theta} = s \quad (3-39c)$$

Substituting (3-39) in (3-38b) results in:

$$\frac{d^2P}{d\vartheta^2} + \frac{1}{\vartheta} \frac{dP}{d\vartheta} + \left[\frac{n(n+1)}{s^2} - \frac{m^2}{\vartheta^2} \right] P = 0 \quad (3-40)$$

To transform equation (3-40) to a similar form of equation (3-38), one sets

$$\frac{n(n+1)}{s^2} = k(k+1) \quad (3-41)$$

Here, the result is:

$$\frac{d^2P}{d\vartheta^2} + \frac{1}{\vartheta} \frac{dP}{d\vartheta} + \left[k(k+1) - \frac{m^2}{\vartheta^2} \right] P = 0 \quad (3-42)$$

The Legendre function of integer degree k and order m is a solution of equation (3-42) (De Santis, 1992). In equation (3-40), n is a real number. It can be calculated as function of k ($n=n(k)$). Using equation (3-41), $n(k)$ reads:

$$n(k) = \sqrt{s^2 k(k+1) + 0.25} - 0.5 \quad (3-43)$$

In equation (3-43), s is the scale factor computed from equation (3-35a). k is the degree parameter in the ASCH model. There is an approximate formula of equation (3-43) that may be used for low degree and order ASCH models; following De Santis et al., (1997), reading:

$$n(k) = s(k + 0.5) \quad (3-44)$$

The ASCH in equation (3-36) have the following advantages compared to the normal SCH in equation (3-2): First, the well-known Legendre function with its recursive formulas is used. Second, there is no need to search for the roots $n(k)$ of Legendre functions and their derivatives according to the conditions in equations (3-9a) and (3-9b), which is time consuming (De Santis, 1992). The conditions in equations (3-9a) and (3-9b) are no longer required to find the roots of Legendre functions.

3.3. Relationship between SCH and SH

Different methods have been developed and proposed in the past to transform the spherical harmonic coefficients of global potential models of type (2-33) to the local SCH of type (3-2). When the SH and SCH have the same pole, only a transformation of the Legendre function with integer degree and order to the Legendre function with real degree and integer order is required, as shown in equation (3-45) (De Santis et al., 1999). This leads to:

$$P_{nm}(\theta) = \sum_{k=m}^{\infty} A_k^{n,m} P_{n(k),m}(\theta) \quad (3-45)$$

The coefficients $A_k^{n,m}$ are then the parameters for the transformation from the global to the cap system. These parameters can be calculated on a grid of points over the cap area. In this case, the local SCH (S'_{nm}, C'_{nm}) can be directly calculated from the coefficients of the global SH (S_{nm}, C_{nm}) with the transformation parameters $A_k^{n,m}$ using equation (3-46).

$$\begin{bmatrix} C'_{nm} \\ S'_{nm} \end{bmatrix} = \sum_{n=m}^{\infty} A_k^{m,n} \begin{bmatrix} C_{nm} \\ S_{nm} \end{bmatrix} \quad (3-46)$$

In the general case, the transformation of SH coefficients to SCH coefficients requires consideration of different poles (De Santis et al., 1996). Generally, a SH function in terms of SH in a coordinate system (ϕ, λ) is a linear combination of another SH in another coordinate system (θ, α) . The transformation equation of the coefficients from global SH to local SCH reads:

$$P_{n,m}(\phi) \begin{Bmatrix} \cos m\lambda \\ \sin m\lambda \end{Bmatrix} = \sum_{\mu=0}^n \left[\begin{Bmatrix} a_{n,\mu}^{\mu} \\ c_{n,\mu}^{\mu} \end{Bmatrix} \cos m\alpha + \begin{Bmatrix} b_{n,\mu}^{\mu} \\ d_{n,\mu}^{\mu} \end{Bmatrix} \cos m\alpha \right] P_{n(k),m}(\theta) \quad (3-47)$$

In equation (3-47), a , b , c and d are the transformation parameters, which can be calculated using a grid of points distributed over the entire cap area. It is worth noting that the transformation parameters can be separately calculated for each degree n . using these parameters. The SCH parameters are given by:

$$C'_{nm} = \sum_{\mu=0}^n (a_{n,\mu}^m C_{n\mu} + c_{n,\mu}^m S_{n\mu}) \quad (3-48a)$$

$$S'_{nm} = \sum_{\mu=0}^n (b_{n,\mu}^m C_{n\mu} + d_{n,\mu}^m S_{n\mu}) \quad (3-48b)$$

3.4. Other modifications of SCH

3.4.1. Translated-Origin Spherical Cap Harmonics (TOSCH)

De Santis (1991) introduced the concept of TOSCH, which is generally applied by moving the origin of the cap coordinate system in the direction of the cap pole (see figure3.3). This enables a smaller minimum wavelength compared to the conventional SCH model (De Santis, 1991).

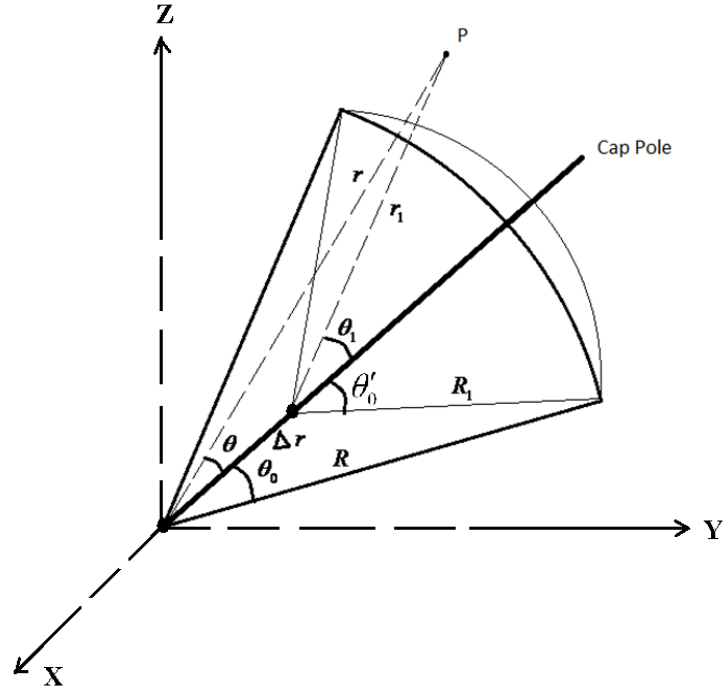


Figure (3.3): The shift of the origin in the TOSCH.

With this new definition of the system origin, a point P with spherical coordinates (r, α, θ) will have new coordinates $(r_1, \alpha_1, \theta_1)$ depending on the origin shift Δr . The new spherical coordinates are:

$$r_1 = \sqrt{r^2 + \Delta r^2 - 2r\Delta r \cos \theta} \quad (3-49a)$$

$$\alpha_1 = \alpha \quad (3-49b)$$

$$\theta_1 = \sin^{-1} \left(\frac{r \sin \theta}{r_1} \right) \quad (3-49c)$$

By substituting $\theta = \theta_0$ and $r = R$ in equation (3-49a), the radius of the cap boundary in the new system R_1 is derived:

$$R_1 = \sqrt{R^2 + \Delta r^2 - 2R\Delta r \cos \theta_0} \quad (3-50)$$

According to the new system, the opening angle for the new cap reads:

$$\theta'_0 = \sin^{-1} \left(\frac{R \sin \theta_0}{R_1} \right) \quad (3-51)$$

The potential in equation (3-36) in the new system reads:

$$V(r_1, \alpha_1, \theta_1) = \frac{GM}{r} \sum_{k=0}^{k \max} \left(\frac{R_1}{r_1} \right)^{n(k)1} \sum_{m=0}^k (C'_{km} \cos m\alpha_1 + S'_{km} \sin m\alpha_1) \bar{P}_{n(k),m}(\cos \theta_1) \quad (3-52)$$

To find the minimum wavelength represented at the original sphere surface, the distance at the pole from the sphere surface to the new origin R_S is required. R_S reads:

$$R_S = \sqrt{R^2 + \Delta r^2 - 2R\Delta r} \quad (3-53)$$

The minimum spatial resolution reads:

$$L_{\min} = \frac{2\pi R_S}{n_{k1}} \quad (3-54)$$

Where, n_{k1} reads:

$$n_{k1} = \frac{90^\circ}{\theta'_0} (k + 0.5) - 0.5 \quad (3-55)$$

By equation (3-54), it is clear, that the spatial resolution of the model is enhanced by the implementation of the TOSCH. This means that a small degree and order of the model can be applied (De Santis, 1991). It is still difficult, however, to determine the optimal translation of origin needed to achieve the required accuracy. Additionally, the physical interpretation of the potential and related quantities such as the gravity and deflections of the vertical are not clear, since the typical definition of the potential and its related quantities are commonly referred to the origin of the Earth. E.g. the first derivative of the gravitational potential V should be the radial gravity component g_r in the direction of the Earth centre not the translated center as it is in the case of TOSCH.

3.4.2. Revised Spherical Cap Harmonic (R-SCH)

Thebault et al. (2004) proposed a new modification of the SCH model to enable the upward continuation of the geomagnetic field and established a relationship to the global SH, referred to previously as R-SCH. The principle is to add more boundary conditions depending on a cone bounded radially between the surface of the Earth (the cap area) and another surface suitable for satellite data (Thebault et al., 2004). The general form of the R-SCH for modeling the geomagnetic field reads:

$$V(r, \alpha, \theta) = R \sum_{k=0}^{k \max} \left(\frac{R}{r} \right)^{n(k)+1} \sum_{m=0}^k (C'_{km} \cos m\alpha + S'_{km} \sin m\alpha) \bar{P}_{n(k),m}(\theta) \quad (3-56)$$

$$+ R \sum_{p=0}^{k \max} R_p(r) \sum_{m=0}^p (A_{pm} \cos m\alpha + B_{pm} \sin m\alpha) K_{pm}(\theta)$$

In equation (3-56), the function $R_p(r)$ is a radial function representing the radial change of the magnetic field in the cone. The functions $K_{pm}(\theta)$ are basis functions known as Mehler functions that contain only one set of Legendre basis functions. P is an integer index. The functions $R_p(r)$ and $K_{pm}(\theta)$ are completely derived and proved Thebault and Pique (2008).

The R-SCH have been widely applied in geomagnetic field research. Unlike SCH, R-SCH includes additional functions to represent the radial change of the geomagnetic field by applying flux correction (Thebault et al., 2006). In addition to the doubled number of unknowns in equation (3-56), the R-SCH converge very slowly compared to SCH. The R-SCH also do not fit different types of data in a solution (Thebault & Pique, 2008). For these reasons, the R-SCH are not commonly applied for gravity potential and the gravity modeling in an integrated solution.

3.5. Other carrier functions for local potential modeling

3.5.1. Spherical Radial Basis Functions (SRBF)

The previously mentioned SRBF are radial symmetric functions, which are localizing in space. The radial basis functions support modeling of the potential in the local or global domain (Jekeli, 2004). A sphere σ_R with radius R is defined so that the sphere is completely inside the topographic masses (Bjerhammar sphere). If two points i and j are considered, then the SRBF of location j evaluated at i reads (Wittwer, 2009):

$$\Psi_j(i, j) = \sum_{l=0}^{\infty} \psi_l \left(\frac{R}{r_i} \right)^{l+1} P_l(\theta_{ij}) \quad (3-57)$$

In equation (3-57), $P_l(\theta_{ij})$ is the Legendre polynomial of degree l . θ_{ij} is the angular spherical distance between points i and j . ψ_l are the Legendre coefficients of the basis function. Different types of SRBF are used for gravity field modeling, depending on the choice of ψ_l , which generate different forms. Selected Legendre coefficients are introduced in table (3.1), (Klees et al., 2008).

Table (3.1) : Examples of Legendre coefficients .

Coefficient name	Coefficient formula
Point mass kernel	$\psi_l = \frac{4\pi R}{2l+1} \left(\frac{r_j}{R} \right)^l$
Poisson wavelet of order m	$\psi_l = l^m \left(\frac{r_j}{R} \right)^l$
Dirac approach of Bjerhammar	$\psi_l = \begin{cases} 4\pi R^3 & l \geq 2 \\ l-1 & l = 0,1 \\ 0 & \end{cases}$
Poisson kernel	$\psi_l = \left(\frac{r_j}{R} \right)^l$

The representation of a harmonic function like the disturbing potential T of point P using SRBF reads (Schmidt et al., 2007):

$$T_p = \frac{GM}{a} \sum_{j=1}^N \alpha_j \Psi_j(P, j) \quad (3-58)$$

In equation (3-58), α_j are the SRBF coefficients that have to be calculated to model the disturbing potential using a grid of observations.

3.5.2. Spherical Harmonic Splines

The Spherical Harmonic Splines are essentially constructed by spherical basis functions. Their basic advantage over the SH is their ability to represent the geoid or potential in local or global areas (Jekeli, 2004). The potential can be modeled using a grid of points on the latitude and longitude lines. The employed Legendre coefficient in equation (3-59) reads (Wittwer, 2009):

$$\psi_l = \sigma_l^2 \quad (3-59)$$

σ_l^2 are the SH degree variances. Different methods are used to calculate the degree variances, and they can be directly calculated using existing gravity models. Torge (2001) has given the Kaula's rule to estimate of degree variance. According to the Kaula's rule σ_l^2 reads:

$$\sigma_l^2 = (2l + 1) \frac{10^{10}}{l^4} \quad (3-60)$$

Tscherning and Rapp (1974) introduced a covariance function, where σ_l^2 reads (Torge, 2001):

$$\sigma_l^2 = \left(\frac{R}{l-1} \right)^2 \begin{cases} 0 & l = 0,1 \\ 754 & l = 2 \\ \frac{A(l-1)}{(l-2)(l+B)} s^{l+2} & l \geq 3 \end{cases} \quad (3-61)$$

In equation (3-61), $A=42528$, $B=24$ and $s=0.999617$.

To find the unknowns α_j (SRBF or Spline coefficients), a grid of points with known quantities as functions of the latitude and longitude must be interpolated. These quantities can be gravity anomalies, gravity disturbances or height anomalies. The grid of points can be used as observation equations to calculate the unknowns α_j of each grid point. Here, each point is to be modeled using the other grid points (Freedden, 1984).

Many kinds of Harmonic Splines have been introduced. Jekeli (2004) introduced several forms and demonstrated their application to the disturbing potential. Another modified spine was used to calculate the geoid height using a grid of gravity anomalies; see Kling et al. (1987) for details.

The use of splines and SRBF has advantages over the SH. First, both support local and global modeling of the gravity potential. Secondly, the calculations are only affected by local errors.

On the other hand, SH models are more easily employed. Furthermore, the calculation of spherical harmonic coefficients is less complicated using integrals and least squares. An important disadvantage in using splines or SRBF is that each grid point j has an unknown α_j , resulting in no redundancy of data for quality control. Finally, the reference points in each model must be in a grid, leading to additional interpolation errors (Jekeli, 2004).

4. Transformation of global SH gravity models to local ASCH

The application of global based space methods for gravity field determination leads to global SH models at first instance. At present, there are several global gravity models freely available on the internet which can be used by the public. The newer and recent models are represented with increasingly high degrees and orders like EIGEN06C with maximum degree and order of 1420 and the space based terrestrially combined EGM2008 model with maximum degree and order of 2190. For several reasons, it is advantageous to represent the regional or local gravity field with a smaller number of parameters and to develop a parameter transformation from the global model to a local ASCH model. An example is the frequent use of a global model for a specific area of interest. The transformation of the global SH model to the local ASCH allows the modelling of regional gravity potential with fewer coefficients and is less demanding in terms of computer memory requirements and the time consumption for computation and storage.

In this chapter, the local ASCH are introduced for the regional gravitational potential representation related to a local pole and a local spherical coordinate system in a cap. In this way, the global gravity models can fully be exploited and mapped to a regional ASCH model, respectively, in the context of the computation of regional geoid models with equivalent resolution.

The adjustment principle is also presented in this chapter. The convergence of unknowns (ASCH coefficients) with respect to the maximum degree and order of the calculated ASCH model is discussed. The area size as well the behavior of the ASCH modeling at the boundaries and their effects on the accuracy are explained. The design of the observations with respect to the extension to the vertical direction is also tested. Finally, a practical application transforming the EGM2008 model to a local ASCH model for the study area of Baden-Württemberg state in Germany is presented and discussed.

4.1. Functional models

The methods of transformation of SH to SCH discussed in chapter (3.3) do not apply for transforming SH models to the ASCH models in an analytical way. The reason is that the coordinates are not only related to different poles but also scaled according to equation (3-35).

A straightforward method for transforming SH to ASCH is to set up a linear equation system for a number of positions $P(r, \vartheta, \lambda)$ with known potential values (V) by means of the global model, as given in equation (4-1):

$$V_{ASCH}(r, \vartheta, \alpha) = \frac{GM}{r} \sum_{k=0}^{k_{max}} \left(\frac{R}{r}\right)^{n(k)+1} \sum_{m=0}^k (C'_{nm} \cos m\alpha + S'_{nm} \sin m\alpha) \bar{P}_{n,m}(\cos \vartheta) = V_{Global}(r, \bar{\varphi}, \lambda) \quad (4-1)$$

The solution of the system of equations based on (4-1) is linear with respect to q coefficients (S'_{nm}, C'_{nm}) by using at least m number positions $(r, \vartheta, \lambda)_i$, $q = (k_{max} + 1)^2$. This method is derived in Jäger (2010). The extension of that approach, presented here, takes into account that both SH of type (2-33) and ASCH of type (3-36) are truncated series. This means that V in equation (2-

33) and V_{ASCH} in equation (4-1) are inconsistent. The computation of the coefficients (S'_{nm}, C'_{nm}) therefore has to be controlled and optimized at the same time. This is done by a least squares estimation of (S'_{nm}, C'_{nm}) related to (4-1) set up in the following way: A 3D grid of points is generated over the cap area, where the minimum number of required grid points is the same or more than the number of unknown parameters $(k_{\max} + 1)^2$. Figure (4.1) shows an example of grid points distributed all over a cap covering the state of Baden-Württemberg in Germany.

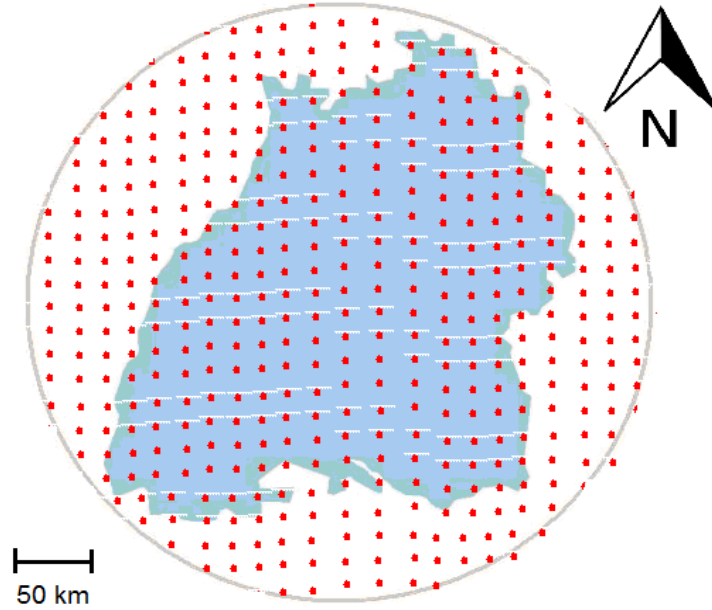


Figure (4.1): Distribution of a sample grid points over the cap area for the example of Baden-Württemberg state in Germany.

The potential value $V(r, \vartheta, \lambda)_i$ for the grid point P_i are taken from a global model V_{Global} using equation (2-33), and used as an observation in equation (4-1). The ASCH coefficients (S'_{nm}, C'_{nm}) are the unknown parameters to be estimated. The number of unknowns in a SCH model is $(k_{\max} + 1)^2$ (Schneid, 2006). The least squares solution of the over-determined problem related to (4-1) reads (Younis et al., 2011):

$$\hat{\mathbf{x}} = (\mathbf{A}^T \mathbf{C}_i^{-1} \mathbf{A})^{-1} \mathbf{A}^T \mathbf{C}_i^{-1} \mathbf{l} \quad (4-2a)$$

The design-matrix \mathbf{A} reads:

$$\mathbf{A} = \begin{bmatrix} \frac{GM}{r_1} & \frac{GM}{r_1} \frac{R}{r_1} P_{10} & \frac{GM}{r_1} \frac{R}{r_1} \cos \alpha_1 P_{11} & \frac{GM}{r_1} \frac{R}{r_1} \sin \alpha_1 P_{10} & & & \\ \frac{GM}{r_2} & \frac{GM}{r_2} \frac{R}{r_2} P_{10} & \frac{GM}{r_2} \frac{R}{r_2} \cos \alpha_2 P_{11} & \frac{GM}{r_2} \frac{R}{r_2} \sin \alpha_2 P_{10} & \dots & \dots & \\ \frac{GM}{r_3} & \frac{GM}{r_3} \frac{R}{r_3} P_{10} & \frac{GM}{r_3} \frac{R}{r_3} \cos \alpha_3 P_{11} & \frac{GM}{r_3} \frac{R}{r_3} \sin \alpha_3 P_{10} & & & \\ \vdots & \vdots & & & \ddots & & \\ \vdots & \vdots & & & & & \\ \vdots & \vdots & & & & & \frac{GM}{r_m} \left(\frac{R}{r_m} \right)^n \sin m \alpha_m P_{nn} \end{bmatrix} \quad (4-2b)$$

The vector of unknowns $\hat{\mathbf{x}}$, the vector of observations \mathbf{l} and the observations covariance matrix \mathbf{C}_l are:

$$\hat{\mathbf{x}} = [\mathbf{C}'_{00} \quad \mathbf{C}'_{10} \quad \mathbf{C}'_{11} \quad \mathbf{S}'_{11} \quad \mathbf{C}'_{20} \quad \dots \quad \mathbf{S}'_{nm}]^T \quad (4-2c)$$

$$\mathbf{l} = [V_1 \quad V_2 \quad V_3 \quad V_4 \quad \dots \quad V_m]^T \quad (4-2d)$$

$$\mathbf{C}_l = \begin{bmatrix} s_{11}^2 & s_{12} & s_{13} & s_{14} & & & s_{1m} \\ & s_{22}^2 & s_{23} & s_{24} & \dots & \dots & s_{2m} \\ & & s_{33}^2 & s_{34} & & & s_{3m} \\ & & & s_{44}^2 & \dots & \dots & s_{4m} \\ & & & & \ddots & & \vdots \\ & & & & & \ddots & \vdots \\ & & & & & & s_{mm}^2 \end{bmatrix}^T \quad (4-2e)$$

Each observation leads to a row in the so-called design matrix \mathbf{A} (4-2a), and the elements of each row are the coefficients of the unknown parameters $\hat{\mathbf{x}}$ (4-2c). The column vector \mathbf{y} are observations computed from the input V_{Global} . \mathbf{C}_l is the fully correlated covariance matrix of the observations $V(r, \vartheta, \lambda)_i$, which must be computed by applying the law of error-propagation using the covariance matrix $\mathbf{C}_{\bar{c}_{nm}, \bar{s}_{nm}}$ of the coefficients of the global model spherical harmonic model (Migliaccio et. al, 2010). Here the covariance matrix of the observations \mathbf{C}_l reads:

$$\mathbf{C}_l = \mathbf{F} \mathbf{C}_{\bar{c}_{nm}, \bar{s}_{nm}} \mathbf{F}^T \quad (4-3a)$$

Where \mathbf{F} reads:

$$\mathbf{F} = \begin{bmatrix} (a_{20})_1 & (a_{21})_1 & (a_{N \max N \max})_1 & (b_{21})_1 & (b_{22})_1 & (b_{N \max N \max})_1 \\ (a_{20})_2 & (a_{21})_2 & (a_{N \max N \max})_2 & (b_{21})_2 & (b_{22})_2 & (b_{N \max N \max})_2 \\ \vdots & \vdots & \vdots & \vdots & \vdots & \vdots \\ (a_{20})_m & (a_{21})_m & (a_{N \max N \max})_m & (b_{21})_m & (b_{22})_m & (b_{N \max N \max})_m \end{bmatrix} \quad (4-3b)$$

For an observation point i ,

$$(a_{jk})_i = \frac{GM}{r_i} \left(\frac{a}{r_i} \right)^j \cos k\lambda_i P_{jk}(\sin \bar{\phi}_i) \quad (4-3c)$$

$$(b_{jk})_i = \frac{GM}{r_i} \left(\frac{a}{r_i} \right)^j \sin k\lambda_i P_{jk}(\sin \bar{\phi}_i) \quad (4-3d)$$

The covariance matrix of the Spherical Harmonics $\mathbf{C}_{\bar{c}_{nm}, \bar{s}_{nm}}$ reads:

$$\mathbf{C}_{\bar{C}_{nm}, \bar{S}_{nm}} = \begin{bmatrix} S_{\bar{C}20}^2 & S_{\bar{C}20\bar{C}21} & S_{\bar{C}20\bar{C}NN} & S_{\bar{C}20\bar{S}20} & S_{\bar{C}20\bar{S}21} & S_{\bar{C}20\bar{S}NN} \\ & S_{\bar{C}21}^2 & S_{\bar{C}21\bar{C}NN} & S_{\bar{C}21\bar{S}20} & S_{\bar{C}21\bar{S}21} & S_{\bar{C}21\bar{S}NN} \\ & & \ddots & & & \\ & & & S_{\bar{C}NN}^2 & S_{\bar{C}NN\bar{S}20} & S_{\bar{C}NN\bar{S}21} & S_{\bar{C}NN\bar{S}NN} \\ & & & & S_{\bar{S}20}^2 & S_{\bar{S}20\bar{S}21} & S_{\bar{S}20\bar{S}NN} \\ & & & & & S_{\bar{S}21}^2 & S_{\bar{S}21\bar{S}NN} \\ & & & & & & \ddots \\ & & & & & & & S_{\bar{S}NN}^2 \end{bmatrix} \quad (4-3e)$$

In equation (4-3c) and (4-3d), GM is the gravitational constant of the global gravity model and a is the reference radius of the spherical harmonic model. λ is the longitude of the point. $\bar{\phi}$ is the spherical latitude of the point. r_i is the radial distance from the origin of the model's ellipsoid to the point. The parameters j and k are the degree and order of the spherical harmonic model.

The full covariance matrix of the Spherical Harmonics $\mathbf{C}_{\bar{C}_{nm}, \bar{S}_{nm}}$ in equation (4-3e) is not always available for public use. Some can be requested from the publisher (e.g. EIGEN05c). Furthermore, they mostly have only the diagonal elements (the variances) without the covariances. In this case, the covariances are assumed to be zero.

4.2. Result of Transforming global SH to local ASCH

To provide a better background about the usability of transformed ASCH models in local areas and to discuss the behavior of this model, different tests were applied to transform the global SH to ASCH models. In the following, the convergence of parameters related to the maximum degree and order is studied to see how the values of the ASCH coefficients would change by altering the maximum degree and order of the model. The convergence of the standard deviations is also observed.

The accuracy of the calculations is studied according to the spatial distribution of the test points in the cap area. The accuracy of the model is dependent on the distance from a point to the cap center (the angle θ). This is discussed to examine the behavior of the model in the inner area of the cap area, as well as on the cap boundaries.

4.2.1. The convergence of coefficients

Different ASCH coefficients were randomly chosen to monitor their convergence under the change of the maximum degree and order of calculations. A test area with a fixed maximum opening cap angle of 1° was chosen to apply the tests; all calculations applied over this cap area.

The calculations were applied over this cap with different maximum degree and order. These maximum degrees and order were 10, 20, 30 ... to 90. Randomly selected coefficients were also analyzed. These coefficients are $C_{0,0}$, $S_{5,5}$, $C_{30,10}$ and $C_{20,10}$. The values of the coefficients and their standard deviations related to different values of the maximum degree and order are

registered to be analyzed with respect to their convergence. The results of the calculations are shown in figure (4.2).

In general, the coefficients have shown fewer changes with higher maximum degrees and orders. The coefficient $C_{0,0}$ converges towards the value of 1 but does not actually reach this value. The reason for this is that the integral formula for calculating the SH coefficient in equation (2-23) is applied all over the whole sphere of Earth due to the orthogonality conditions of SH, while in the ASCH this is not valid, because the cap covers only a partial part of the sphere. In addition, the coefficient $C_{0,0}$ is changing as the cap and input change.

The other coefficients were consistently around the same value with only small changes. The standard deviations also had fewer changes. The coefficients consistently had smaller standard deviation, as the maximum degree and order of the calculated ASCH got higher. These were the expected results, as when the degree and order gets higher, smaller standard deviations of the coefficients should appear. The reason for this is that the errors in the observations will be distributed over more coefficients.

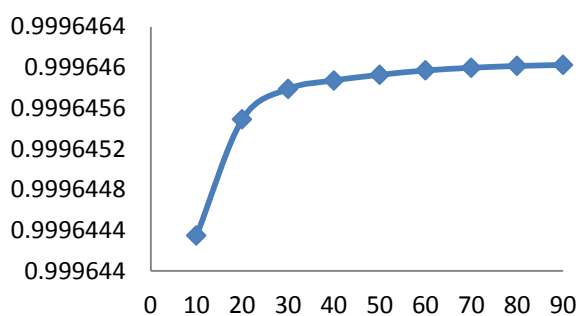
4.2.2. The boundary problem

Because the ASCH models are applied in a local area with a maximum opening angle, the behavior of ASCH on the boundary of this cap area is unknown. The reason is that the observation data applied in the adjustment according to equation (4-1) are only available inside this boundary and on the other side of the boundary there is no control in the adjustment.

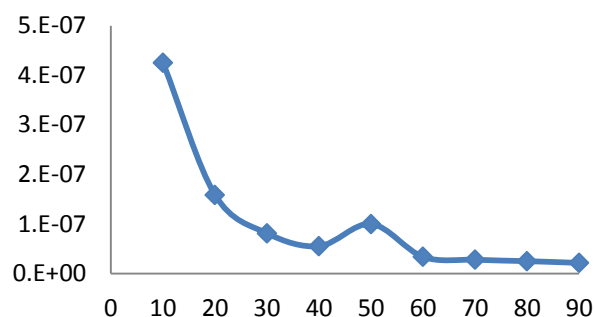
To test the behavior of ASCH on the boundary of the area of interest, data in a local cap with a maximum opening angle of 1° were predicted using EIGEN05c global model. The ASCH model was calculated over this area. To examine the effect on the boundary, the ASCH model in the test area was calculated using different maximum opening angle sizes larger than the area of interest. The calculations were applied by adding 0.1° , 0.2° , 0.3° and 0.4° to the original opening angle of the test area. Higher degrees and orders were used in the calculations to keep the same spatial resolution. The results of the different calculations in the original test area are shown in figure (4.3).

It is clear that the solution shows deteriorated residuals at the boundary of the cap. Furthermore, by an examination of the relationship between the residuals and the opening angle, it can be easily seen that the accuracy has an inverse relationship to the angle θ (see figure 4.4). By making the maximum cap size larger than the area of interest and with increasing the maximum degree and order, the accuracy within the area of interest could be enhanced. In the test, the residuals in the area of interest were getting smoother by applying solutions with a maximum cap size larger than the area of interest with 0.2° or higher. It is important always to consider the need for higher maximum degree and order in the adjustment to keep the same accuracy and resolution.

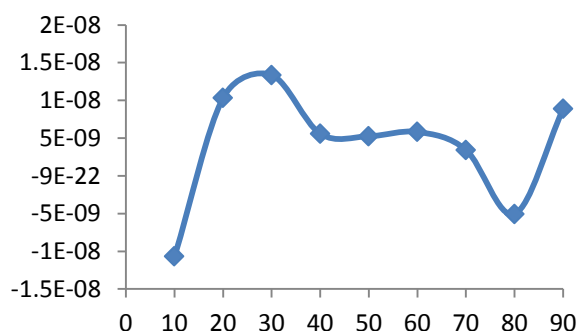
a.1) The coefficient $C_{0,0}$



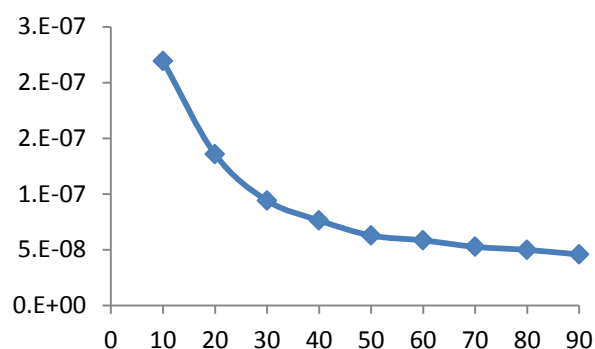
a.2) the standard deviation of $C_{0,0}$ ($s_{C_{0,0}}$)



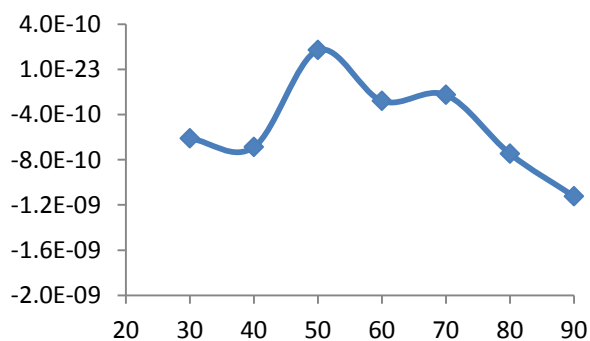
b.1) the coefficient $S_{5,5}$



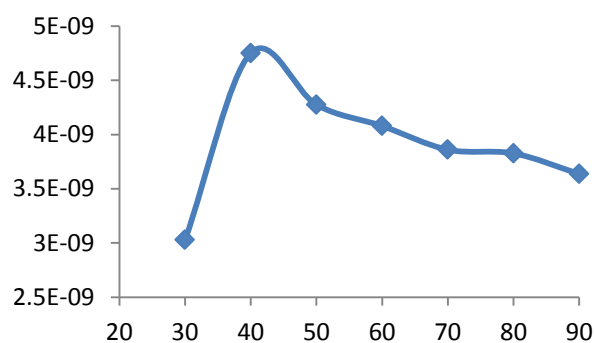
a.2) the standard deviation of $S_{5,5}$



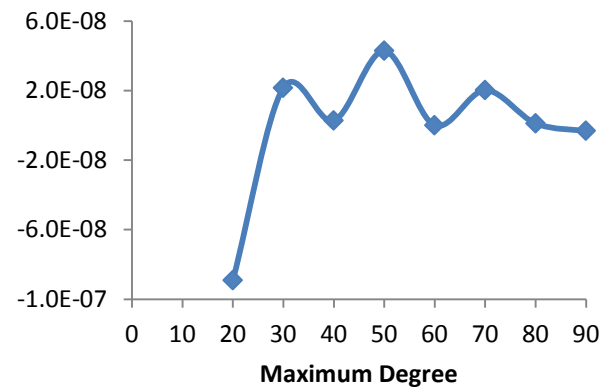
c.1) the coefficient $C_{30,10}$



a.2) the standard deviation of $C_{30,10}$



d.1) the coefficient $C_{20,10}$



a.2) the standard deviation of $C_{20,10}$

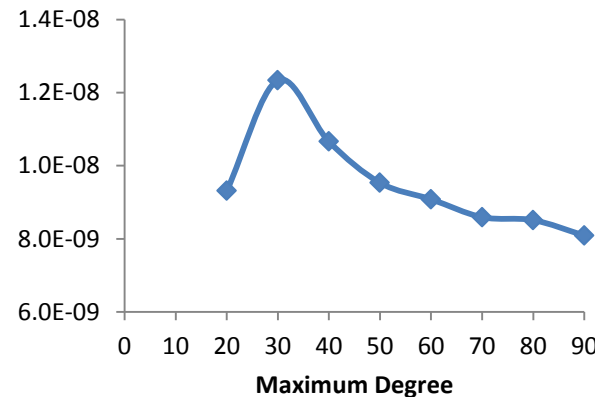


Figure (4.2): The relation between the calculated coefficients and the maximum degree and order.

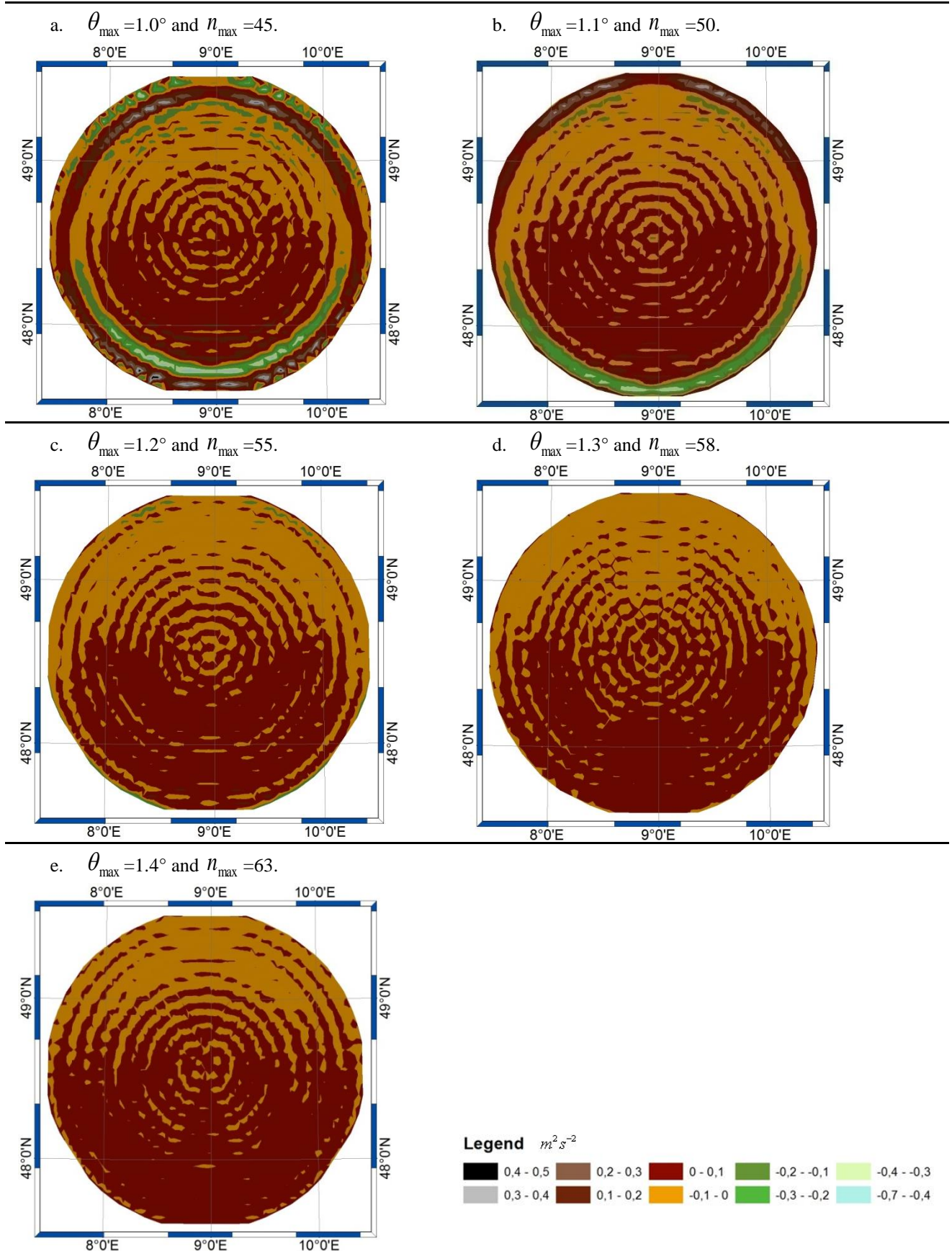
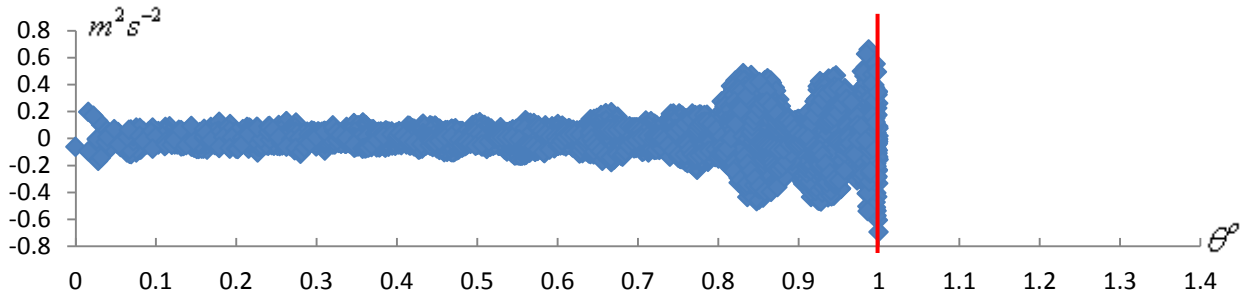
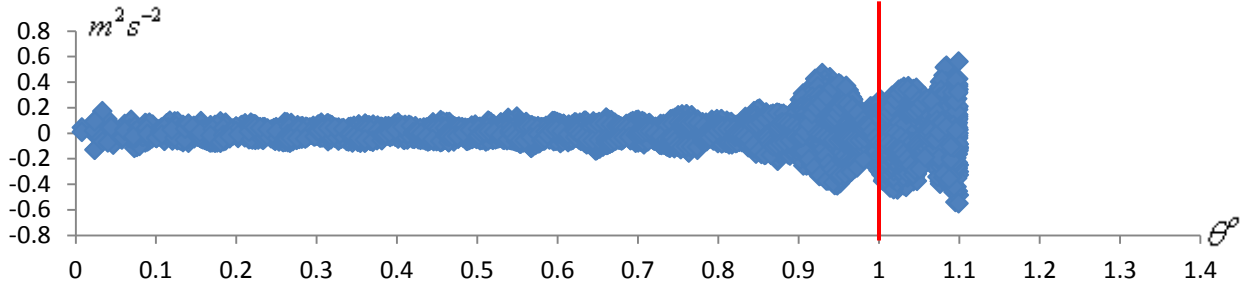


Figure (4.3): The behavior of ASCH at the boundary of the cap area with opening angle $\theta_{\max} = 1.0^\circ$, the figure shows the residuals of the potential (V) in $m^2 s^{-2}$.

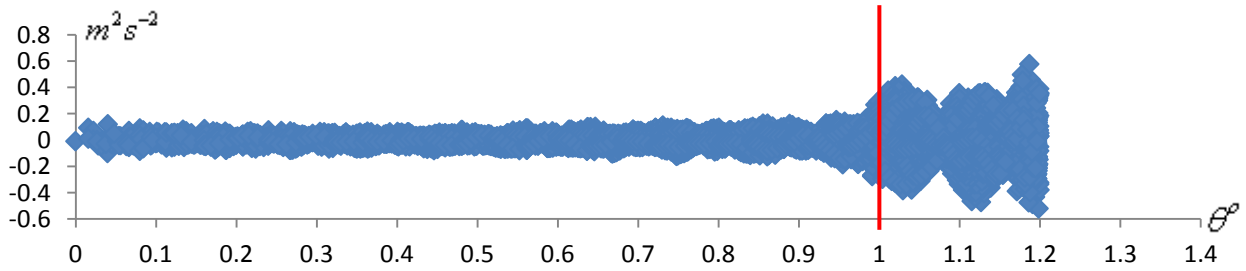
a. The relation between the residuals and the cap coordinates (θ) with $\theta_{\max} = 1.0^\circ$ and $n_{\max} = 45$.



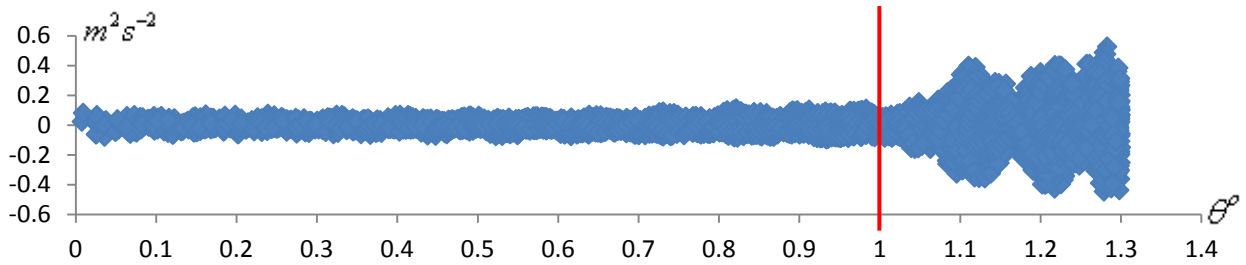
b. The relation between the residuals and the cap coordinates (θ) with $\theta_{\max} = 1.1^\circ$ and $n_{\max} = 50$.



c. The relation between the residuals and the cap coordinates (θ) with $\theta_{\max} = 1.2^\circ$ and $n_{\max} = 55$.



d. The relation between the residuals and the cap coordinates (θ) with $\theta_{\max} = 1.3^\circ$ and $n_{\max} = 58$.



e. The relation between the residuals and the cap coordinates (θ) with $\theta_{\max} = 1.4^\circ$ and $n_{\max} = 63$.

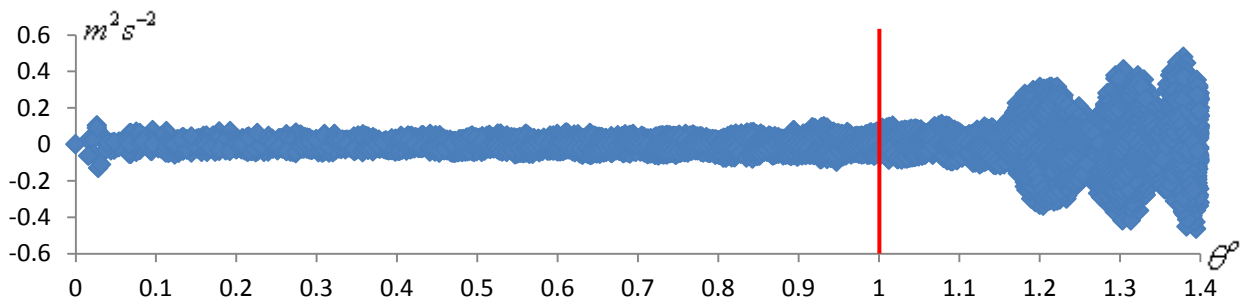


Figure (4.4): The behavior of ASCH at the boundary of the cap area, the figure shows the residuals of the potential (V) in $m^2 s^{-2}$ with respect to the angle θ .

4.2.3. Design of the observations in the vertical direction

It is necessary to find the optimal design of the observations in the vertical direction. Different tests were applied using three dimensional grids of observations. Each grid was designed in layers above the spherical surface of the cap. The observations were predicted using the EIGEN05c model. To test the results, 15000 topographic points in the state of Baden-Württemberg were used. The heights of these points lie within the range of 100m to 1500m. The original height anomaly for each point was predicted using the EIGEN05c model. These height anomalies were then compared with the height anomaly predicted using ASCH. In table (4.1), the different grids and the results are shown.

Table (4.1): Tests of observations design in the vertical direction using the height anomalies.

<i>Nr.</i>	<i>Min h</i>	<i>Max h</i>	<i>Nr. Layers</i>	<i>Max</i>	<i>RMSE</i>	<i>Min error</i>	<i>Max error</i>
		(m)	(m)	degree	(cm)	(cm)	(cm)
1	0	1000	2	45	0.31	-1.66	1.47
2	0	2000	2	45	0.55	-3.13	2.16
3	0	2000	4	45	0.55	-3.13	2.16
4	0	2000	4	60	0.35	-1.76	1.08
5	0	5000	2	45	1.35	-7.70	5.68
6	0	5000	4	45	0.53	-2.81	1.88
7	0	5000	4	60	0.40	-1.98	1.64
8	0	10000	2	45	3.62	-18.27	8.84
9	0	10000	4	45	4.61	18.75	16.40
10	0	10000	4	60	3.47	-12.96	10.33
11	0	10000	4	80	2.72	-7.52	6.87

The results in table (4.1) show that the grids of observations arranged in layers very close to the topography of the area of interest will provide the best results. The tests using maximum heights of between 1000m and 2000m above the sphere of the cap also provide good results, as they are very close to the actual topography. The grids with a maximum height of 5000m in two layers above the sphere provide worse results, but those with a maximum height of 5000m in four layers above the sphere provide good results. The reason is that the grids have layers of observations near the topography. Finally, the solution can always be enhanced in the vertical direction by adding a higher degree and order in solution of the ASCH; this is clearly demonstrated by the test results using 3D grids within the range of 0m to 10000m.

4.3. Transformation of EGM2008 to a local ASCH

A practical example of the transformation of a global SH model to a local ASCH model is to transform the EGM2008 model to a local ASCH in the state of Baden-Württemberg. The EGM2008 has a maximum degree and order of 2190, which contains 4800481 spherical harmonic coefficients. The defining elements of the EGM2008 are shown in table (4.2). For frequent application of the model in this specific area, using such a large number of coefficients will result in significant computing time and memory costs.

Table (4.2): The defining parameters of the EGM2008.

Parameter	Description	Value
<i>GM</i>	Earth's gravitational constant	$3986004.415 \times 10^8 \text{ m}^3 / \text{s}^2$
<i>a</i>	Semi-major axis of the EGM2008 reference ellipsoid	6378136.3 m
<i>n_max</i>	Maximum degree and order of the model	2190

The transformation was applied in the State of Baden-Württemberg with proper ASCH model defining parameters, chosen so that the cap area covers the whole area of interest (see table 4.3). The area size could be covered by an opening angle of 1.35° , which was rounded up to 1.5° . The radius was selected as the distance to the geocentre of the origin of the cap area using ellipsoidal height equal to zero.

Table (4.3): The defining parameters of the ASCH model in Baden-Württemberg with a cap size of 1.5° .

Parameter	Description	Value
GM	Gravitational constant of the Earth ²	$3986005 \times 10^8 \text{ m}^3 \text{ s}^{-2}$
R	Selected reference radius	6366166.378729511 m
ϕ_0	Latitude of origin	$48^\circ.6112600518$
λ_0	Longitude of origin	$9^\circ.0410298719$
<i>s</i>	Scale	$90^\circ / 1^\circ.5 = 60.0$
<i>n_max</i>	Maximum degree and order of the model	70

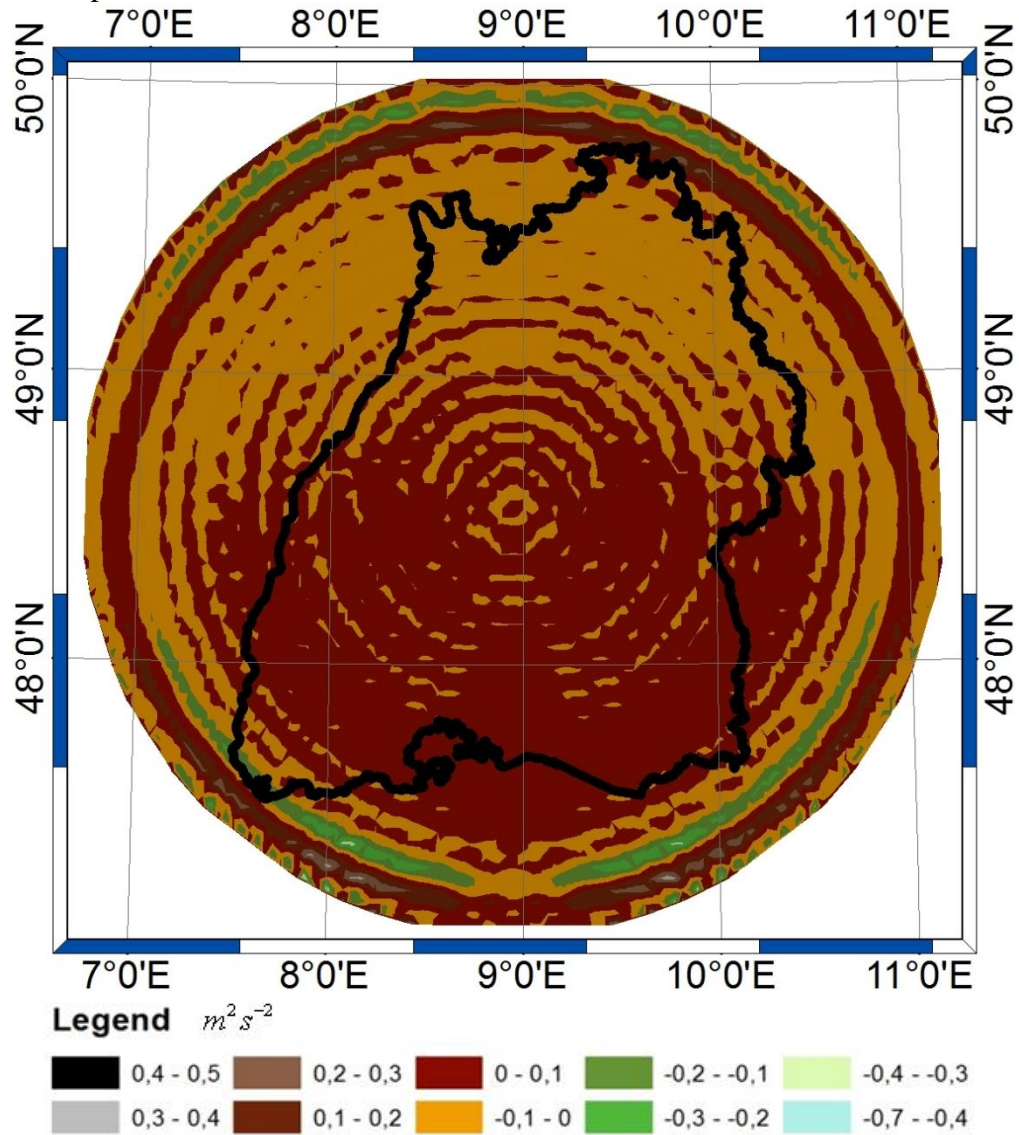
The input data from EGM2008 were calculated at ellipsoidal height levels of 0m, 1000m and 2000m. This enabled area coverage in the vertical direction, where the topography varies from between 100m and 1500m above the GRS80 ellipsoid (ellipsoidal heights). The calculations were applied with ASCH with maximum degree and order of 70 with a grid spatial resolution of 0.03° . The results representing the EGM2008 in Baden-Württemberg are shown in figure (4.5). The residuals of the calculated gravitational potential *V* in figure (4.5) are essentially larger at the boundary of the cap than of those in the inside the boundary. To achieve better results in the area of interest, the cap was oversized to an opening angle of 1.7° . To keep the spatial resolution the calculations were applied with a maximum degree and order of 80. The results of the same area are shown in figure (4.6). It is clear that at the boundary the residuals are less deteriorated as compared to those in figure (4.5).

Table (4.4): The defining parameters of the ASCH model in Baden-Württemberg with cap size of 1.7° .

Parameter	Description	Value
GM	Gravitational constant of the Earth	$3986005 \times 10^8 \text{ m}^3 \text{ s}^{-2}$
R	Selected Reference Radius	6366166.378729511 m
ϕ_0	Latitude of origin	$48^\circ.6112600518$
λ_0	Longitude of origin	$9^\circ.0410298719$
<i>s</i>	Scale	$90^\circ / 1^\circ.7 = 52.9411765$
<i>n_max</i>	Maximum degree and order of the model	80

² (GRS80).

a. The spatial distribution of the residuals



b. The relation between the residuals and the cap coordinates (θ)

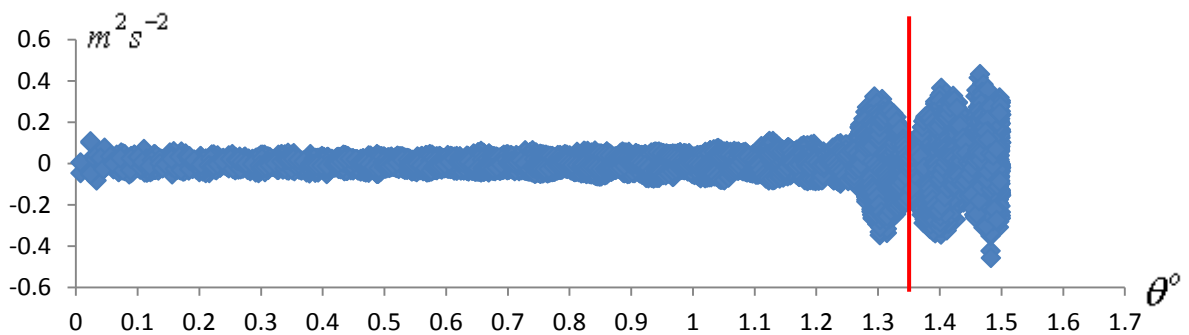
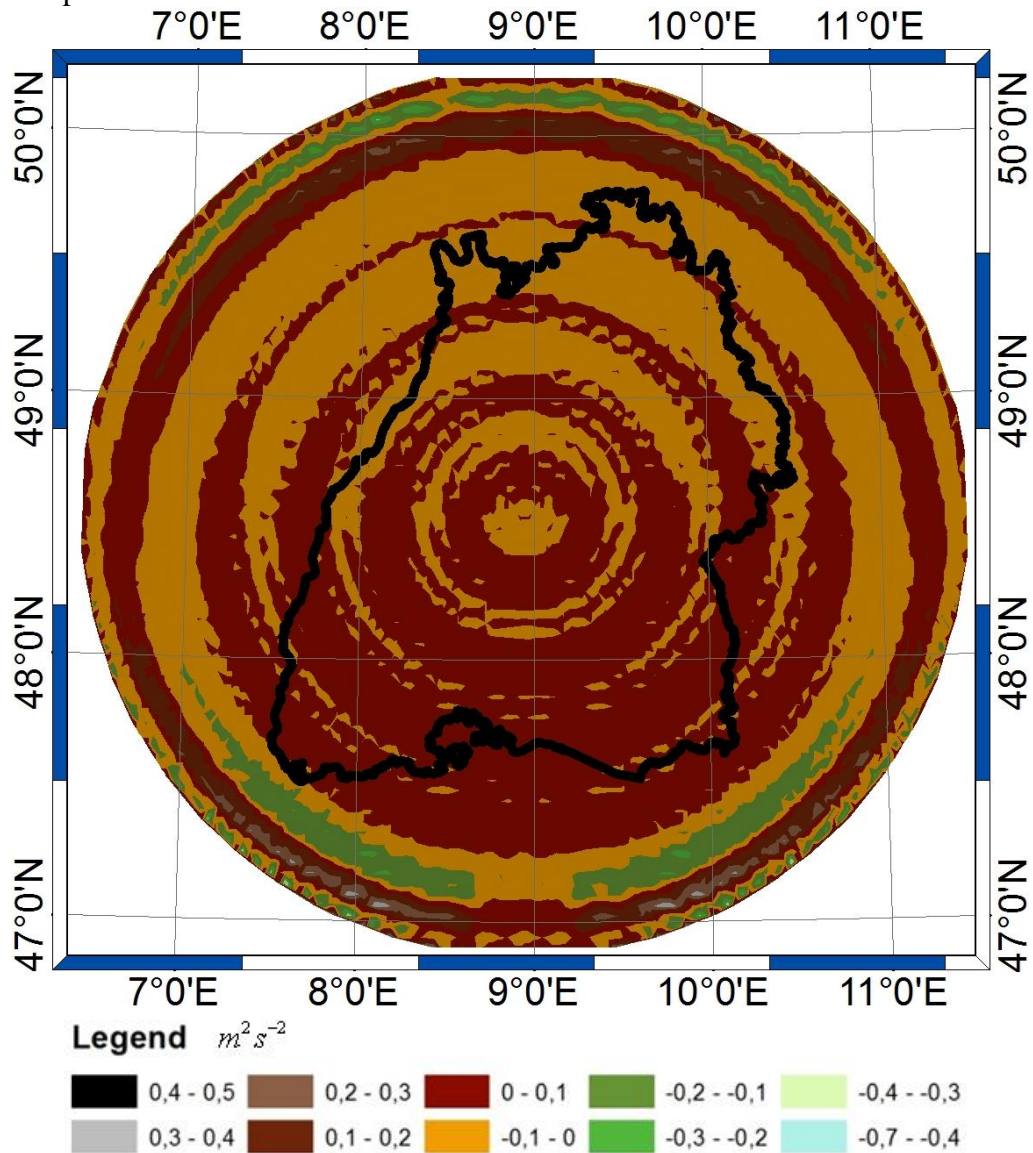


Figure (4.5): The residuals of the gravitational potential ($m^2 s^{-2}$) for the transformation of EGM2008 to a local ASCH model with cap opening angle of 1.5° .

a. the spatial distribution of the residuals



b) the relation between the residuals and the cap coordinates (θ)

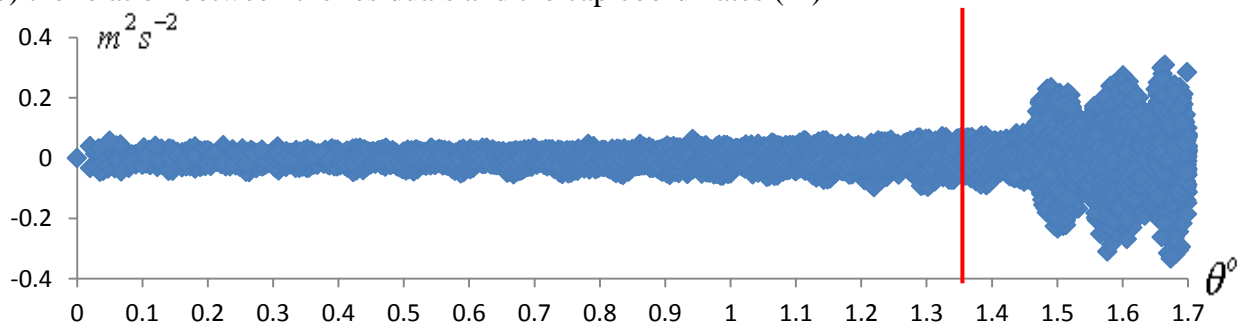


Figure (4.6): The residuals of the gravitational potential ($m^2 s^{-2}$) for the transformation of EGM2008 to a local ASCH model with cap opening angle of 1.7° .

In figure (4.6), the residuals in the area of interest were all less than $0.1 \text{ m}^2\text{s}^{-2}$ or equivalently less than 1 cm in the height anomalies. The covariance matrix of the coefficients was calculated, and the standard deviations of the ASCH-coefficients (C_{nm}, S_{nm}) are shown in figure (4.7).

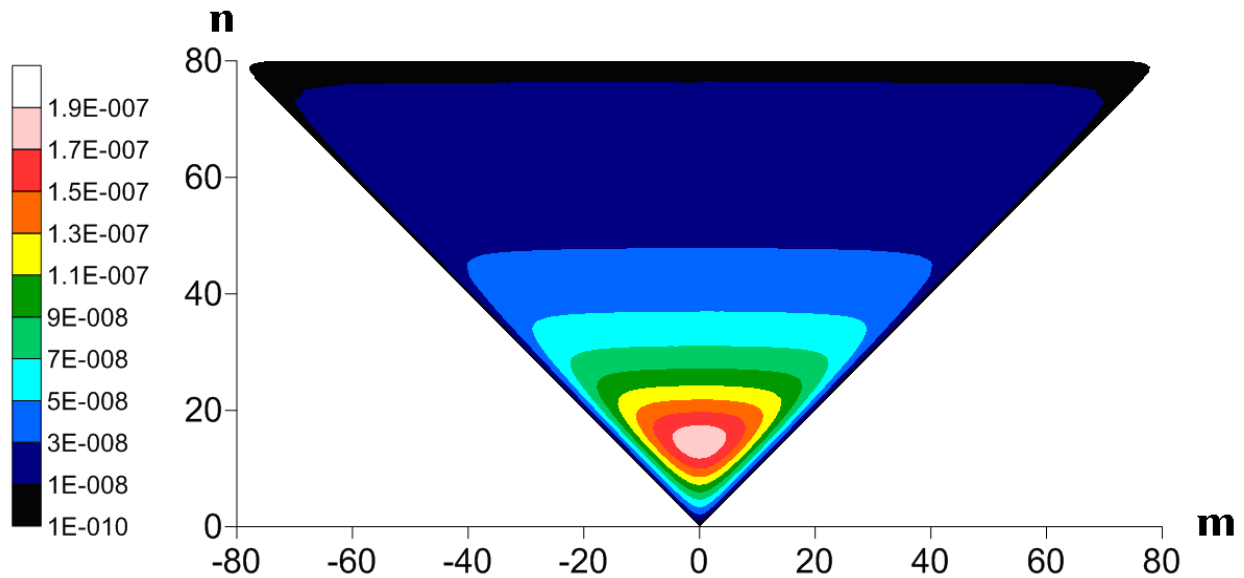


Figure (4.7): The standard deviations of the ASCH coefficients. The positive sign indicates C_{nm} and the negative sign indicates S_{nm} .

To test the reliability of the solution, 15000 topographic points distributed over the State of Baden-Württemberg (the gravity network points) were used to test the model. These points were not used in the adjustment. The points have known horizontal position (λ, ϕ) and normal heights (H^*). To calculate the spherical coordinates ($\lambda, \bar{\phi}, r$) the ellipsoidal height is needed. The ellipsoidal heights of the points were calculated by adding the height anomalies (ζ) from the official Height Reference Surface of Baden-Württemberg, which was calculated using the DFHRS-Software with 1-2cm accuracy (www.dfhbf.de). The topographic model of Baden-Württemberg above the GRS80 ellipsoid (ellipsoidal heights) is shown in figure (4.8).

In modern surveying procedures, the ellipsoidal heights (h) are directly measured by means of GNSS. For points with only normal heights (H^*), height anomalies (ζ) must always be considered; these can be calculated existing using precise geoid models or iteratively by ASCH.

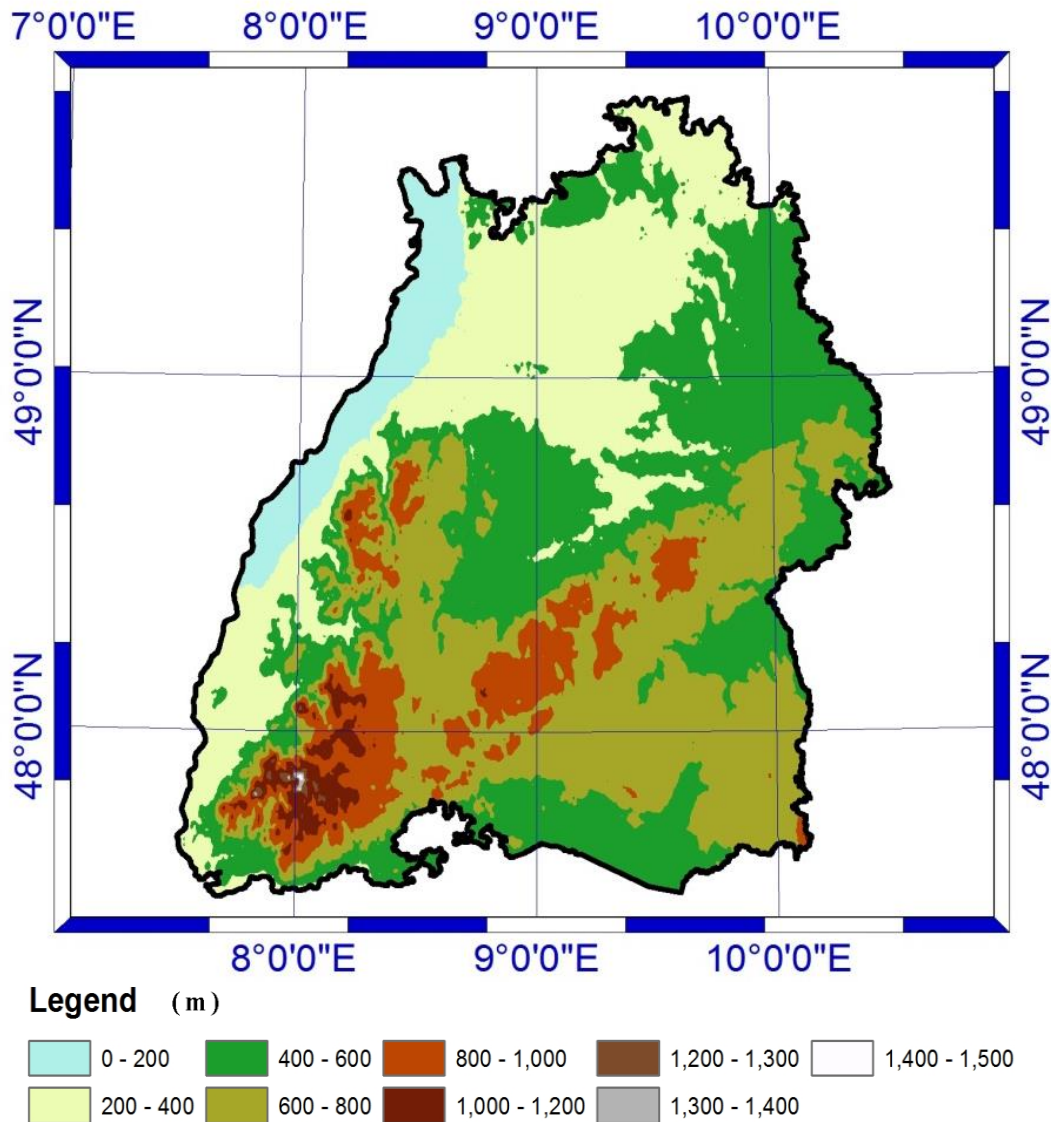


Figure (4.8): The ellipsoidal height (m) in Baden-Württemberg above the GRS80 ellipsoid in meters.

The calculated height anomalies of the Quasigeoid over Baden-Württemberg using the developed integrated ASCH approach are shown in figure (4.9). The differences between the height anomalies calculated by the EGM2008 and the ASCH model in Baden-Württemberg are shown in figure (4.10). In all 15000 points, the maximum difference was less than 5mm, indicating that the local ASCH model could accurately model the EGM2008 in the local area without effect of the heights or positions. A direct advantage of using ASCH modeling is that during the calculations of the 15000 test points, the EGM2008 model requires 4800481SHcoefficients, while the ASCH model needs only 6561 coefficients. The large difference in the number of coefficients leads to significant differences in required computer memory and calculation times. For example, calculating the 15000 points using the original EGM2008 and a single CPU needed more than one hour of time; in contrast, less than 5 minutes of calculation time was needed for the ASCH model with a maximum degree and order of 80.

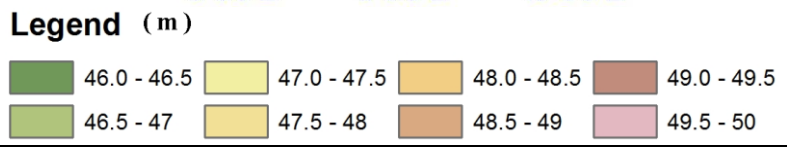
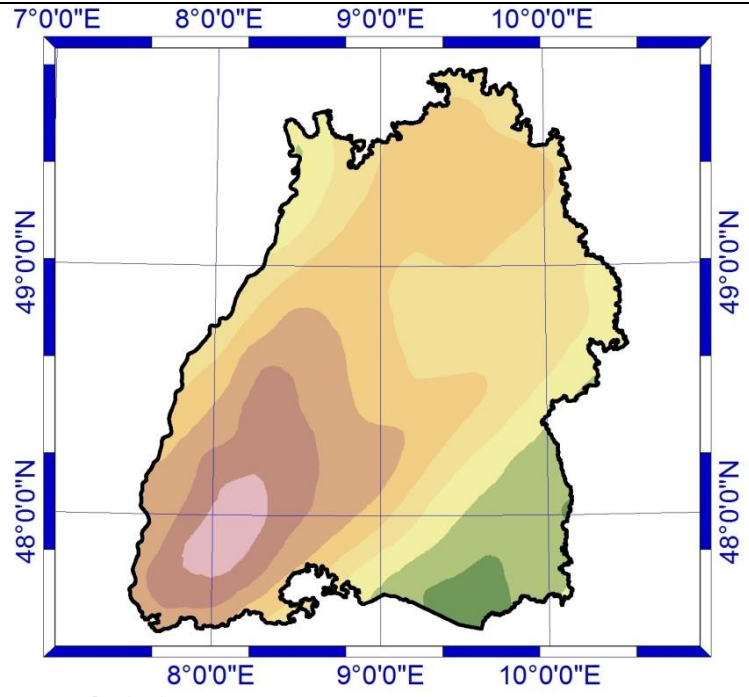


Figure (4.9): The height anomalies heights in Baden-Württemberg calculated by means of ASCH model with maximum degree and order of 80 in meters.

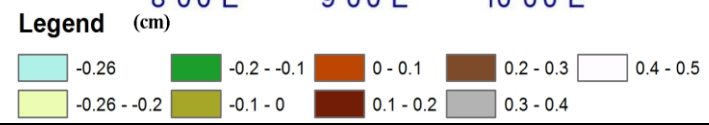
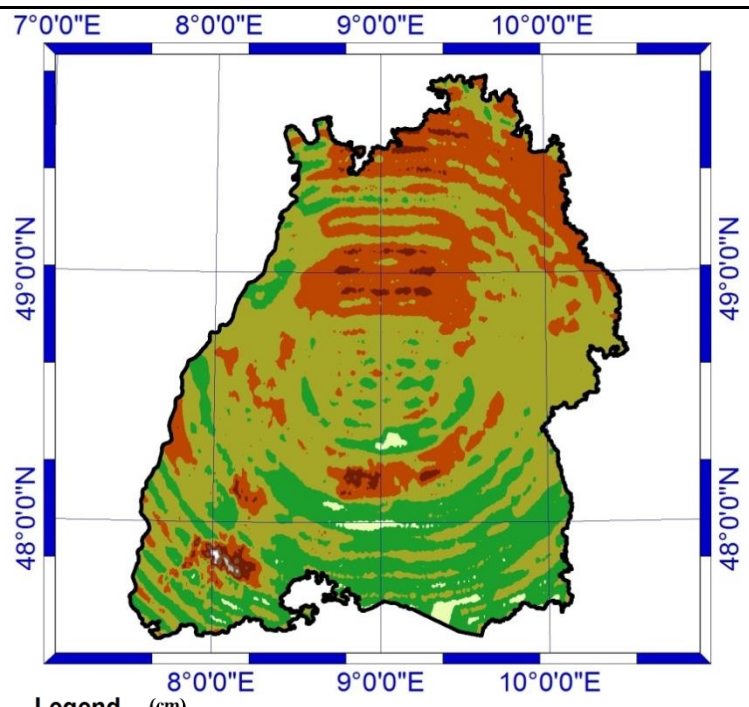


Figure (4.10): The difference between the height anomalies calculated by the EGM2008 with $N_{max}=2190$ and the height anomalies calculated by means of ASCH with a maximum degree and order of 80.

5. Integrated Solution for ASCH modeling

The different types of SCH were discussed in chapter (3). The parameterization of ASCH has advantages over the other types of SCH, since they do not require the search for the roots of Legendre function and its derivatives $(n(k), m)$ to satisfy the orthogonality requirements in equations (3-9a) and (3-9b). In ASCH, equation (3-43) is used to find the roots of Legendre function and its derivative to satisfy the Laplace equation. Another advantage of ASCH is that the Legendre function of integer degree and order are used, enabling the use of the well-known recursive and non-iterative formulas.

The advantages discussed above made it simple and easy to implement the ASCH model for local gravity/potential representation, making it ideal for this study. The principles of adjustment, observation equations and the required reductions and transformations of different types of observations are discussed in detail in this chapter.

To accomplish a complete solution, the observation equations for each type of observation are also discussed in detail in this chapter. All required reductions needed for each type of observation are introduced. The solution algorithms and the applied numerical methods are also explained.

5.1. Solution introduction

The ASCH parameterization can be used to model the potential V of the Earth according to chapter (3.2). The potential V in terms of ASCH reads:

$$V(r, \alpha, \vartheta) = \frac{GM}{r} \sum_{k=0}^{k_{\max}} \left(\frac{R}{r}\right)^{n(k)} \sum_{m=0}^k (C'_{k_{nm}} \cos m\alpha + S'_{k_{nm}} \sin m\alpha) \bar{P}'_{km}(\cos \vartheta) \quad (5-1)$$

According equation (5-1), an ASCH model has a group of defining parameters that are chosen so that the cap covers the whole area of interest. The following are the defining parameters of ASCH (Younis et al., 2011):

GM : Geocentric gravitational constant of the Earth.

R : The mean radius of the cap area.

θ_0 : The maximum opening angle of the cap area, where the scale factor of the ASCH model in equation (3-35) is $s = 90^\circ / \theta_0$

λ_0, ϕ_0 : The latitude and longitude of the cap's origin. They are used to calculate the cap coordinates as shown in figure (3.1).

The task of modeling the gravity potential using ASCH requires the computation of the unknown coefficients (S'_{nm}, C'_{nm}) in equation (5-1) using different types of observations available in the area of interest. These observations are terrestrial gravity measurements, height fitting points, deflections of the vertical and the available global gravity models GGM (e.g. EGM2008, EIGEN05c).

The prior information of ASCH coefficients is achieved by solving a linear equation system for a number of direct observations with positions $P(r, \mathcal{G}, \lambda)$ as shown in chapter (5.2) and the mapped global SH to ASCH using the approach in chapter (4). The solution of the system of equations based on (5-1), or one of its derivatives, is linear with respect to the unknown coefficients (S'_{nm}, C'_{nm}) by using a number of observations with positions $(r, \mathcal{G}, \lambda)_i$ at least equal to the number of unknown coefficients; the minimum number of required observation points is therefore equal to or greater than the number of unknown coefficients $(k_{\max} + 1)^2$ (Younis et al., 2011). For an observation l_i with a residual v_i at the position $(r, \mathcal{G}, \lambda)_i$, the observation equation reads:

$$l_i + v_i = \mathbf{A}_i \hat{\mathbf{x}} \quad (5-2)$$

The column vector of unknowns reads:

$$\hat{\mathbf{x}} = [C'_{00} \quad C'_{10} \quad C'_{11} \quad S'_{11} \quad C'_{20} \quad \dots \quad S'_{nn}]^T \quad (5-3)$$

The row vector \mathbf{A}_i is a row in the design matrix \mathbf{A} . The elements of \mathbf{A}_i are the coefficients of the unknown parameters in an observation equation, which are explained in the following parts of this chapter.

The least squares solution for the system of linear equations according to (5-2) reads:

$$\hat{\mathbf{x}} = (\mathbf{A}^T \mathbf{W}_u \mathbf{A})^{-1} \mathbf{A}^T \mathbf{W}_u \mathbf{l} \quad (5-4)$$

The square matrix $\mathbf{W}_u = \sigma_0^2 \mathbf{C}_u^{-1}$ is the weight matrix of the observations with covariance matrix \mathbf{C}_u . \mathbf{l} is the column vector of the observations. Using the solved unknowns in equation (5-4), the residuals vector \mathbf{v} of the observations reads:

$$\mathbf{v} = \mathbf{A} \hat{\mathbf{x}} - \mathbf{l} \quad (5-5)$$

The reference variance of the adjustment with r redundant observations reads:

$$\hat{s}_0^2 = \frac{\mathbf{v}^T \mathbf{W}_u \mathbf{v}}{r} \quad (5-6)$$

Using the error propagation, the covariance matrix of the unknowns \mathbf{C}_{xx} reads:

$$\mathbf{C}_{xx} = \hat{s}_0^2 (\mathbf{A}^T \mathbf{W}_u \mathbf{A})^{-1} = \hat{s}_0^2 \mathbf{N}^{-1} = \hat{s}_0^2 \mathbf{Q}_{xx} \quad (5-7)$$

The covariance matrix $\mathbf{C}_{\hat{y}}$ of the adjusted observations is given by:

$$\mathbf{C}_{\hat{y}} = \hat{s}_0^2 \mathbf{A} (\mathbf{A}^T \mathbf{W}_u \mathbf{A})^{-1} \mathbf{A}^T = \hat{s}_0^2 \mathbf{A} \mathbf{N}^{-1} \mathbf{A}^T = \hat{s}_0^2 \mathbf{Q}_{\hat{y}} \quad (5-8)$$

5.2. Observations

5.2.1. Terrestrial gravity observation

Many countries have constructed national gravimetric networks with high accurate surface gravity measurements. By the year 2000, the USA was covered by more than 150 absolute gravity stations used as a reference for geodetic and geodynamic applications (Torge, 2001). In Germany, the first gravity network was built in the 1930s with relative pendulum gravimeters tied to the Potsdam absolute gravity value. The achieved accuracy was $0.01\text{--}0.1\text{ mGal}$. In 1976/1977 a base network (Deutsche Schweregrundnetz DSGN76) of absolute/relative gravity stations was built in Western Germany, and extended in 1994/1995 to the eastern region including 30 absolute gravity points. The 30km space network of relative gravity points over the entire country has the accuracy of $\mp 0.01\text{ mGal}$. The network is called the German Primary Gravity Network (DHSN96) (BKG, 2011). Depending on the DHSN96, a densification of nearly 15000 gravity points using relative gravimeters has been established in Baden-Württemberg by the year 2010 (see figure 5.1).

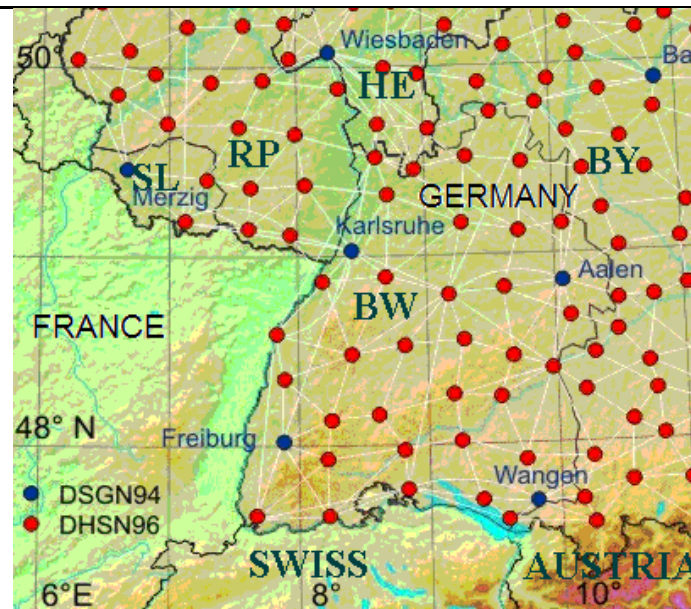


Figure (5.1): First order gravity network in the state of Baden-Württemberg (BW) and the neighboring states in Germany (BKG, 2011).

The modern positioning equipment (GNSS+gravity) enabled the use of the directly measured gravity (g) with its ellipsoidal height instead of using the gravity anomaly (Δg)/disturbance (δg) which need the physical height (H/H^*). The directly measured gravity value (apparent gravity) g takes the down direction of the plumb line without tangential components (Local Astronomical Vertical system -LAV) (Chatfield, 1997) (see figure 5.2). The gravity vector in LAV-system reads:

$$\vec{g} = \vec{g}_{LAV} = \begin{bmatrix} 0 \\ 0 \\ -g \end{bmatrix}^{LAV} \quad (5-9)$$

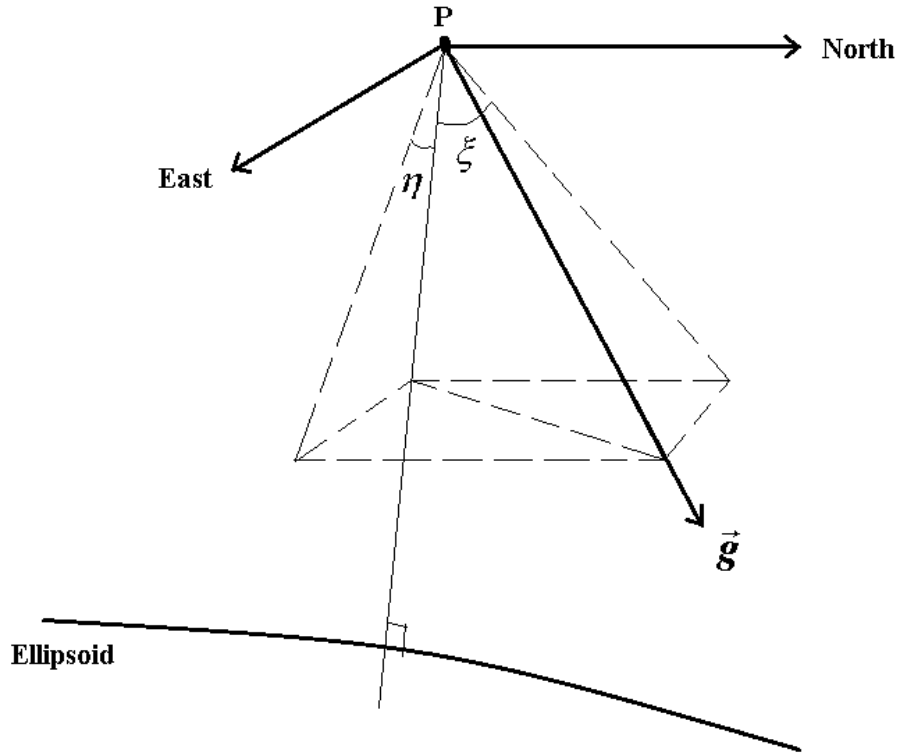


Figure (5.2): The direction of the measured gravity vector.

The gravity vector is $\vec{g} = grad(W)$. The gravity potential $W=V+\Omega$ contains of the gravitational part V and centrifugal part Ω (Torge, 2001). The centrifugal part Ω is related to the Earth rotation and must be reduced in the observations, in order to use the parameterization of V . Further observed gravity vectors have also to be transformed to the local cap system for modeling the gravitational potential V using ASCH. The following steps must be performed to get the final observation equation:

Step-1: The gravity vector is to be transformed from the Local Astronomical Vertical frame (LAV) to the Local Geodetic Vertical System (LGV). Here, the deflections of the vertical in the north-south direction (η) and the east-west direction (ξ) are required to calculate the astronomical position. The astronomical latitude and longitude are given by Fan (2004):

$$\Phi = \phi + \xi \quad (5-10)$$

$$\Lambda = \lambda + \frac{\eta}{\cos \phi} \quad (5-11)$$

The transformation from LAV to LGV reads:

$$\vec{g}_{LGV} = \begin{bmatrix} g_{\phi} \\ g_{\lambda} \\ g_r \end{bmatrix} = \mathbf{R}_{LAV}^{LGV} \vec{g}_{LAV} \quad (5-12)$$

The rotation matrix \mathbf{R}_{LAV}^{LGV} between LAV and LGV systems is (Chatfield, 1997):

$$\mathbf{R}_{LAV}^{LGV} = \begin{bmatrix} \sin \phi \sin \Phi \cos(\Lambda - \lambda) + \cos \phi \cos \Phi & \sin \phi \sin(\Lambda - \lambda) & \cos \phi \sin \Phi - \sin \phi \cos \Phi \cos(\Lambda - \lambda) \\ -\sin \Phi \sin(\Lambda - \lambda) & \cos(\Lambda - \lambda) & \cos \Phi \sin(\Lambda - \lambda) \\ \sin \phi \cos \Phi - \cos \phi \sin \Phi \cos(\Lambda - \lambda) & -\cos \phi \sin(\Lambda - \lambda) & \cos \phi \cos \Phi \cos(\Lambda - \lambda) + \sin \phi \sin \Phi \end{bmatrix} \quad (5-13)$$

Step-2: The gravity from the LGV-system is transformed to Earth-Centered-Earth-Fixed system (e-system). The transformation reads:

$$\vec{\mathbf{g}}_e = \begin{bmatrix} g_x \\ g_y \\ g_z \end{bmatrix} = \mathbf{R}_{LGV}^e \vec{\mathbf{g}}_{LGV} \quad (5-14)$$

The rotation matrix between LGV and e-system reads (Jekeli, 2001):

$$\mathbf{R}_{LGV}^e = \begin{bmatrix} -\sin \phi \cos \lambda & -\sin \lambda & \cos \phi \cos \lambda \\ -\sin \phi \sin \lambda & \cos \lambda & \cos \phi \sin \lambda \\ \cos \phi & 0 & \sin \phi \end{bmatrix} \quad (5-15)$$

Step-3: centrifugal gravity vector $\vec{\mathbf{z}}$ related to the rotation of the Earth is removed to generate a reduced gravity vector related to V in the e-system $\vec{\mathbf{g}}'_e$. The centrifugal gravity vector reads (Torge, 2001):

$$\vec{\mathbf{z}} = \omega^2 \vec{\mathbf{P}} = \begin{bmatrix} \omega^2 X \\ \omega^2 Y \\ 0 \end{bmatrix} \quad (5-16)$$

Accordingly, the reduction of the centrifugal acceleration reads:

$$\vec{\mathbf{g}}'_e = \begin{bmatrix} g'_x \\ g'_y \\ g'_z \end{bmatrix} = \begin{bmatrix} g_x \\ g_y \\ g_z \end{bmatrix} - \begin{bmatrix} \omega^2 X \\ \omega^2 Y \\ 0 \end{bmatrix} \quad (5-17)$$

Step-4: As the ASCH in equation (5-1) need a spherical coordinate system $(\lambda, \bar{\phi}, r)$, the reduced geocentrical gravity vector $\vec{\mathbf{g}}'_e$ has to be transformed back again, but now to the spherical-LGV of the Cap system. The transformation reads (Seeber, 2003):

$$\vec{\mathbf{g}}_{LGV_Sphere} = \begin{bmatrix} g_{\bar{\phi}} \\ g_{\lambda} \\ g_r \end{bmatrix} = (\mathbf{R}_{LGV_sphere}^e)^{-1} \vec{\mathbf{g}}'_e \quad (5-18)$$

The rotation matrix $\mathbf{R}_{LGV_sphere}^e$ reads (Becker and Hehl, 2012):

$$\mathbf{R}_{LGV_sphere}^e = \begin{bmatrix} -\sin \bar{\phi} \cos \lambda & -\sin \lambda & \cos \bar{\phi} \cos \lambda \\ -\sin \bar{\phi} \sin \lambda & \cos \lambda & \cos \bar{\phi} \sin \lambda \\ \cos \bar{\phi} & 0 & \sin \lambda \end{bmatrix} \quad (5-19)$$

The accuracy of tangential gravity components $g_{\bar{\phi}}$ and g_{λ} is too heavily influenced by the accuracy of the deflections of the vertical. The tests have shown that 1 second accuracy in deflections of vertical leads to nearly 0.4 *mGal* in $g_{\bar{\phi}}$ and g_{λ} , but less than 0.001 *mGal* in the radial component g_r . For this reason, the tangential components are excluded from the adjustment, while the radial component g_r appears to be free of vertical errors and suits the accuracy of (0.01-0.02) *mGal* of terrestrial gravimeters.

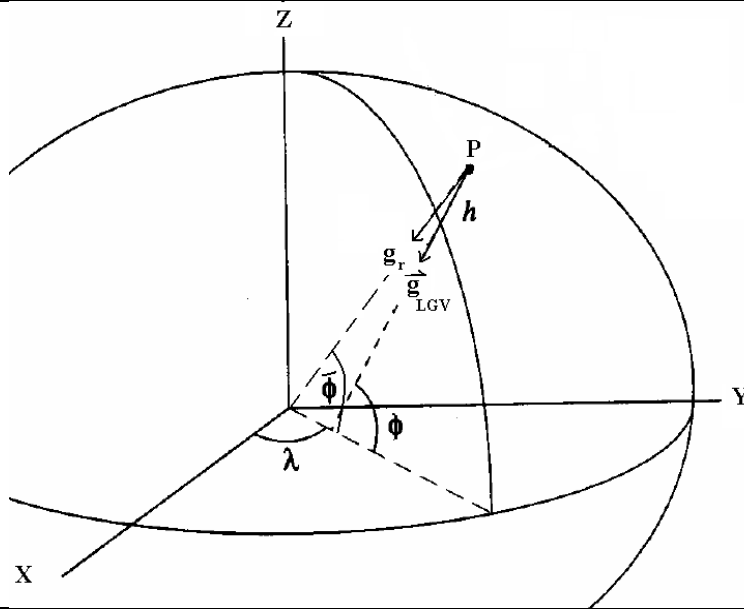


Figure (5.3): The gravity vector in the LGV-system and its radial component (after the reduction of the centrifugal acceleration part).

The radial component of the gravity g_r in (5-18) is the first radial derivative of the gravitational potential V (Hofmann-Wellenhof & Moritz 2005):

$$g_r = \frac{\partial V}{\partial r} \quad (5-20)$$

Inserting equation (5-20) in equation (5-1), it is seen that the terrestrial gravity has the observation equation (5-21). The geographic coordinates $(\lambda, \bar{\phi}, r)$ have to be transformed to the cap coordinates (r, θ, λ) , the cap coordinates (r, θ, λ) are the adjusted coordinates (scaled) to the adjusted Cap system $(r, \mathcal{G}, \lambda)$ using equation (3-35).

$$g_r + v_i = -\frac{GM}{r^2} \sum_{k=0}^{k \max} \left(\frac{R}{r} \right)^{n(k)+1} (n(k)+1) \sum_{m=0}^k (C'_{km} \cos m\alpha + S'_{km} \sin m\alpha) \bar{P}_{km}(\cos \mathcal{G}) \quad (5-21)$$

5.2.2. Height fitting points

As the conventional methods deal with points on the geoid W_0 , there is now a need to obtain the gravity anomalies and disturbance above or below the geoid because of the new methods of positioning (e.g. GNSS). Molodensky (1945) introduced a new approach. The point P, with ellipsoidal h in figure (5.4), is located on an equipotential surface $W=W_p$. There exists other surface called the telluroid whose normal potential U_Q is equal to the actual potential at the point W_p . The distance between the two surfaces through the normal line is the height anomaly ζ . This difference defines the quasigeoid. Where the ellipsoidal height of point Q in figure (3.8) is called the normal height, this height is the normal height of the point P (Hofmann-Wellenhof & Moritz, 2005).

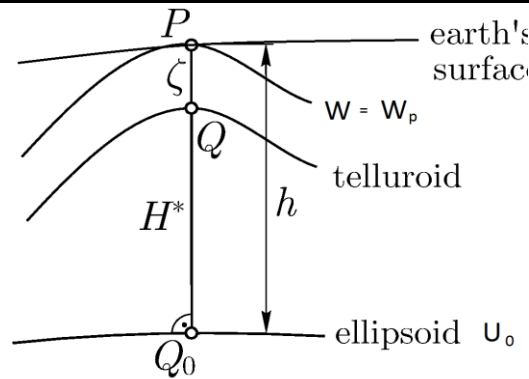


Figure (5.4): Definitions of Molodensky's approach (Hofmann-Wellenhof & Moritz, 2005).

The height fitting points with both normal height H^* and ellipsoidal height h in a country can be used to model the gravitational potential by means of ASCH. According to Molodensky's theory, the quasigeoid height (height anomaly) reads:

$$\zeta = h_P - H_p^* = h_P - h_Q \quad (5-22)$$

By the definition of Molodensky's theory, the normal gravity potential of the point Q (U_Q) on the telluroid is the same of the gravity potential of point P (W_p) on the Earth's surface.

$$U_Q = W_p \quad (5-23)$$

The ellipsoidal normal potential of a point reads (Moritz, 1967):

$$U(u, \beta) = \frac{GM}{E} \tan^{-1} \frac{E}{u} + \frac{1}{2} w^2 a^2 \frac{q}{q_0} \left(\sin^2 \beta - \frac{1}{3} \right) + \frac{1}{2} w^2 (u^2 + E^2) \cos^2 \beta \quad (5-24a)$$

The quantity q is an arbitrary quantity. q_0 is $q(u = b)$. The values of q and q_0 are given by:

$$q = \frac{1}{2} \left[\left(1 + 3 \frac{u^2}{E^2} \right) \tan^{-1} \frac{E}{u} - 3 \frac{u}{E} \right] \quad (5-24b)$$

$$q_0 = \frac{1}{2} \left[\left(1 + 3 \frac{b^2}{E^2} \right) \tan^{-1} \frac{E}{b} - 3 \frac{b}{E} \right] \quad (5-24c)$$

These coordinates (λ, β, u) are the harmonic coordinates (Hofmann-Wellenhof & Moritz, 2005). The formulas to calculate harmonic coordinates using the Cartesian coordinates are given by:

$$\lambda = \tan^{-1} \left(\frac{Y}{X} \right) \quad (5-25a)$$

$$u = \left(X^2 + Y^2 + Z^2 - E^2 \right) \left[\frac{1}{2} + \frac{1}{2} \sqrt{1 + \frac{4E^2 Z^2}{(X^2 + Y^2 + Z^2 - E^2)^2}} \right] \quad (5-25b)$$

$$\tan \beta = \frac{Z \sqrt{u^2 + E^2}}{u \sqrt{X^2 + Y^2}} \quad (5-25c)$$

$$E = \sqrt{a^2 - b^2} \quad (5-25d)$$

In terms of the potential, the quasigeoid height ζ using Molodensky theory reads:

$$\zeta = \frac{T_p}{\gamma_q} \quad (5-26)$$

T is the disturbing potential, reading:

$$T_p = W_p - U_p = U_Q - U_p \quad (5-27a)$$

$$T_p = (V_p + \Omega_p) - (V'_p + \Omega_p) = V_p - V'_p \quad (5-27b)$$

Here, Ω is the centrifugal potential due to the Earth rotation ω . where Ω reads:

$$\Omega = 0.5 \omega^2 r^2 \cos^2 \bar{\phi} = \frac{1}{2} \omega^2 (x^2 + y^2) \quad (5-28)$$

Using equations (5-26) and (5-27), the gravitational potential V of point P is derived as follows:

$$V_p = W_p - \Omega = U_p + \gamma_q \zeta - \Omega \quad (5-29)$$

When the height fitting points have orthometric heights instead of normal heights, the orthometric heights have to be transformed to normal heights (see figure 5.5). The relationship between orthometric height H and normal height H^* reads:

$$H^* - H = N - \xi = \frac{\bar{g} - \bar{\gamma}}{\bar{\gamma}} \quad (5-30)$$

\bar{g} is the mean gravity along the plumb line of point P, and can be calculated using the global gravity models. Alternatively, it can be approximately assumed to be equal to the Bouguer gravity correction. In this context, \bar{g} reads (Sneeuw, 2006):

$$\bar{g} = g_P + 0.0424 \frac{Gal}{km} H \quad (5-31)$$

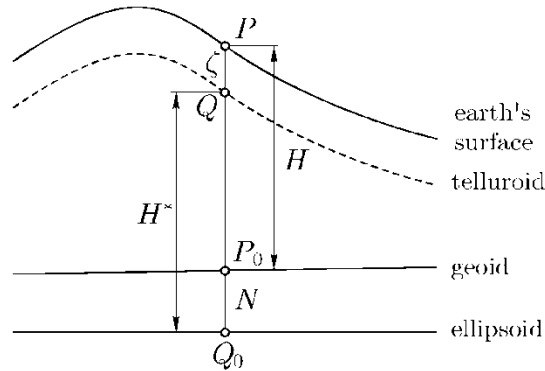


Figure (5.5): The normal height H^* and the orthometric height H (Hofmann-Wellenhof & Moritz, 2005).

$\bar{\gamma}$ is the mean ellipsoidal normal gravity from the point Q down to the ellipsoid along the normal line of point P . $\bar{\gamma}$ can be calculated strictly in an iterative procedure using the reference ellipsoid GRS80. $\bar{\gamma}$ can be calculated with lower accuracy by applying half of free air correction to the normal gravity at point Q . $\bar{\gamma}$ then reads (Sneeuw, 2006):

$$\bar{\gamma} = \gamma_P + 0.1543 \frac{Gal}{km} H \quad (5-32)$$

In modern geodesy and the definition of reference frames, the height reference surface is related to reference potential value W_0 of the Earth gravity field. To achieve consistency the normal gravity potential of the reference ellipsoid surface is set equal to W_0 (Wahr, 1996).

$$W_0 = U_0 \quad (5-33)$$

The height is related to the difference between the reference gravity potential W_0 and the actual gravity potential W_P at the point P . The difference is called the geopotential number C_P .

$$C_P = W_0 - W_P \quad (5-34)$$

Then the normal height H^* reads (Fan, 2004):

$$H^* = \frac{C_P}{\bar{\gamma}} \quad (5-35)$$

An example of a vertical reference system is the European Vertical Reference System (EVRS2000). The reference point for its realization is the *Normaal Amsterdam Peil NAP*. The reference ellipsoid is GRS80 with $C_{NAP} = 0$. The EVRS2007, however, is defined by a fixed geopotential number of $7.0259 \text{ m}^2 \text{ s}^{-2}$ or equivalently 0.716 m . The latest EVRS developed in

Europe is the EVRS2007, which was defined using 13 points distributed keeping the level datum of EVRS2000. The national height reference surfaces in Europe must also be realized using different tide gauges. This introduces differences of height systems in the neighboring countries, which are different from the EVRS2000. Figure (5.6) shows the differences between the national height reference surfaces and the EVRS2007 (ΔV) (BKG, 2011).

The use of different tide gauges (height datums) requires adding the datum difference between the local area height reference surface and the gravity reference by referencing the height fitting points to gravity. This implies an additional unknown parameter (ΔV) to the functional model of the integrated adjustment approach, which has to be applied for the computations of the observation equations of the height fitting points. For the i -th gravity point, we have:

$$V_i = \left[\frac{GM}{r} \sum_{k=0}^{k_{max}} \left(\frac{R}{r} \right)^{n(k)} \sum_{m=0}^k (C'_{km} \cos m\alpha + S'_{km} \sin m\alpha) \bar{P}_{km}(\cos \vartheta) \right] + \Delta V \quad (5-36)$$

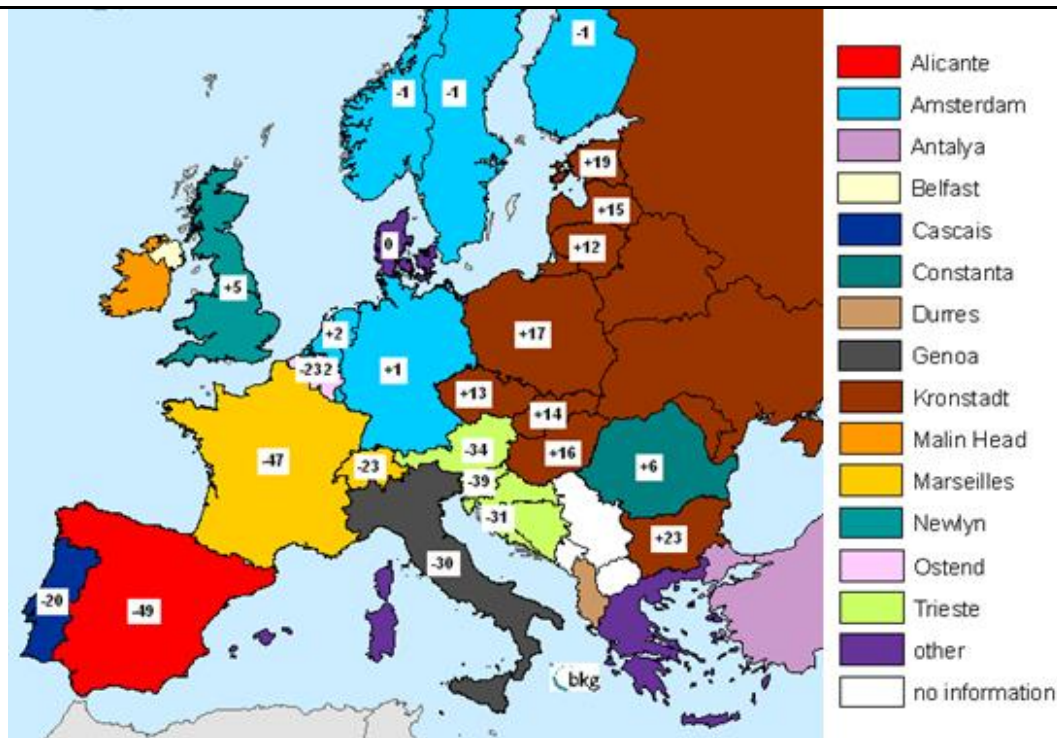


Figure (5.6): Differences between the EVRF2007 and national reference tide gauges in cm (BKG, 2011).

5.2.3. Deflections of the vertical

The directly measured deflections of the vertical using astronomical methods like zenith cameras can be used as direct input in the integrated adjustment approach. The measured deflections of the vertical are given in the east and north directions. As the deflections of the vertical are functions of the disturbing potential, they can be related to the potential W . The east-west η direction reads (Torge, 2001):

$$\eta = - \frac{1}{\gamma_Q(N+h)\cos\phi} \frac{\partial T}{\partial \lambda} \quad (5-37)$$

The north-south component of the deflections of the vertical ξ reads:

$$\xi = -\frac{1}{\gamma_Q(M+h)} \frac{\partial T}{\partial \phi} \quad (5-38)$$

Here, M and N are radii of curvature of the ellipsoid in longitude and latitude directions.

5.2.3.1. First method of deriving the observation equations

To integrate the deflections of vertical in (5-37) and (5-38) in the ASCH model, the direction of the plumb line is transformed to the spherical cap system. This can be achieved using the astronomical latitude and longitude (Φ, Λ) . The relationship between the astronomical and geographic latitude and longitude reads:

$$\Phi = \phi + \xi \quad (5-39)$$

$$\Lambda = \frac{\eta}{\cos \phi} + \lambda \quad (5-40)$$

The direction vector of the plumb line \bar{r} in the e-system reads (Hofmann-Wellenhof et al., 2001):

$$\bar{r} = \begin{bmatrix} \cos \Phi \cos \Lambda \\ \cos \Phi \sin \Lambda \\ \sin \Phi \end{bmatrix}_e = \begin{bmatrix} r_x \\ r_y \\ r_z \end{bmatrix}_e = \bar{r}(\lambda, \phi, \eta, \xi) \quad (5-41)$$

The transformation of the direction vector \bar{r} in the cap system \bar{r}_{cap} reads:

$$\bar{r}_{cap} = \begin{bmatrix} r_{x'} \\ r_{y'} \\ r_{z'} \end{bmatrix} = (\mathbf{R}_{LGV_sphere}^e)^{-1} \bar{r} = \bar{r}(\lambda, \phi, \eta, \xi / \lambda_0, \phi_0, \lambda, \bar{\phi}) \quad (5-42)$$

The rotation matrix $\mathbf{R}_{LGV_sphere}^e$ reads:

$$\mathbf{R}_{LGV_sphere}^e = \begin{bmatrix} -\sin \bar{\phi}_0 \cos \lambda_0 & -\sin \lambda_0 & \cos \bar{\phi}_0 \cos \lambda_0 \\ -\sin \bar{\phi}_0 \sin \lambda_0 & \cos \lambda_0 & \cos \bar{\phi}_0 \sin \lambda_0 \\ \cos \bar{\phi}_0 & 0 & \sin \bar{\phi}_0 \end{bmatrix} \quad (5-43)$$

In equation (5-43), $\bar{\phi}_0$ and λ_0 are the spherical latitude and longitude of the cap pole. The direction vector of the plumb line in the cap system \bar{r}_{cap} in terms of astronomical cap coordinates (Θ, A) reads:

$$\bar{r}_{cap} = \begin{bmatrix} \sin \Theta \cos A \\ \sin \Theta \sin A \\ \cos \Theta \end{bmatrix}_{cap} \quad (5-44)$$

In equation (5-44), the angle Θ between the cap pole and the direction of the plumb line at point and the cap astronomical azimuth A are:

$$\Theta = \tan^{-1} \frac{\sqrt{r_{x'}^2 + r_{y'}^2}}{r_{z'}} \quad (5-45)$$

$$A = \tan^{-1} \frac{r_{y'}}{r_{x'}} \quad (5-46)$$

The transformed deflections of the vertical in the local spherical cap system η' and ξ' are:

$$\eta' = (A - \alpha) \sin \theta = \eta'(\eta, \xi / \lambda, \phi, h / \lambda_0, \bar{\phi}_0, \lambda, \bar{\phi}) \quad (5-47)$$

$$\xi' = \Theta - \theta = \xi'(\eta, \xi / \lambda, \phi, h / \lambda_0, \bar{\phi}_0, \lambda, \bar{\phi}) \quad (5-48)$$

The relationships between the transformed ξ' , η' and the potential read:

$$\eta' = -\frac{1}{\gamma_Q r \sin \theta} \frac{\partial T}{\partial \alpha} = -\frac{1}{\gamma_Q r \sin \theta} \left(\frac{\partial V}{\partial \alpha} - \frac{\partial(U - \Omega)}{\partial \alpha} \right) \quad (5-49)$$

$$\xi' = -\frac{1}{\gamma_Q r} \frac{\partial T}{\partial \theta} = -\frac{1}{\gamma_Q r} \left(\frac{\partial V}{\partial \theta} - \frac{\partial(U - \Omega)}{\partial \theta} \right) \quad (5-50)$$

To model the gravitational potential part, (5-49) and (5-50) can be rewritten as follows:

$$Q_1 = \eta' - \frac{1}{\gamma_Q r \sin \theta} \frac{\partial(U - \Omega)}{\partial \alpha} = -\frac{1}{\gamma_Q r \sin \theta} \frac{\partial V}{\partial \alpha} \quad (5-51)$$

$$Q_2 = \xi' - \frac{1}{\gamma_Q r} \frac{\partial(U - \Omega)}{\partial \theta} = -\frac{1}{\gamma_Q r} \frac{\partial V}{\partial \theta} \quad (5-52)$$

In equation (5-52), the derivative of the potential $\frac{\partial V}{\partial \theta}$ is in terms of θ , but the ASCH model depends on the scaled angle $\vartheta = s \theta$. $\frac{\partial V}{\partial \theta}$ in equation (5-52) then reads:

$$\frac{\partial V}{\partial \theta} = \frac{\partial V}{\partial \vartheta} \frac{\partial \vartheta}{\partial \theta} = s \frac{\partial V}{\partial \vartheta} \quad (5-53)$$

Inserting (5-53) in (5-52) gives in:

$$Q_2' = -\frac{s}{\gamma_Q r} \frac{\partial V}{\partial \vartheta} \quad (5-54)$$

The derivatives of the gravitational potential with respect to α and ϑ in ASCH are:

$$\frac{\partial V}{\partial \alpha} = \frac{GM}{r} \sum_{k=0}^K \left(\frac{R}{r} \right)^{n_k(m)} \sum_{m=0}^k m (\bar{S}'_{k,m} \cos(m\alpha) - \bar{C}'_{k,m} \sin(m\alpha)) \bar{P}_{n,m}(\vartheta) \quad (5-55)$$

$$\frac{\partial V}{\partial \vartheta} = \frac{GM}{r} \sum_{k=0}^K \left(\frac{R}{r} \right)^{n_k(m)} \sum_{m=0}^k (\bar{C}'_{n,m} \cos(m\alpha) + \bar{S}'_{n,m} \sin(m\alpha)) \frac{\partial \bar{P}_{n,m}(\vartheta)}{\partial \vartheta} \quad (5-56)$$

In equations (5-55) and (5-56), $\bar{P}_{n,m}(\vartheta)$ and $\frac{\partial \bar{P}_{n,m}(\vartheta)}{\partial \vartheta}$ are the fully normalized Legendre functions of degree n and order m and their derivatives, as shown in chapter (2.1.3). Finally, the observation equations related to the deflections of the vertical are built using equations (5-55) and equation (5-56):

$$Q_1^{+v_i} = -\frac{1}{\gamma_Q r \sin \theta} \frac{\partial V}{\partial \alpha} \quad (5-57)$$

$$Q_2^{+v_i} = -\frac{s}{\gamma_Q r} \frac{\partial V}{\partial \vartheta} \quad (5-58)$$

5.2.3.2. Second method of deriving the observation equations

Another method for transforming the deflections of the vertical in equations (5-37) and (5-38) to derivatives of the potential V in equations (5-55) and (5-56) is to apply direct derivatives. Equations (5-37) and (5-38) can be rewritten as:

$$\eta = -\frac{1}{\gamma_Q (N+h) \cos \phi} \frac{\partial (V - (U - \Omega))}{\partial \lambda} \quad (5-59a)$$

$$\xi = -\frac{1}{\gamma_Q (M+h)} \frac{\partial (V - (U - \Omega))}{\partial \bar{\phi}} \frac{\partial \bar{\phi}}{\partial \phi} \quad (5-59b)$$

Using equations (5-59a and b), the derivatives of the gravitational potential with respect to λ and $\bar{\phi}$ read:

$$\frac{\partial V}{\partial \lambda} = -\eta \gamma_Q (N+h) \cos \phi + \frac{\partial (U - \Omega)}{\partial \lambda} \quad (5-60a)$$

$$\frac{\partial V}{\partial \bar{\phi}} = \frac{-\xi \gamma_Q (M+h)}{\frac{\partial \bar{\phi}}{\partial \phi}} + \frac{\partial (U - \Omega)}{\partial \bar{\phi}} \quad (5-60b)$$

The final derivatives of the potential in equations (5-55) and (5-56) read:

$$\frac{\partial V}{\partial \alpha} = \frac{\partial V}{\partial \bar{\phi}} \frac{\partial \bar{\phi}}{\partial \alpha} + \frac{\partial V}{\partial \lambda} \frac{\partial \lambda}{\partial \alpha} \quad (5-61a)$$

$$\frac{\partial V}{\partial \theta} = \frac{\partial V}{\partial \bar{\phi}} \frac{\partial \bar{\phi}}{\partial \theta} + \frac{\partial V}{\partial \lambda} \frac{\partial \lambda}{\partial \theta} \quad (5-61b)$$

5.2.3.3. Third method of deriving the observation equations

The new CCD technologies (Charged Coupled Devices) enable the foundation of imaging sensors to track the celestial objects. These sensors are known as “zenith cameras”. One purpose of the zenith cameras is to determine the deflections of the vertical (Hirt et al, 2010). Generally, the observations of deflections of the vertical are reading

$$\xi = \Phi_{astr} - \phi \quad (5-62a)$$

$$\eta = (\Lambda_{astr} - \lambda) \cdot \cos \phi \quad (5-62b)$$

Here (ϕ, λ) are observed by GNSS with high accuracy, and can be regarded as fixed parameters. And (Φ, Λ) are the result of astronomical observations using zenith cameras based on the fundamental equation for celestial navigation (Hofmann-Wellenhof et al, 2003).

$$\mathbf{R}_e^{LAV}(\Phi, \Lambda) \cdot \mathbf{r}^{e,s}(t) - \mathbf{R}_{LGV}^{LAV}(\Phi, \Lambda, \eta, \xi) \cdot \mathbf{R}_b^{LGV}(p, y, r) \cdot \mathbf{r}_{SI}^b = \mathbf{0} \quad (5-63a)$$

In equation (5-63a), (r=roll, p=pitch and y=yaw) are the rotation angles between the body-frame and the navigation-frame. \mathbf{r}_{SI}^b is the normalized image vector of the celestial object. In the case of zenith camera observation situation, we rewrite equation (5-63a) for a LAV-horizontal zenith camera as

$$\mathbf{R}_e^{LAV}(\lambda, \phi, \eta, \xi) \cdot \mathbf{r}^{e,s}(t) - \mathbf{R}_b^{LAV}(r_{LAV}, p_{LAV}, y_{LAV}) \cdot \mathbf{r}_{SI}^b = \mathbf{0} \quad (5-63b)$$

Due to horizontalation, $r_{LAV} = p_{LAV} = 0$, while r_{LAV} is occurring as an auxiliary unknown. (η, ξ) are the further and essential unknowns in the nonlinear observation equation (5-63b). With $\mathbf{g} = [W_x \ W_y \ W_z]^T = -g \cdot [\cos \Phi \cdot \cos \Lambda \ \cos \Phi \cdot \sin \Lambda \ \sin \Phi]^T$, we directly arrive at the observation equations for resultant deflections of the vertical (η, ξ) reading

$$\eta = \left[\tan^{-1} \left(\frac{W_y}{W_x} \right) - \lambda \right] \cdot \cos \phi = \left[\tan^{-1} \left(\frac{V_y + Z_y}{V_x + Z_x} \right) - \lambda \right] \cdot \cos \phi \quad (5-64a)$$

$$\xi = \tan^{-1} \left(\frac{-W_z}{\sqrt{W_x^2 + W_y^2}} \right) - \phi = \tan^{-1} \left(\frac{-(V_z + Z_z)}{\sqrt{(V_x + Z_x)^2 + (V_y + Z_y)^2}} \right) - \phi \quad (5-64b)$$

The GNSS-positions (ϕ, λ) on the right side can be regarded as fix parameters. Based on the location (x, y, z) of the observations (η, ξ) , all components on the right side are also to be parameterized (e.g. $r = r(x, y, z)$, $\alpha = \alpha(x, y, z)$ and $\vartheta = \vartheta(x, y, z)$ in case of the CAP coordinates and V-ASCH) directly or implicitly by (x, y, z) . So the occurring partial derivatives in the nonlinear observation equations (5-64a,b) can be set up directly or by using the chain rule.

5.2.4. Global gravity models

The global gravity model (GGM) can be integrated in the local ASCH model in different ways. One method is to use the locally transformed coefficients described in chapter (4). The transformed parameters of global SH models to ASCH model can be used as additional observations in the adjustment. The observation equation then reads:

$$l_i + v_i = x_{iASCH_EGM} \quad (5-65)$$

In matrix form, equation (5-65) reads:

$$\mathbf{l} + \mathbf{v} = \mathbf{A}\mathbf{x}_{ASCH_EGM} \quad (5-66)$$

The block of the design matrix \mathbf{A} related to the global model reads:

$$\begin{bmatrix} 1 & 0 & 0 & 0 & 0 & 0 & 0 \\ 0 & 1 & 0 & 0 & 0 & 0 & 0 \\ 0 & 0 & 1 & 0 & 0 & 0 & 0 \\ \vdots & & \ddots & & & & \vdots \\ \vdots & & & \ddots & & & \vdots \\ 0 & 0 & 0 & \dots & \dots & 1 & 0 \\ 0 & 0 & 0 & \dots & \dots & 0 & 1 \end{bmatrix} \quad (5-67)$$

The block of the observation matrix \mathbf{L} related to the global model reads:

$$\mathbf{l}_{EGM} = \mathbf{x}_{ASCH_EGM} = [C'_{00} \quad C'_{10} \quad C'_{11} \quad S'_{11} \quad C'_{20} \quad \dots \quad S'_{nn}]^T \quad (5-68)$$

5.3. Numerical Methods

5.3.1. Storage Usage

The solution of a least squares problem using a system of linear equations (5-4) is (Ghilani & Wolf, 2006):

$$\hat{\mathbf{x}} = (\mathbf{A}^T \mathbf{W}_w \mathbf{A})^{-1} \mathbf{A}^T \mathbf{W}_w \mathbf{l} = \mathbf{N}^{-1} \mathbf{c} \quad (5-69)$$

Here, \mathbf{N} is the normal equations matrix, and \mathbf{c} is the constants matrix. \mathbf{N} and \mathbf{c} read:

$$\mathbf{N} = (\mathbf{A}^T \mathbf{W}_w \mathbf{A}) \quad (5-70)$$

$$\mathbf{c} = \mathbf{A}^T \mathbf{W}_w \mathbf{l} \quad (5-71)$$

In the case of a large number of observations and unknowns, significant memory would be required to store the matrices \mathbf{A} , \mathbf{W} , \mathbf{N} and \mathbf{L} . The Matrix \mathbf{N} and the vector matrix \mathbf{c} can be calculated directly using the observations and their weights (Jäger et al., 2005). In this way, the size required to store the matrices \mathbf{A} will be reduced to only one row of the matrix. As the normal matrix \mathbf{N} is symmetric, only the upper or the lower part of the \mathbf{N} matrix must be saved. The calculations for the elements of the upper part of \mathbf{N} and the elements of the \mathbf{c} vector using only one row of the design matrix \mathbf{A} related to the i -th observation read (Niemeier, 2001):

$$n_{m,n} = n_{m,n} + a_m a_n w_i \quad (5-72)$$

$$c_m = c_m + a_m w_i l_i \quad (5-73)$$

In the case of a very large number of unknowns, it is possible to get Software/System-failure through the calculation of (5-70) due to computer memory limits. To avoid this problem, the matrix \mathbf{N} is divided into sub-matrices (blocks). Only one or a limited number of blocks are then

loaded in the memory (Smith, 2001). The other blocks are stored in the hard drive in ASCII or Binary files. The block matrix form of the normal equations matrix N reads (Okrah, 2005):

$$N = \begin{bmatrix} N_{11} & N_{12} & N_{13} & \cdots & N_{1m} \\ & N_{22} & N_{23} & \cdots & N_{2m} \\ & & N_{33} & \cdots & N_{3m} \\ & & & \ddots & \vdots \\ & & & & N_{mm} \end{bmatrix} \quad (5-74)$$

5.3.2. Cholesky block matrix decomposition

The calculation time required to find the solution to a system of linear equations (5-4) can be reduced by implementing the Cholesky decomposition, in which a positive symmetric definite matrix N can be represented by a lower triangle L matrix or an upper triangle matrix U multiplied by its transpose (Rothberg & Gupta, 1994).

$$N = LL^T = U^T U \quad (5-75a)$$

$$L = \begin{bmatrix} l_{11} & 0 & \cdots & 0 \\ l_{21} & l_{22} & \cdots & 0 \\ \vdots & \vdots & \ddots & \vdots \\ l_{n1} & l_{n2} & \cdots & l_{nn} \end{bmatrix} \quad (5-75b)$$

$$U = \begin{bmatrix} U_{11} & U_{11} & \cdots & U_{1n} \\ 0 & U_{22} & \cdots & U_{2n} \\ \vdots & \vdots & \ddots & \vdots \\ 0 & 0 & \cdots & U_{nn} \end{bmatrix} \quad (5-75c)$$

The factorization of the lower triangle matrix L according to the Cholesky Decomposition reads:

$$l_{jj} = \sqrt{n_{jj} - \sum_{i=1}^{j-1} l_{ji}^2} \quad (5-76)$$

$$l_{vj} = \left(n_{vj} - \sum_{i=1}^{j-1} l_{ji} l_{vi} \right) / l_{jj} \quad (5-77)$$

By having the factorized L matrix, the solution with respect to the unknowns can be obtained without the need to invert the normal equations matrix N . The matrix form of the linear system of equations according to the Cholesky decomposition reads:

$$Nx = LL^T x = c \quad (5-78)$$

Equation (5-78) can be rewritten as follows:

$$Ly = c \quad (5-79)$$

$$L^T y = x \quad (5-80)$$

This makes it easy to solve the system of equations without the need to invert the matrix L or L^T . This is because L is a lower triangle matrix (Aledeld & Mayer, 1993). Solving the system of equations $Ly = c$ with respect to y is called **forward substitution**. The elements of the vector matrix y are:

$$y_j = \left(c_j - \sum_{i=1}^{j-1} l_{ji} y_i \right) / l_{jj} \quad (5-81)$$

The solution of the system of equations $L^T y = x$ with respect to the unknowns vector x is called **backward substitution**. The values of the elements of the unknowns' vector x are:

$$x_j = \left(y_j - \sum_{i=j+1}^n l_{ij} x_i \right) / l_{jj} \quad (5-82)$$

The implementation of the block matrix Cholesky decomposition is applied similarly to the normal Cholesky decomposition. Each block is handled as an element of a matrix (Nool, 1992). The factorization of the block lower triangle matrices reads (Schaefer, 2003):

$$L_{jj} = \mathbf{Decomp} \left(N_{jj} - \sum_{i=1}^{j-1} L_{ji} L_{ji}^T \right) \quad (5-83)$$

$$L_{ij} = \left[\mathbf{Bforsub} \left(L_{jj}, N_{ji} - \sum_{i=1}^{j-1} L_{ji} L_{ji}^T \right) \right]^T \quad (5-84)$$

In equation (5-83), the term $\mathbf{Decomp}(A)$ is the application of Cholesky factorization of Matrix A using equations (5-76) and (5-77). The term $\mathbf{Bforsub}(A, B)$ is calculated by using the forward substitution in equation (5-81) of the matrix A and the columns of B in equation (5-85). Having B_i as the i 'th column of matrix B , $\mathbf{Bforsub}(A, B)$ reads:

$$\mathbf{Bforsub}(A, B) = (\mathbf{Forsub}(A, B_1), \mathbf{Forsub}(A, B_2), \mathbf{Forsub}(A, B_3), \dots) \quad (5-85)$$

The forward substitution to find the block element Y_j of the vector y using the block elements C_j of the vector c reads:

$$Y_j = \mathbf{Forsub} \left(L_{jj}, C_j - \sum_{i=1}^{j-1} L_{ji} Y_i \right) \quad (5-86)$$

The backward substitution to find the block element X_j of the unknowns' vector x using the block elements Y_j of the vector y reads:

$$X_j = \mathbf{Backsub} \left(L_{jj}^T, Y_j - \sum_{i=j+1}^k L_{ij}^T X_i \right) \quad (5-87)$$

The function $\mathbf{Backsub}()$ is the implementation of backward substitution in equation (5-82).

5.3.3. Parallel processing

In most modern computers, many processors are available (e.g. duo processor, quad processor, i3, i5, i7). Classical programming languages (e.g.: VC++, VB, java ... etc.) use only one processor at a time. Implementing the principle of threading enables the use of all processors or a customized number of processors (Schiebl, 1999) (see figure 5.7). The principle of calculating the normal matrix directly from the observations enables application of threading (Breyman, 2005), meaning that many blocks can be calculated in simultaneously, with each block reserving a single processor (Nool, 2001).

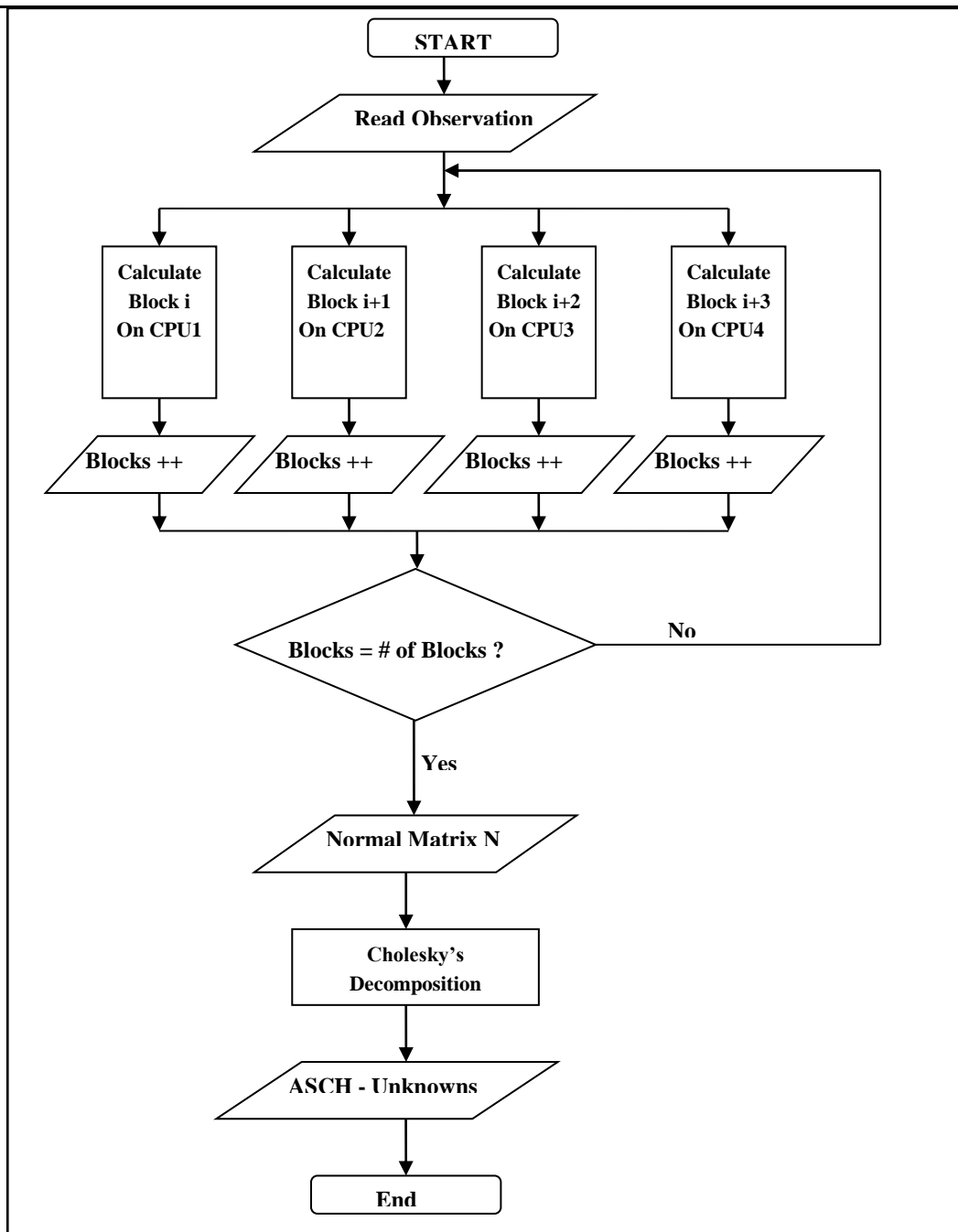


Figure (5.7): Flowchart for calculating ASCH coefficients using parallel processing.

6. Tests and Analysis of the Integrated Approach

The ASCH were theoretically proven for their proper use to model the Earth gravity potential in a local area. In this chapter, the practical tests of ASCH and their proper use to model the gravity potential of the Earth in a local area are presented; the ASCH models are implemented with an integrated approach using groups of available heterogeneous data types, such as terrestrial gravity data, height fitting points and the available global gravity models. The accuracy of gravity representation and prediction using ASCH modeling, as well as the accuracy of the height anomalies, are demonstrated.

Different tests were performed to validate the ASCH for Earth potential modeling by applying the solutions with different types of observations. The first test applied ASCH modeling using height fitting points only. In the second testing phase, the height fitting points in combination with the global SH gravity models were used to apply ASCH modeling in an integrated approach. Here, the global SH models transformed to ASCH models in chapter (4) were used. The final testing phase for ASCH modeling is the integrated solution using height fitting points, global gravity models and the terrestrial gravity observations. These tests were applied using data available in the state of Baden-Württemberg, which required higher maximum degrees and orders. For this reason, the tests were first applied over a smaller area with an opening cap angle of 0.5° ; this was done to have smaller number of unknowns and observations and to save time when the tests were applied. The results of this test validate ASCH in an integrated solution. Finally, a combined solution for the state Baden-Württemberg with a maximum degree and order of 300 was applied.

The convergences of the solution as well as the RMSE of the observations were studied. The reliability of the models is also tested by examining reference points that were not used in the adjustment. These points were predicted using the official height reference surface (DFHRS-DB) of Baden-Württemberg. In addition, the ASCH predicted height anomalies in Baden-Württemberg were compared with the German quasigeoid (GCG2011).

6.1. ASCH modeling using height fitting points

In Baden-Württemberg, 129 height fitting points were available. These points had the projected coordinates (E, N, h, H) according to the DHDN system. The easting and northing have been transformed from the DHDN system to the ETRF89 system by means of CoPaG database of Germany with 3-5cm accuracy (www.geozilla.de). These points are distributed over the state of Baden-Württemberg (see fig 6.1), and have a height accuracy of 7mm holding for the normal height (H^*) and the ellipsoidal height (h), respectively.

The ASCH are used to model the gravitational potential of the Earth. The height anomalies of the height fitting points are transformed to gravitational potential V . The gravitational potential V parameterization related to the height fitting points reads:

$$V_i = \frac{GM}{r} \sum_{k=0}^{k_{max}} \left(\frac{R}{r} \right)^{n(k)} \sum_{m=0}^k (C'_{km} \cos m\alpha + S'_{km} \sin m\alpha) \bar{P}_{km}(\cos \vartheta) + \Delta V \quad (6-1)$$

The transformation of V using the height fitting points in integrated approach reads:

$$V_i = U_p + \gamma_q (h - H) - \Omega \quad (6-2)$$

Here, U_p is the ellipsoidal normal potential in equation (5-24). Ω is the centrifugal potential in equation (5-28). γ_q is the ellipsoidal normal gravity at the ellipsoidal height on the telluroid (see figure 5.4).

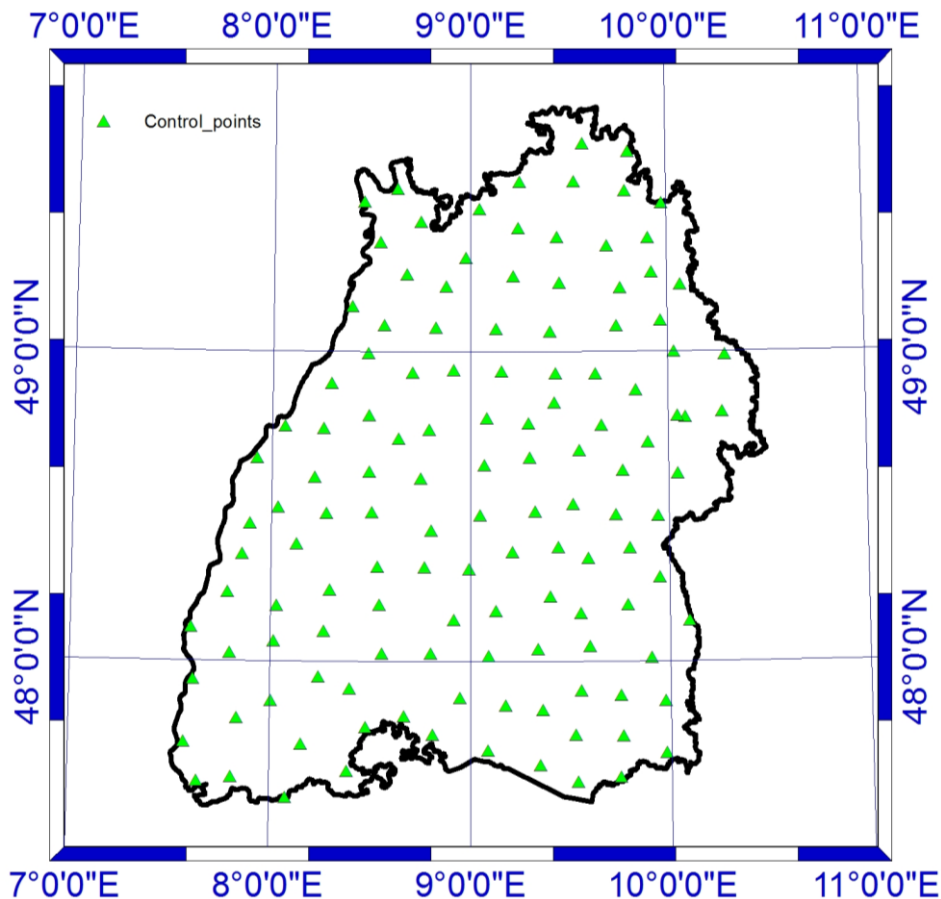


Figure (6.1): The distribution of the height fitting points in the state of Baden-Württemberg.

The height fitting points were used to calculate the gravity potential model using ASCH in the study area. These points were sufficient only to obtain an ASCH model with a maximum degree and order of 10. The calculated height anomalies predicted by the ASCH models by means of the height fitting points only are shown in figure (6.2).

To test the validity of the model, the ASCH was used to predict the height anomalies over 15000 topographic test points. The points have known height anomalies by means of the DFHRS-DB, which is the official reference surface in Baden-Württemberg with accuracy of 1cm. The results show that the maximum difference between the height anomalies by the ASCH model and the height anomaly by the DFHRS-DB was 1.7m (see figure 6.3).

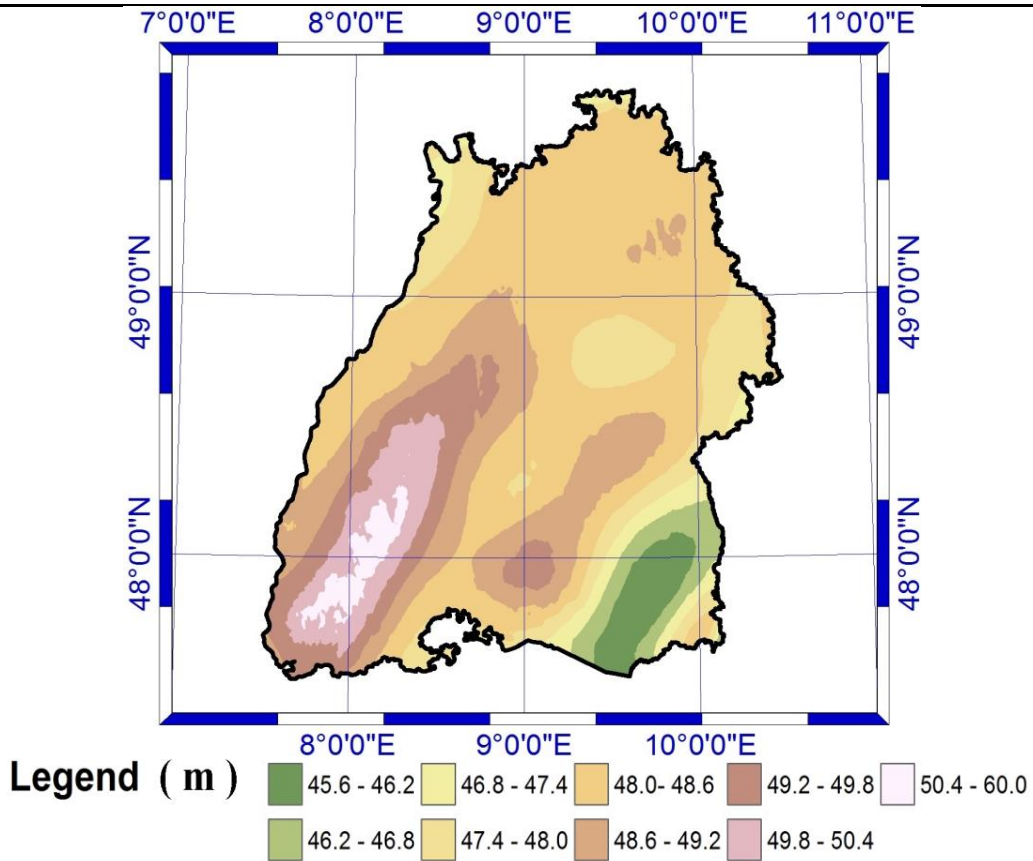


Figure (6.2): The calculated height anomaly over the state of Baden-Württemberg using ASCH with maximum degree and order of 10.

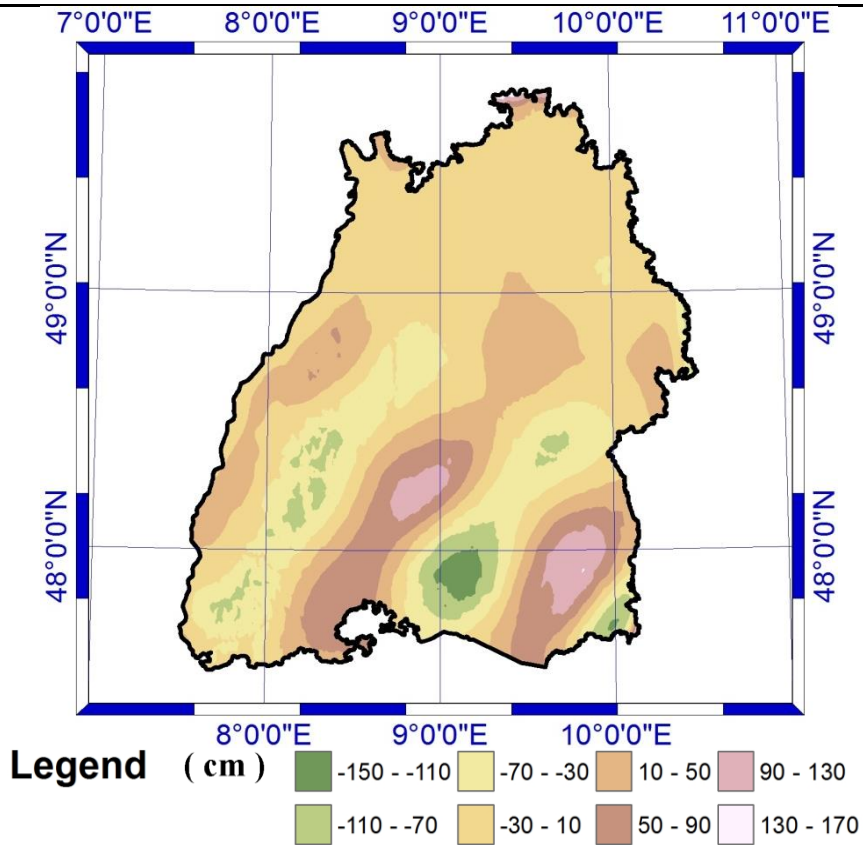


Figure (6.3): Difference between the reference DFHRS-DB and the ASCH model using height fitting points only.

6.2. The combination of height fitting points and global models

To enhance the accuracy the ASCH models in chapter (6.1), a higher maximum degree and order is needed. The higher degrees and orders require more observations as input in the adjustment to find the ASCH coefficients. These additional observations can be obtained from the available global models (e.g. EIGEN05c and EGM2008). These models first have to be transformed to a local ASCH models. The observation equations in the common adjustment of the EGM transformed ASCH coefficients are given in equations (5-65) to (5-67).

The problem with such data is that the height fitting points do not have a direct potential value; rather, they represent the height above a given reference equipotential surface W_E . The height anomaly calculated by the global models is referred to as a reference ellipsoid (e.g. GRS80). The GRS80 reference ellipsoid has a reference potential value of $W_0 = U_0 = 62636860.850 m^2 s^{-2}$. In contrast, the height fitting points in Baden-Württemberg are referred to the NAP reference point (Normaal Amsterdam's Peil), which has a reference potential value of $W_E = 62636857.280 m^2 s^{-2}$ (Ihde et al., 2007). The difference between the reference potential value of the NAP and the reference normal potential of the GRS80 ellipsoid is $\Delta W = W_E - U_0 = 3.57 m^2 s^{-2}$. The value of ΔW has to be modeled in the adjustment as an additional unknown related to height fitting points observation equation (6-1).

To test the utility of the combination of the global SH gravity models transformed to ASCH models with the height fitting points, two models (EIGEN05c and the EGM2008) were used to apply these tests. The global gravity models were transformed to local ASCH models as explained in Chapter (4). At this stage, height anomalies (or equivalently the potential values Grids from global models) were predicted with a 2km spatial resolution in 3 discrete layers with ellipsoidal heights of (h=0, h=750 and h=1500) with the given covariance matrix using error propagation.

The calculated height anomalies over the entire state of Baden-Württemberg using a combination of height fitting points and the EIGEN05c are shown in figure (6.4). The height anomalies in Baden-Württemberg by the combined solution between the height fitting points and EGM2008 model height anomalies are shown in figure (6.5). The combined models were tested using 15000 topography points. These points had given height anomalies from the DFHRS-DB of Baden-Württemberg. The differences between the DFHRS-DB and the EIGEN05c with height fitting points in a combined solution are shown in figure (6.6). The use of the EIGEN05c model introduced errors up to 45cm. The differences between the DFHRS-DB and the combination of EGM2008 with height fitting points are shown in figure (6.7). The use of EGM2008 significantly improved the solution in comparison to the EIGEN05c. The maximum residual of the height fitting points was 3 cm, while the RMSE were less than 5mm. The standard deviations of the calculated ASCH coefficients and the degree variances of the EGM2008 and the height fitting points combined solution are shown in figure (6.8).

Table (6.1): The results of ASCH modeling of height anomalies as compared to DFHRS-DB.

Parameter	FP+EIGN05c	FP+EGM2008
Nmax	80	80
RMSE (cm)	16	1.8
Max (cm)	43	3.4
Min (cm)	-41	-4.4

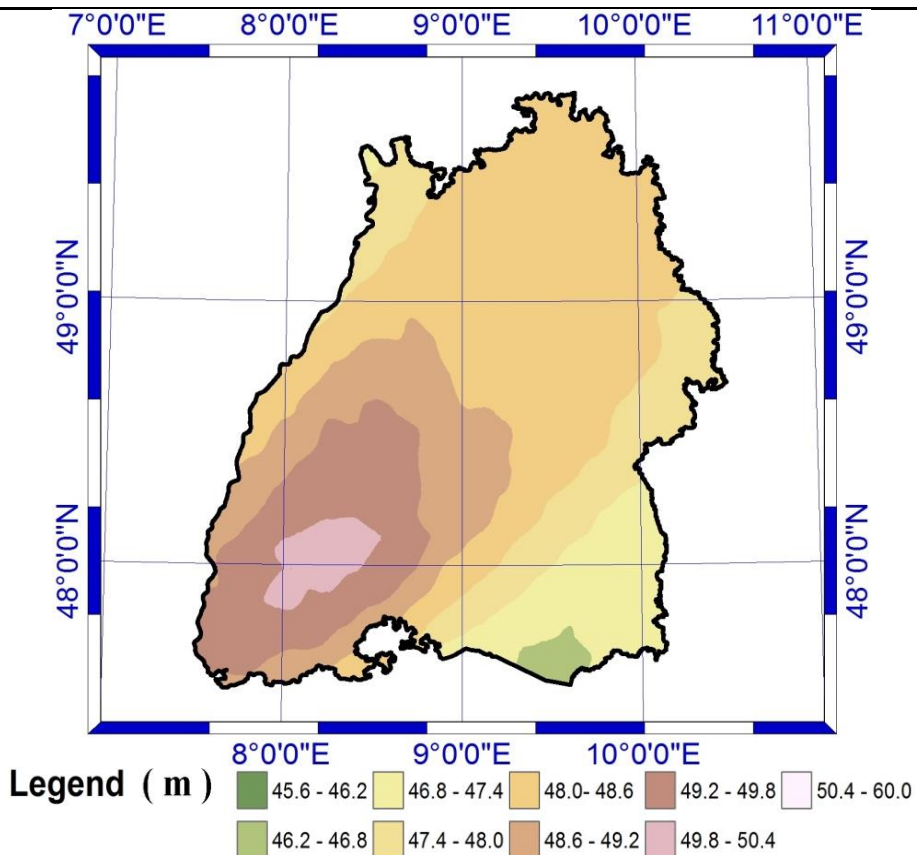


Figure (6.4): The height anomalies in BW by ASCH using the combining height fitting points and the EIGEN05c.

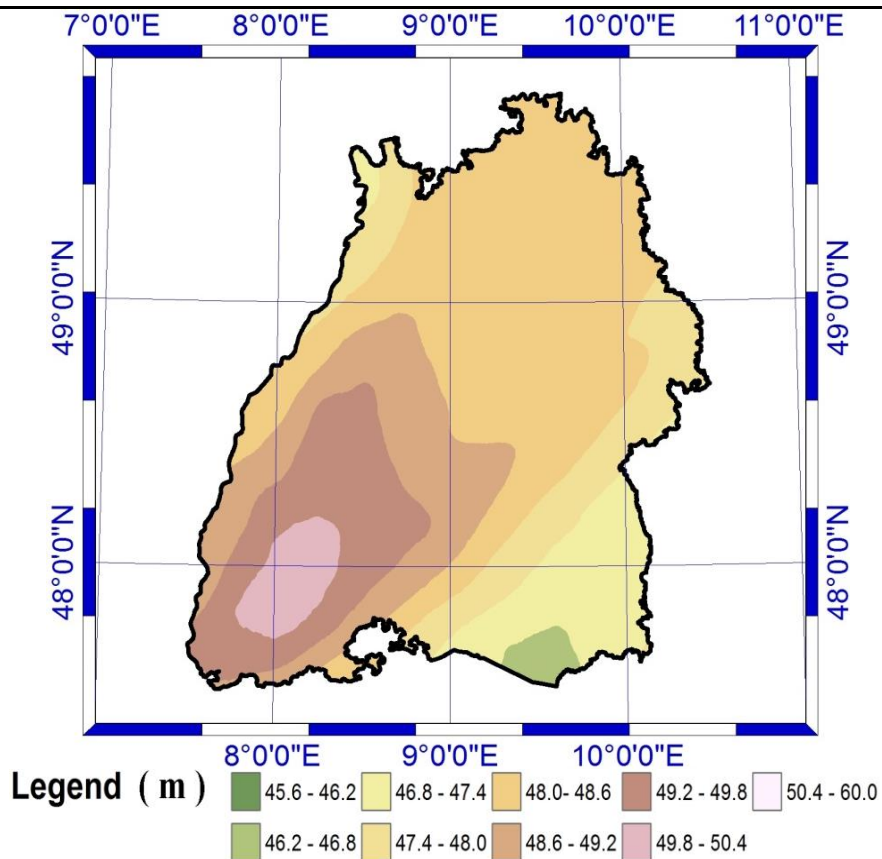


Figure (6.5): The height anomalies in BW by ASCH using the combining height fitting points and the EGM2008.

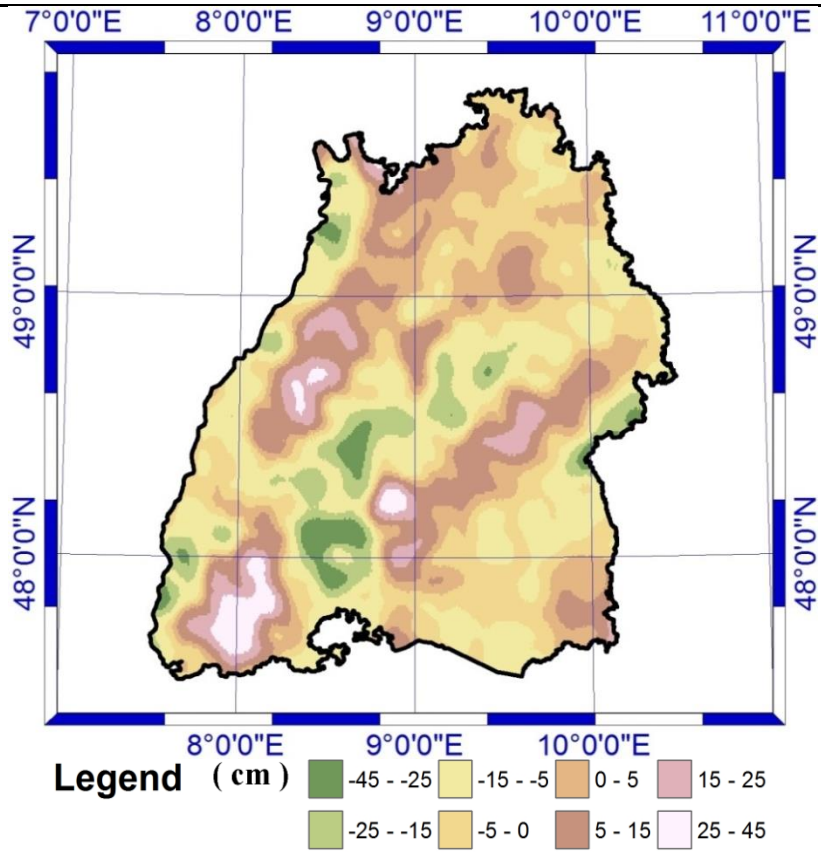


Figure (6.6): The differences between DFHRS-DB and the combination of height fitting points and EIGEN05c.

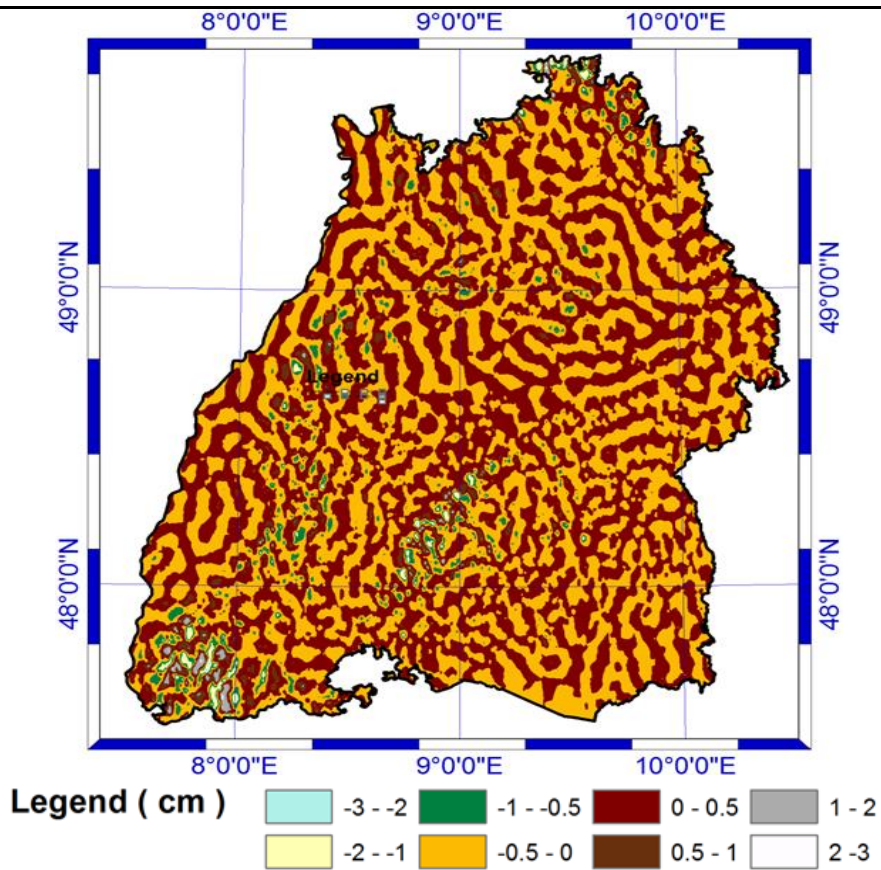
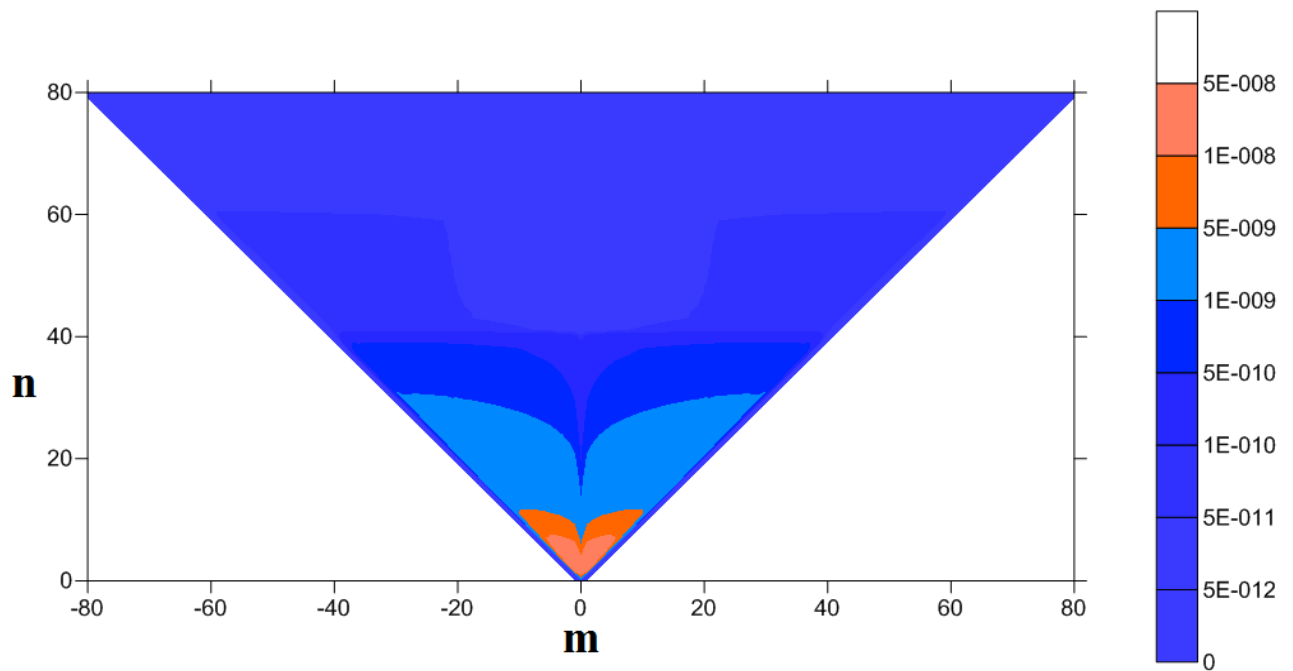


Figure (6.7): The differences between DFHRS-DB and the combination of height fitting points and EGM2008.

a. The standard deviations of the coefficients



b. The degree variances of the coefficients

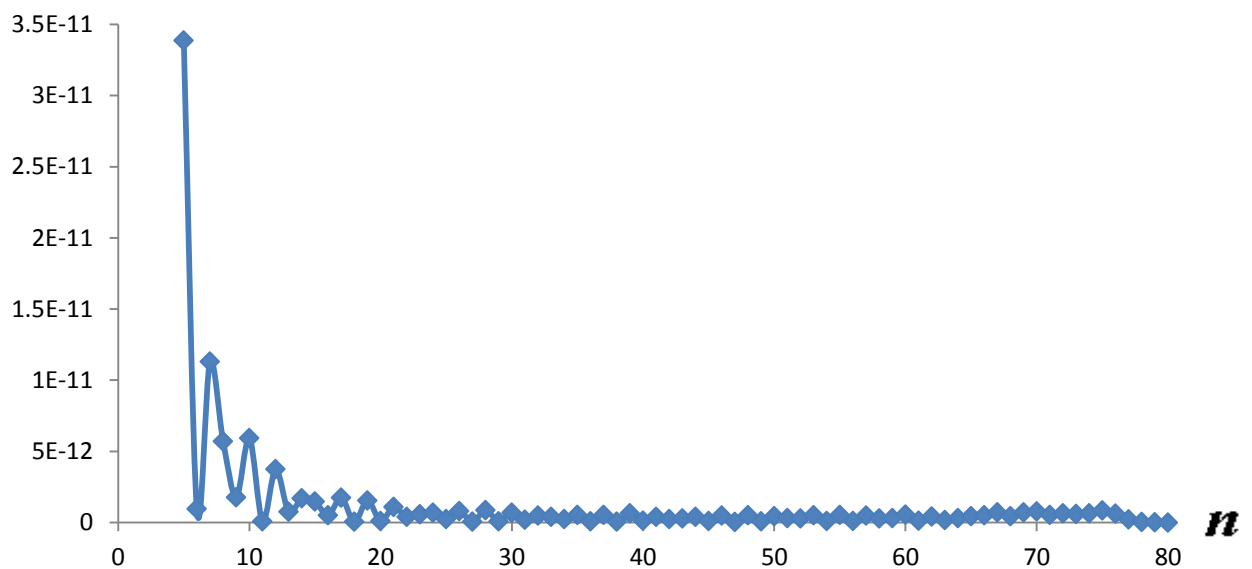


Figure (6.8): The standard deviations and the degree variances of the ASCH coefficients for Baden-Württemberg using combination of EGM2008 and height fitting points. In figure (a) the negative sign represents S_{nm} and the positive sign represents C_{nm} .

6.3. Gravity prediction by means of ASCH

To test the accuracy of the gravity data predicted with the ASCH model, the EIGEN05c model was used. The resulting ASCH models were used to predict not only the gravitational potential (or equivalently the height anomalies), but also the gravity values. The 15000 topographic test points from Baden-Württemberg were used with the radial gravity component predicted by means of the original EIGEN05c model represented using the ordinary SH. These gravity data are compared to the gravity data predicted by the same model transformed to a local ASCH model according to the transformation principle explained in chapter (4).

The solution was applied with different maximum degrees and orders, in order to determine how the accuracy of the predicted gravity data converges with the change of the maximum degree and order. The applied maximum degrees (N_{\max}) were 30, 45 and 80. The results by $N_{\max}=30$ had errors of up to ± 70 mGal, see figure (6.9). These results were enhanced to a maximum error of better than ± 30 mGal with $N_{\max}=45$, see figure (6.10). Accuracy better than ± 15 mGal was achieved by using $N_{\max}=80$ in figure (6.11). Comparing these results with the accuracy of the height anomalies, the predicted gravity produced by the ASCH model using height anomalies only need much higher degree and order to get accuracy of sub-mGal. In contrast, the accuracy of the height anomalies were less than 5mm with $N_{\max}=80$, see figure (6.12).

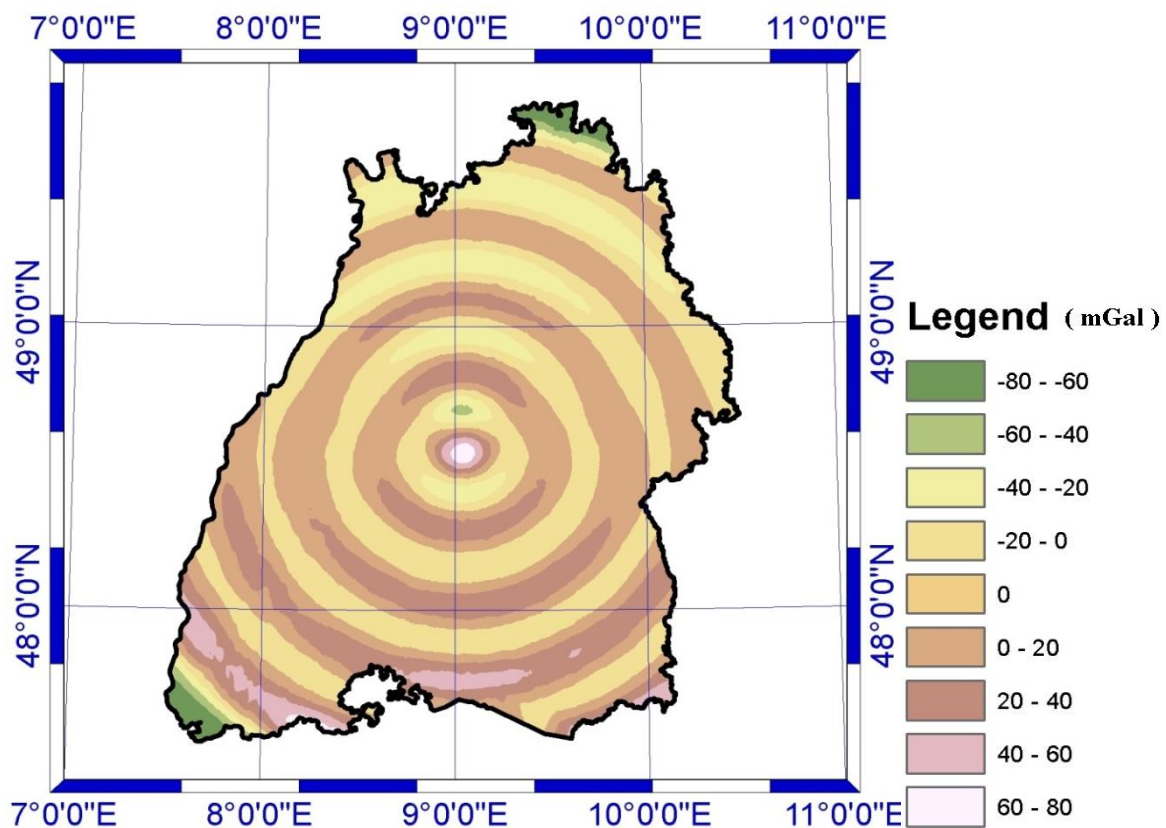


Figure (6.9): Gravity values differences between original EIGEN model predicted values and the ASCH model with maximum degree and order of 30.

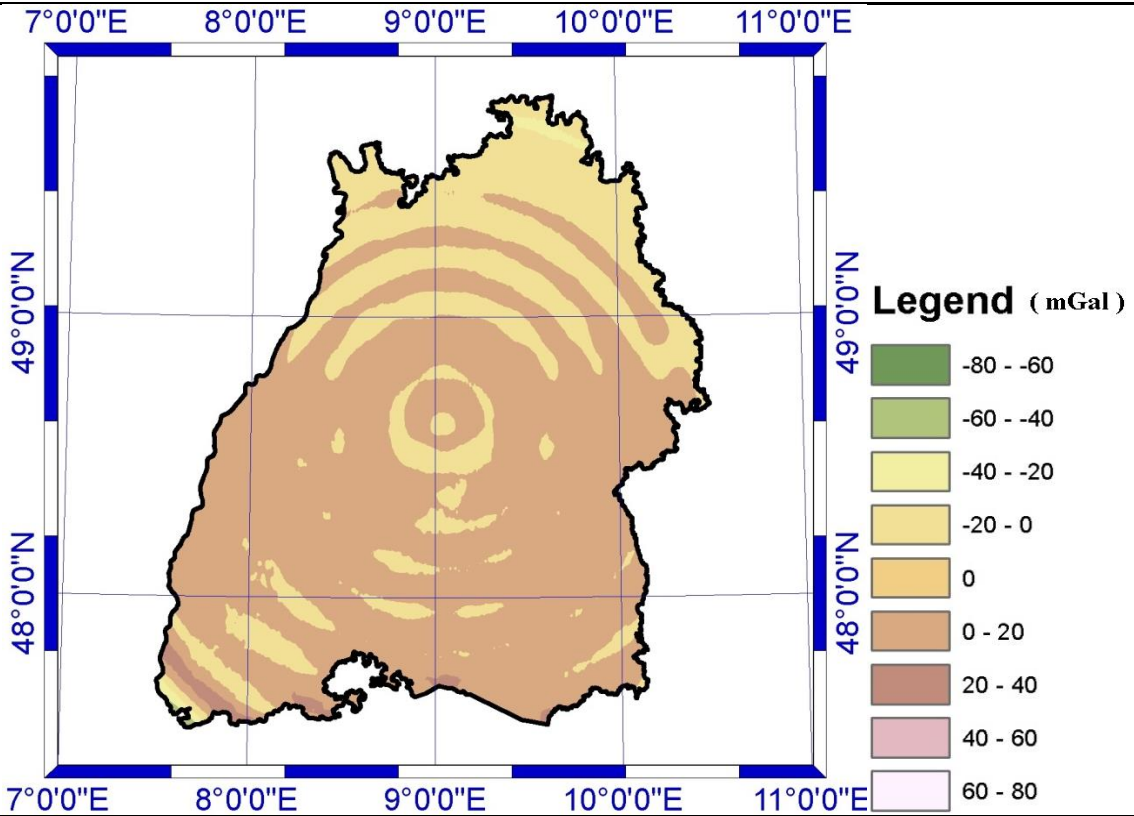


Figure (6.10): Gravity values differences between original EIGEN model predicted values and the ASCH model with maximum degree and order of 45.

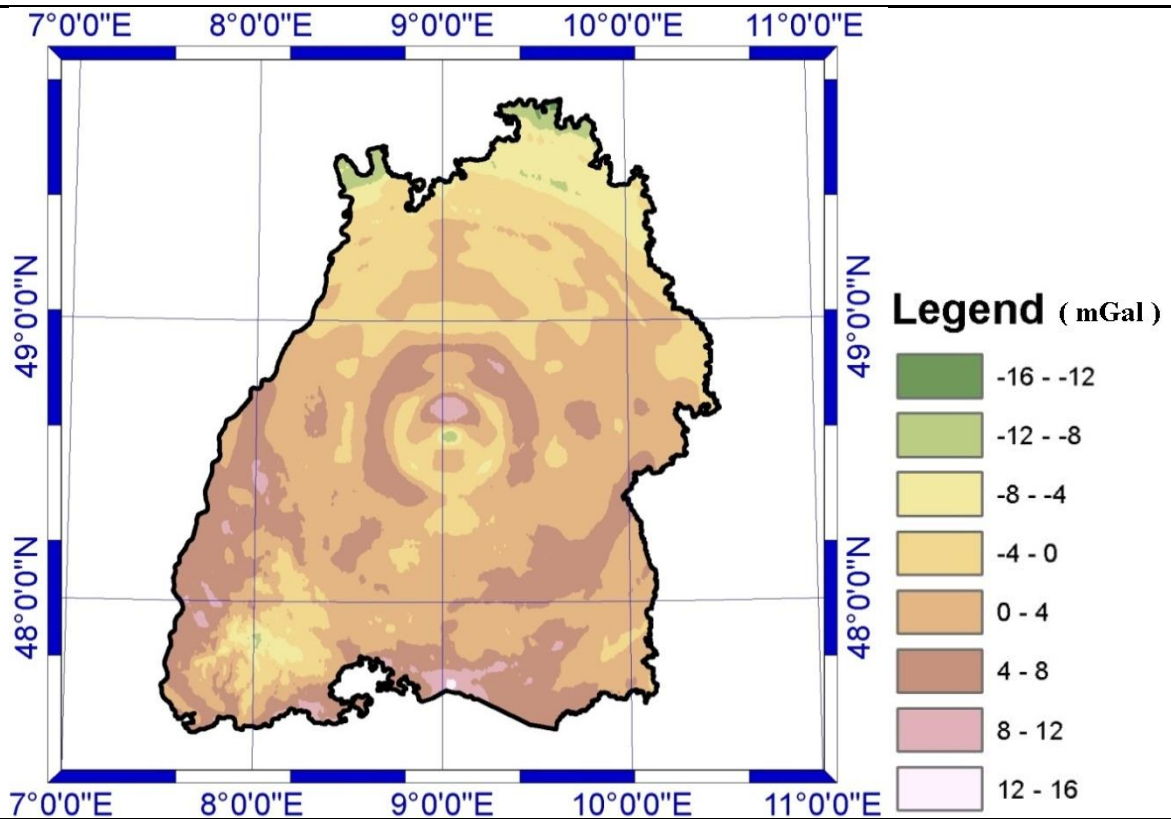


Figure (6.11): Gravity values differences between original EIGEN model predicted values and the ASCH model with maximum degree and order of 80.

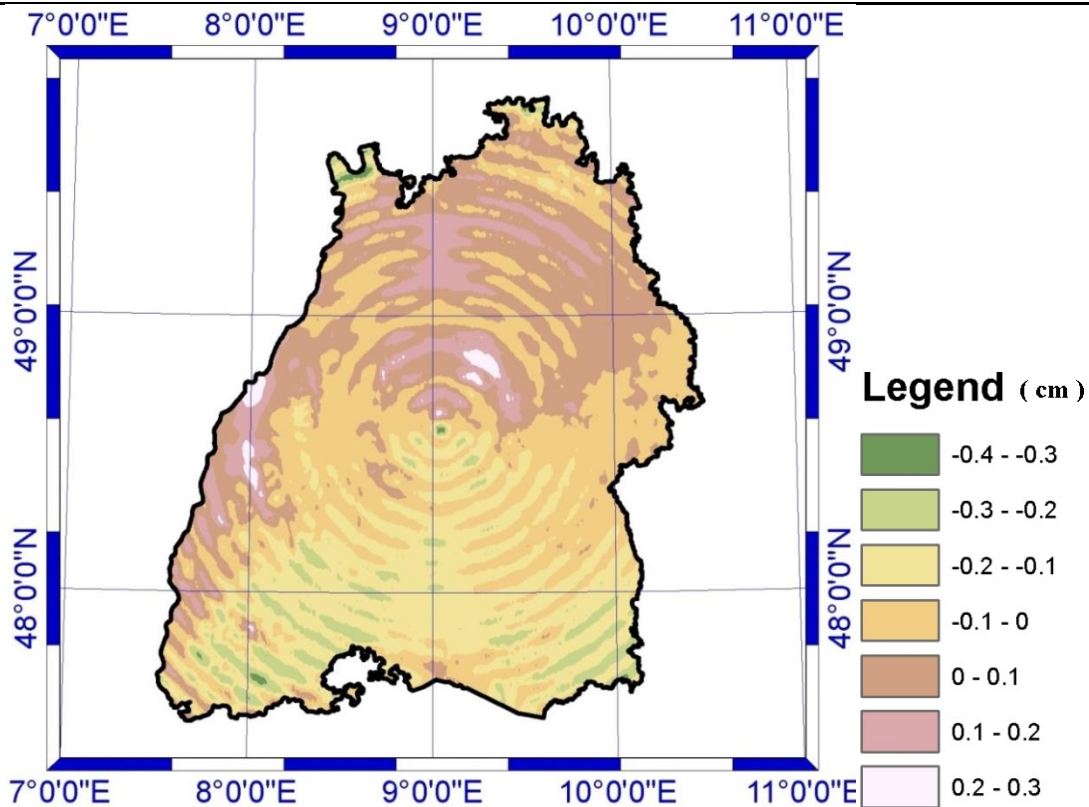


Figure (6.12): Height anomalies differences (m) between original EIGEN model predicted values and the ASCH model with maximum degree and order of 80.

The use of height fitting points only in the adjustment of ASCH models with a maximum degree and order of 10 did not provide any information about the gravity. Figure (6.13) shows the differences between the 15000 terrestrially measured gravity points with 0.01 mGal and the calculated gravity by means of the ASCH model. Higher degrees and orders have been applied with the support of global models, resulting in better modeling of gravity. Table (6.2) shows the accuracy achieved by different solutions of ASCH model. The results were obtained by comparing the calculated and the measured gravity; see the results in figure (6.13), figure (6.14) and figure (6.15).

The best results were achieved by combining the EGM2008 with the height fitting points, as the maximum error was within the range of -60 to 40 mGal. In contrast, the combination of EIGEN05c with height fitting points had errors within (-90 to 180 mGal). In all cases, the use of height anomalies only in the adjustment could not provide good accuracy of modeling the gravity compared to the measured gravity with accuracy of 0.01mGal.

Table (6.2): The results of ASCH modeling related to real gravity measurements.

Parameter	FP only	FP+EIGEN05c	FP+EGM2008
Nmax	10	80	80
RMSE (mGal)	420	43	17
Max (mGal)	1688	162	33
Min (mGal)	-1521	-74	-55

FP = height fitting points

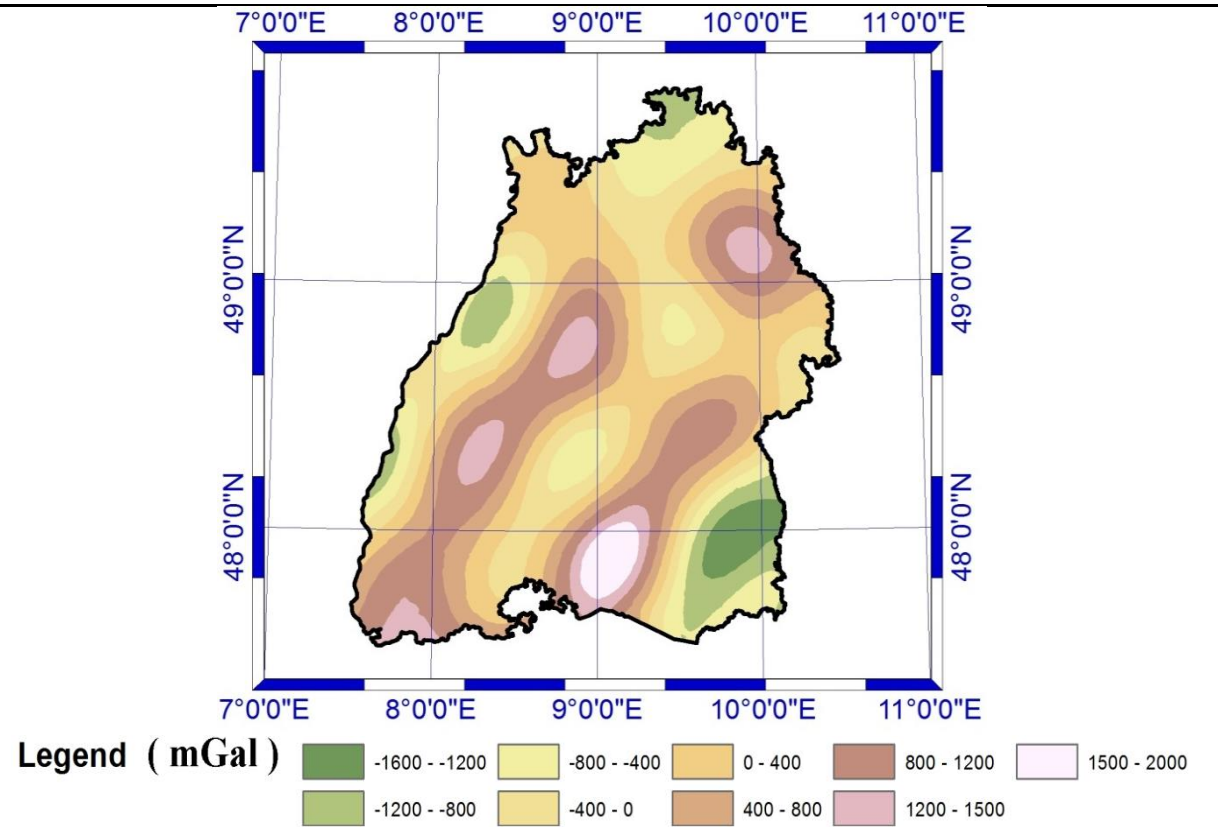


Figure (6.13): Gravity value using ASCH model depending on height fitting points only with maximum degree and order of 10.

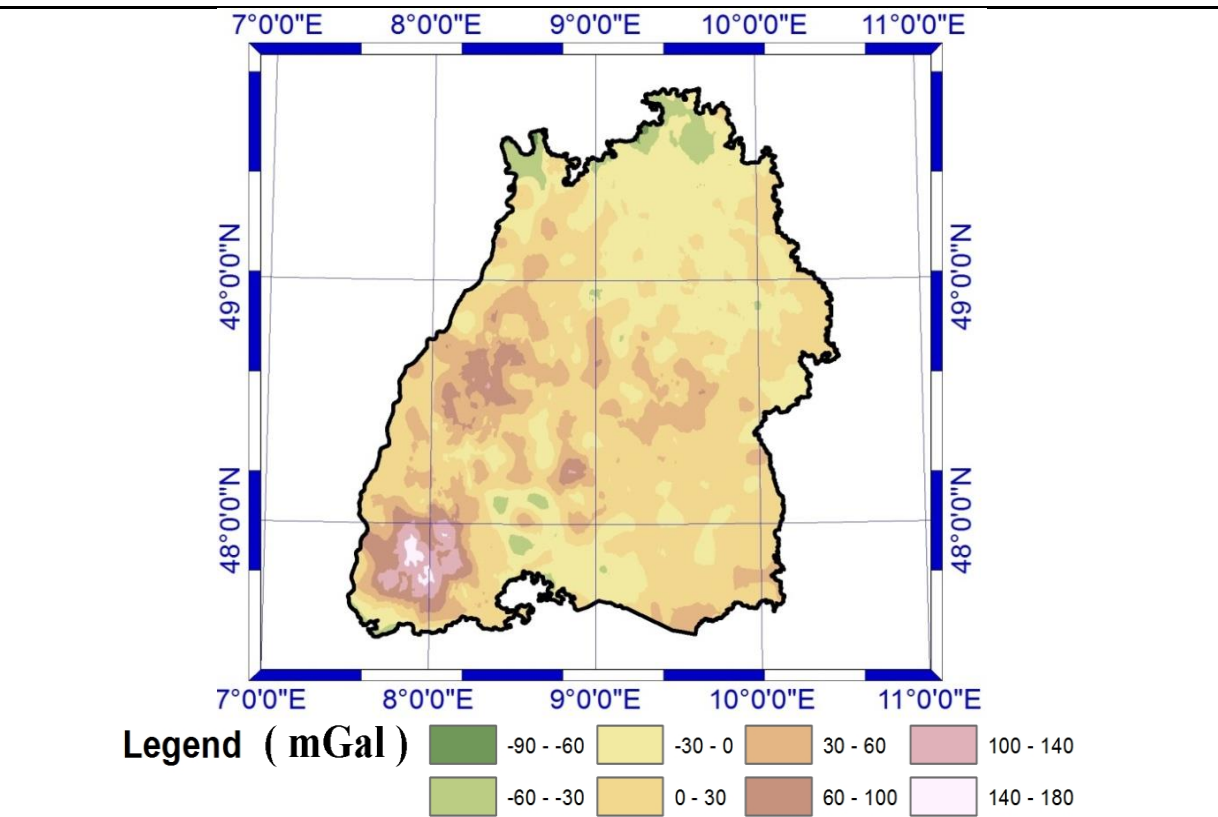


Figure (6.14): Gravity value using ASCH model depending on height fitting points combined with EIGEN05c model with maximum degree and order of 80.

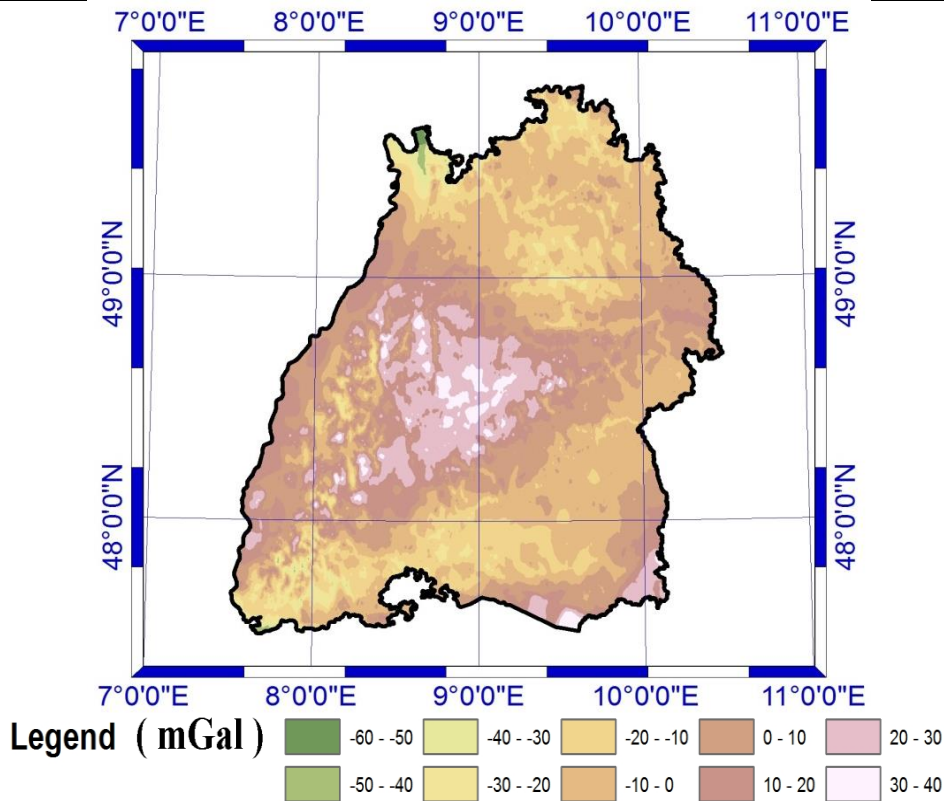


Figure (6.15): Gravity value using ASCH model depending on height fitting points combined with EGM2008 model with maximum degree and order of 80.

6.4. ASCH modeling using terrestrial gravity observations in the integrated approach

The 15000 terrestrially measured gravity points in the study area have a measurement accuracy of 0.02 mGal as a part of the Germany gravity network (DHSN96: Deutsches Hauptschwerenetz 1996). These points, however, were measured over decades, resulting in a reduced average accuracy of approximately 0.05 mGal (Torge, 2001).

The gravity related to the mass of the Earth is modeled by ASCH. The centrifugal parts of the gravity have to be reduced. As the ASCH are presented in a spherical coordinate system, the measured observations have to be transformed from the LAV-system to the $LGV_{Spherical}$ using the transformation steps in equations (5-10) through (5-19). Deflections of the vertical in the north-south direction (η) and the east-west direction (ξ) are required as input in equations (5-10) and (5-11). The values of (η) and (ξ) were obtained from the DFHRS-DB (the official height reference surface of Baden-Württemberg with 1cm accuracy).

As discussed in chapter (5.2.1), and after applying the transformations to the terrestrial gravity values g , the observation equation is then only the radial component of the transformed gravity vector. The tangential components of the gravity are not used as observations in the adjustment, since they are much too sensitive to the deflections of the vertical. As an example, the rule of error propagation was applied for the gravity values. Assuming the deflections of the vertical have a standard deviation of 1 arc second, this could produce errors in the tangential components of the gravity up to 0.4 mGal. The resulting standard deviation in the radial component of the gravity was less than 0.001 mGal. This shows that the radial component can

be assumed to be free of errors related to the deflections of the vertical. The observation equation for the radial component of the transformed gravity vector reads:

$$g_r + v_i = -\frac{GM}{r^2} \sum_{k=0}^{k_{\max}} \left(\frac{R}{r}\right)^{n(k)+1} (n(k)+1) \sum_{m=0}^k (C'_{km} \cos m\alpha + S'_{km} \sin m\alpha) \bar{P}_{km}(\cos \vartheta) \quad (6-6)$$

The use of the 15000 terrestrial gravity points as the only input in the ASCH model adjustment enabled a solution up to a maximum degree and order of 120. The results obtained by applying different degrees and orders of the adjustment are shown in table (6.3). The results of adjustment introduced a RMSE of 0.42 mGal. The maximum residual were 3.87 mGal and the minimum is -4.26 mGal (see figure 6.16). This accuracy does not support the measurement accuracy. In addition, a very poor representation of the potential was achieved (or equivalently, the height anomalies). To achieve a higher accuracy, additional information and observations are required. In the following parts of this chapter, the combination of different observation types with terrestrial observations for ASCH modeling are tested and discussed.

Table (6.3): The results of ASCH adjustment using terrestrial observations only.

Maximum degree	RMSE (mGal)	Min residual (mGal)	Max residual (mGal)
20	5.35	-18.68	20.41
45	1.86	-12.92	13.74
60	1.12	-8.98	9.34
80	0.87	-6.29	6.83
120	0.42	-4.26	3.87

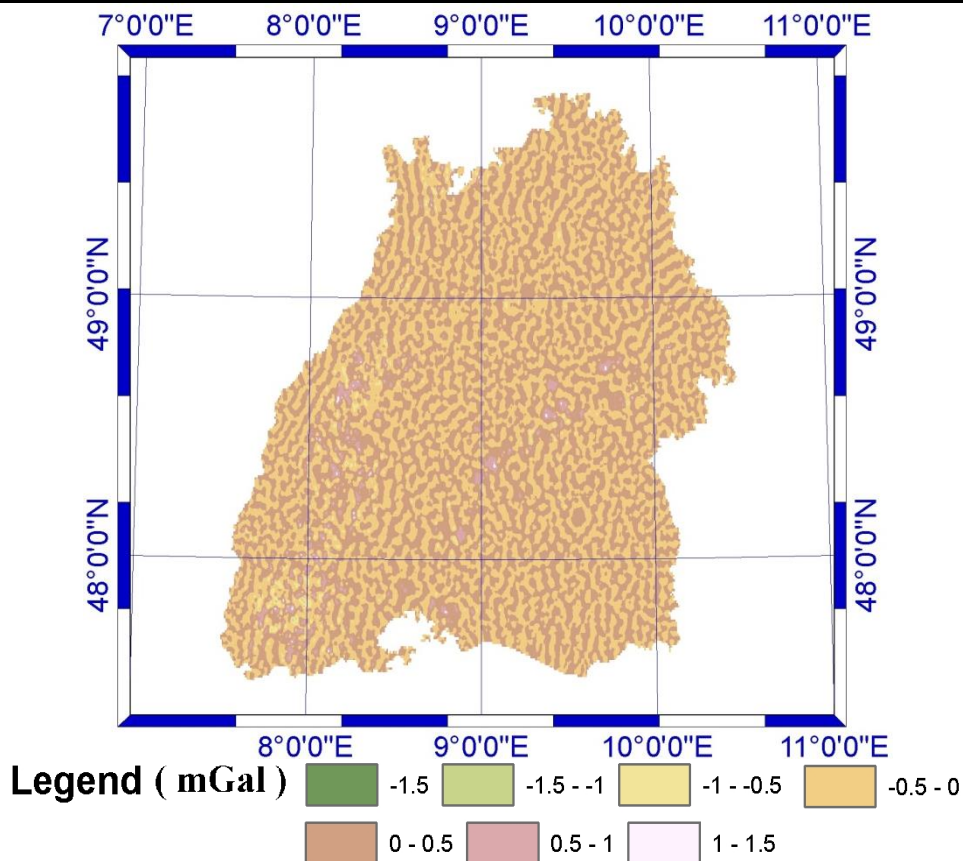


Figure (6.16): Residuals of ASCH adjustment using terrestrial gravity observations only.

6.5. Combined solution

The modeling of the gravity field with an accuracy of up to 0.01 mGal using the ASCH would require higher maximum degrees and orders. For this reason, 15000 terrestrial gravity points and the 129 height fitting points are not enough for this degree of accuracy, and more observations are required to overcome this problem. The solution is applied using a combination of different available data types, including the terrestrial gravity points, the height fitting points and the global gravity models.

In this principle, use of the global gravity models is advantageous. The global SH models were first transformed to local ASCH models as explained in chapter (4). These models provide very special advantages. First, they provide sufficient additional observations for successful modeling. Secondly, the EGM models are transformed from SH to ASCH with data gridded at different layers of height (see chapter 4.2.3). This supports the ASCH in the vertical direction. In contrast, the height fitting points and the terrestrial gravity points only define the ASCH model at the Earth surface.

The observation equations of the global models in the least squares solution using the combination of data are presented by the locally transformed ASCH coefficients with their full covariance matrix in chapter (4). The observation equations are the transformed coefficients (C'_{nm}, S'_{nm}). The observation equations are:

$$l_i + v_i = x_{iASCH_EGM} \quad (6-3)$$

The derivations of the observation equations of the terrestrial gravity points and the and the gravitational potential V transformed from height fitting points were explained in the previous chapters(5.2.1) and (5.2.2), respectively. Their observation equations are given in equation (6-4) and equation (6-5):

$$g_r + v_i = -\frac{GM}{r^2} \sum_{k=0}^{k_{max}} \left(\frac{R}{r}\right)^{n(k)+1} (n(k)+1) \sum_{m=0}^k (C'_{kmm} \cos m\alpha + S'_{km} \sin m\alpha) \bar{P}_{km}(\cos \vartheta) \quad (6-4)$$

$$V_i + v_i = \Delta W + \frac{GM}{r} \sum_{k=0}^{k_{max}} \left(\frac{R}{r}\right)^{n(k)} \sum_{m=0}^k (C'_{kmm} \cos m\alpha + S'_{km} \sin m\alpha) \bar{P}_{km}(\cos \vartheta) \quad (6-5)$$

Due the huge number of observations and unknowns in the least squares solution for the area of Baden-Württemberg, a smaller test area was first selected for the validations of ASCH in an integrated solution using a cap size of $\theta_{max} = 0.5^\circ$. In this area there are 33 height fitting points in addition to 3900 terrestrial gravity points. The EGM2008 model transformed to an ASCH model of this cap were used as additional observation equations according to equation (6-3). The least squares solution was applied with a maximum degree and order of 120. The results of the adjustment are shown in table (6.4).

Table (6.4): The results of ASCH modeling using combined solution.

Parameter	Height fitting points	Gravity points
Number of observations	33	3907
RMSE	0.55 cm	0.001 mGal
Maximum residual	1.52 cm	0.0413 mGal
Minimum residual	-1.96 cm	-0.0382 mGal

In the results shown in table (6.4), the residuals in gravity observations were mostly in the expected accuracy in comparison with measurement accuracy, as the average accuracy in the German gravity network is about 0.05 mGal (Torge, 2001). In addition, the assumed measurement accuracy is 0.01-0.02 mGal. There were only seven gravity observations with absolute residuals larger than 0.01 mGal. This is less than 0.2% of the gravity observation. In contrast, the height fitting points all had absolute residuals of less than 2cm.

The comparison of height anomalies calculated by means the ASCH model and the reference DFHRS-DB are shown in figure (6.17). It is clear that the differences in the internal area are less than 5cm, while higher residuals of up to 10cm exist on the boundary.

Based on the results shown in figure (6.17) and table (6.4), it can be concluded that the ASCH are valid to model the potential and the gravity using a combination of heterogeneous groups of data types. Based on these results, the calculations over the entire state of Baden-Württemberg can be applied, with the caveat that a cap size larger than the area of interest must be used to avoid the boundary problem. The computations over the entire study area with combined heterogeneous data are discussed in the chapter (6.6).

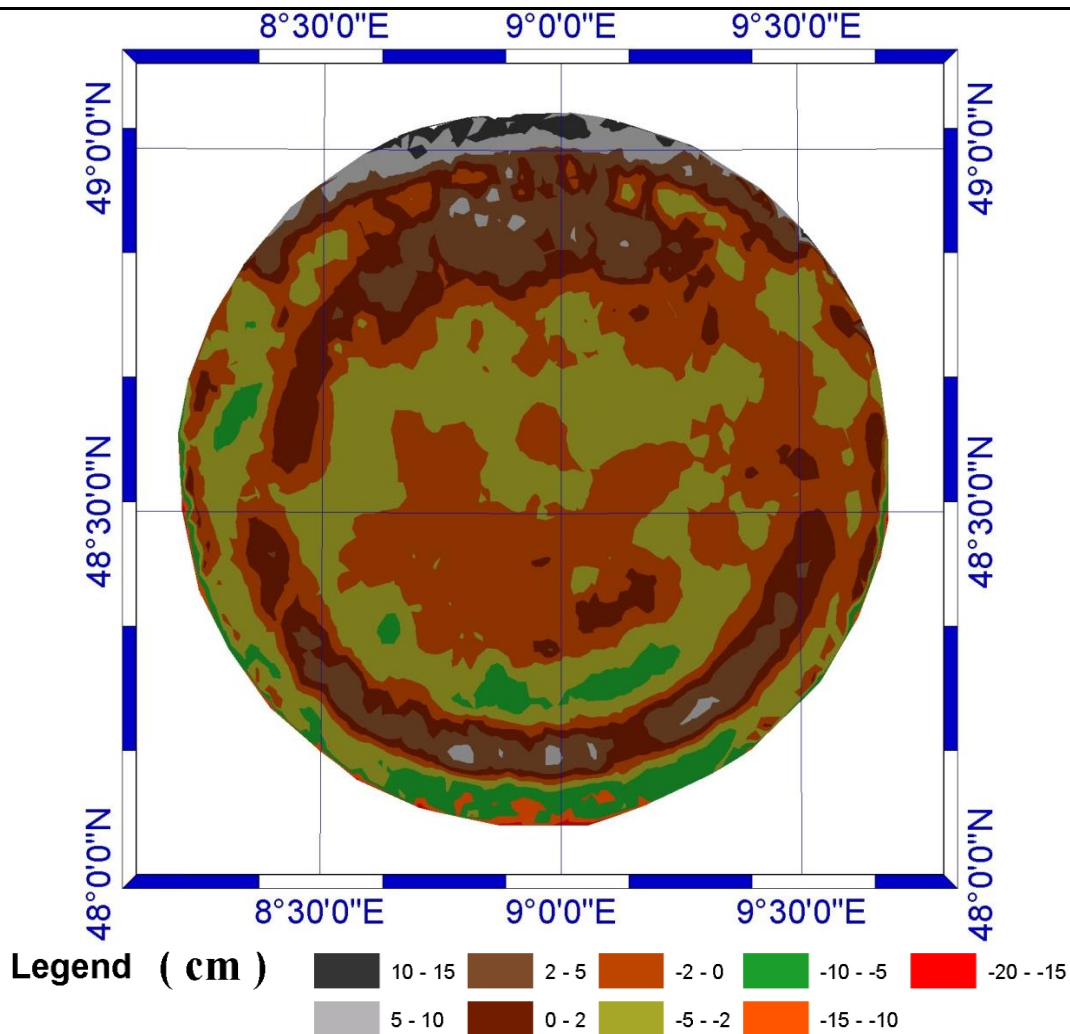


Figure (6.17): The comparison between the height anomalies by the DFHRS-DB and the ASCH model.

6.6. Combined ASCH model of Baden-Württemberg

ASCH modeling was applied in the state of Baden-Württemberg in Germany. There exist 130 height fitting points with known ellipsoidal height (h) and normal height (H^*) in the study area. Another group of available data is the terrestrial gravity network composed of nearly 15000 terrestrial gravity stations, which were measured over several years and even decades. The accuracy of these points varies between 0.01 mGal to 0.05 mGal (Torge, 2001).

Prior tests of the input data were applied. For height fitting points, the measured height anomalies $\zeta = h - H$ were compared with the reference DFHRS-DB of Baden-Württemberg. 129 points were in the range 0 to 3 cm, with one point having an error 1.25m. This point was removed as blunder. The terrestrial gravity points were tested for their positions, since there is no available reference data source for testing the values of the gravity with an accuracy of 0.01-0.05 mGal. The gravity points were compared with a Digital Terrain Model of Baden-Württemberg with height accuracy of better than 5cm. The test was directly applied by the Technicians/Engineers of the Land Surveying Department of Baden-Württemberg. Many points were found to have very large height differences, with some reaching an absolute error of up to 30m. 13694 points were ultimately chosen due to their acceptable positional accuracy. An aposteriori test was applied after the adjustment using the principle of data snooping. The summary of the blunders detection is given in table (6.5).

Table (6.5): The detection of the blunders in the observations for Baden-Württemberg observations.

Parameter	Gravity points	Height fitting points
Number of points	15002	130
Number of blunders using the apriori test	13694	1
Number of blunders using the aposteriori test	23	0
Number of observations used in the final solution	13671	129

Additional observations from the global gravity model in the adjustment were used from the EGM2008, which is one of the most recent of these. It has a degree and order of 2190. This model first had to be transformed to a local ASCH model as explained in chapter (4.3).

The calculations of the ASCH coefficients were finally applied using a combination of 13671 terrestrial gravity points, 129 height fitting points and EGM2008. The maximum degree and order of the calculations was 300. The selected cap opening angle was 1.7° according to the test results presented in chapter (4.2.2). The EGM2008 was first transformed to a local ASCH model with a degree and order of 300.

The final solution was applied by combining the locally transformed EGM2008 model with the terrestrial gravity points and the height fitting points in the adjustment using observation equations (5-36), (5-65) and (5-21). The average residual of the gravity data was $0.0032mGal$, the maximum gravity residual was $0.032mGal$ and the minimum residual was $-0.041 mGal$. The residuals of the terrestrial gravity observations are shown in figure (6.21). The residual of the height fitting points were less than 1 cm in most of areas in the study area. In the south-western part of the state, however, the residuals in some cases went up to 3 cm. Table (6.6) summarizes the residuals of the height fitting points and the gravity points.

Figures (6.18) and (6.19) show the relative frequency histograms of the height fitting points residuals and terrestrial gravity residuals, respectively. The shapes of the relative frequency histograms in figure (6.18) and (6.19) are approximately similar to the shape of the normal distribution curve, indicating that there are no systematic errors present in the observations.

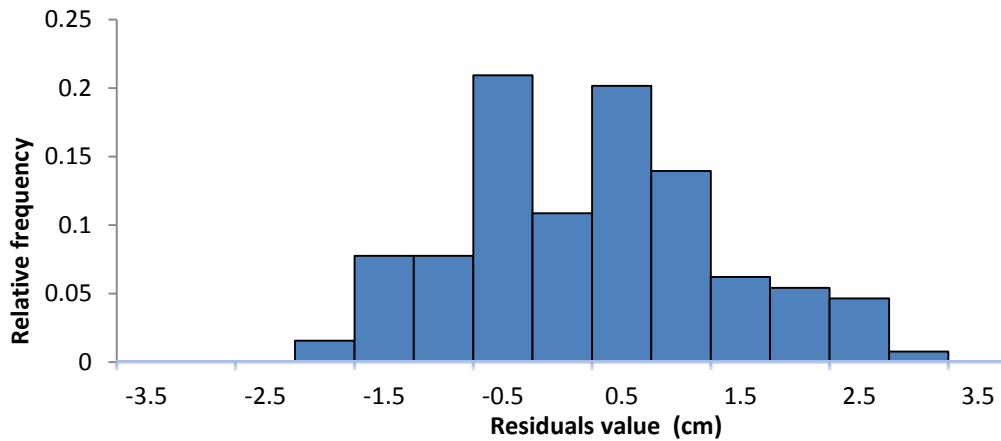


Figure (6.18): The relative frequency histogram of the height fitting points residuals.

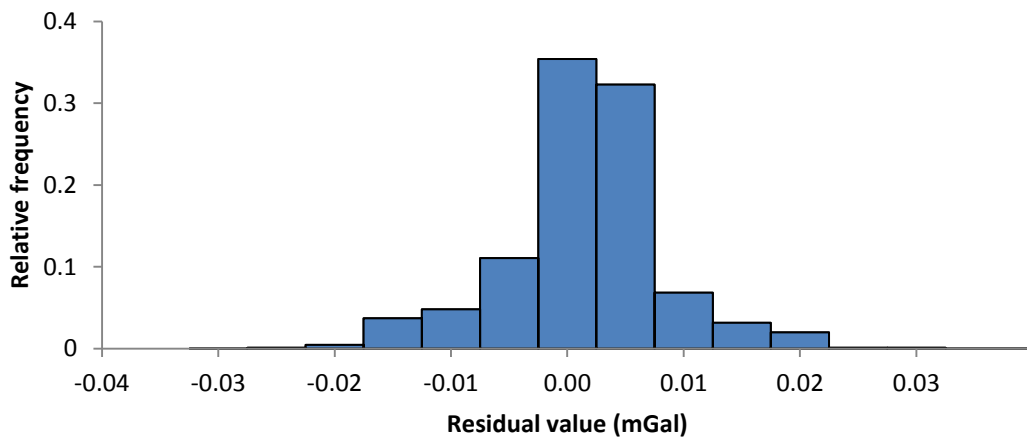


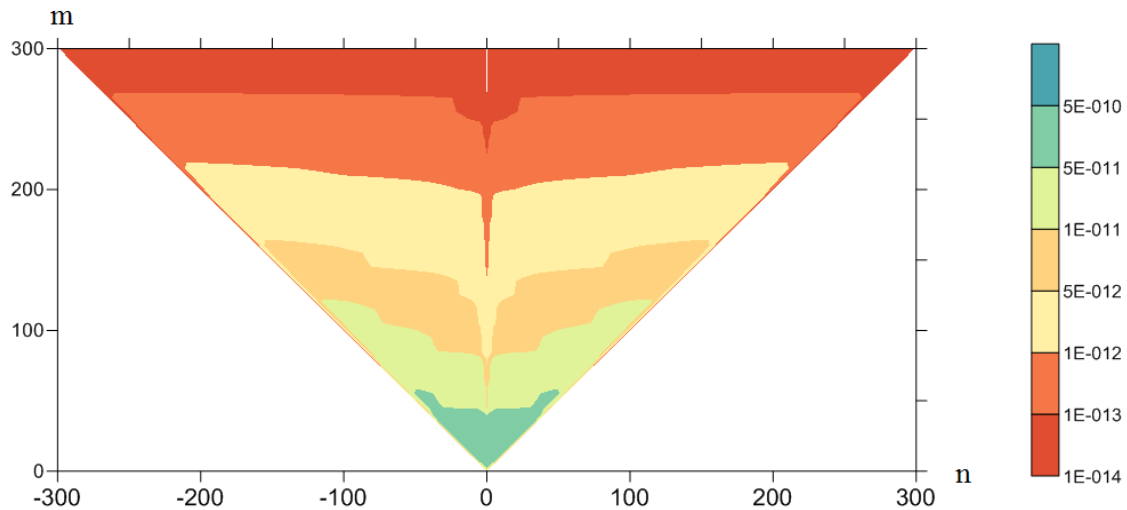
Figure (6.19): The relative frequency histogram of the terrestrial gravity points residuals.

Table (6.6): The results of the final adjustment of the combined ASCH model in Baden-Württemberg with maximum degree of 300.

Parameter	Gravity points	Height fitting points
Number of points	13671	129
RMSE	0.0032 mGal	0.8 cm
Maximum residual	0.032 mGal	3.3 cm
Minimum residual	0.041 mGal	-2.4 cm

Finally, the ASCH model was calculated. The solution with respect to the unknown ASCH coefficients and their related covariance matrix was successfully applied. The standard deviations of the ASCH coefficients using the combined solution with a maximum degree and order of 300 are given in figure (6.20).

a. Standard deviations of the ASCH coefficients



b. The degree variance of the ASCH model

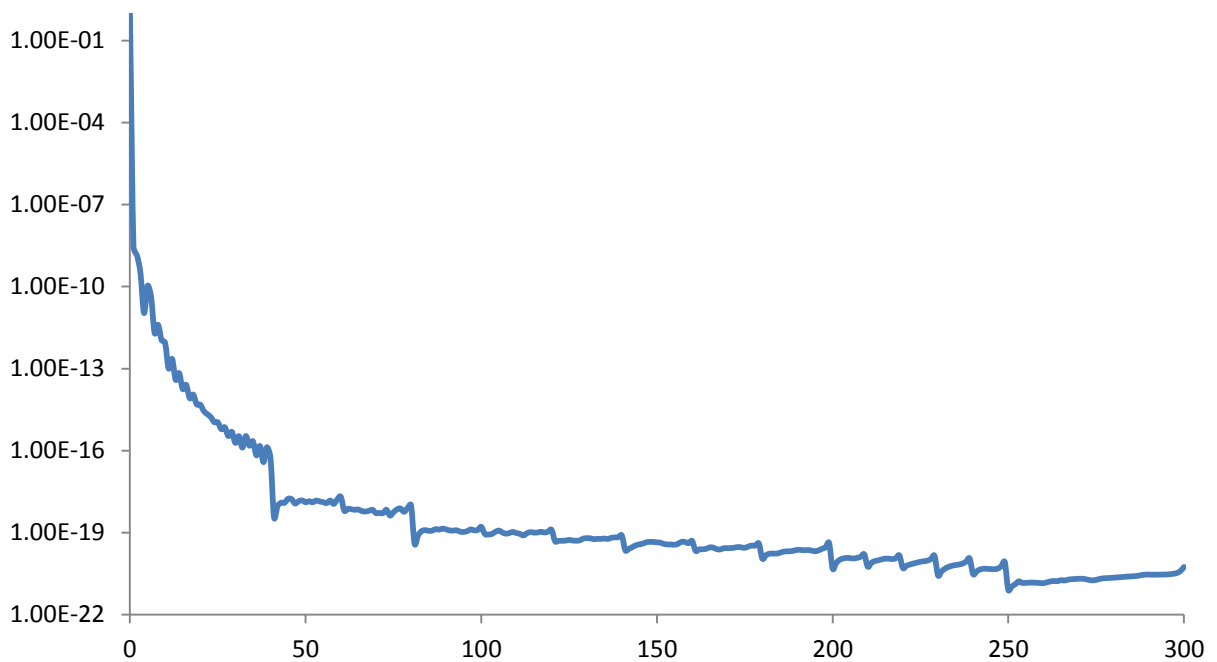


Figure (6.20): The standard deviations and the degree variances of the ASCH coefficients using the combined solution of the state of Baden-Württemberg. The negative sign represents S_{nm} and the positive sign represents C_{nm} .

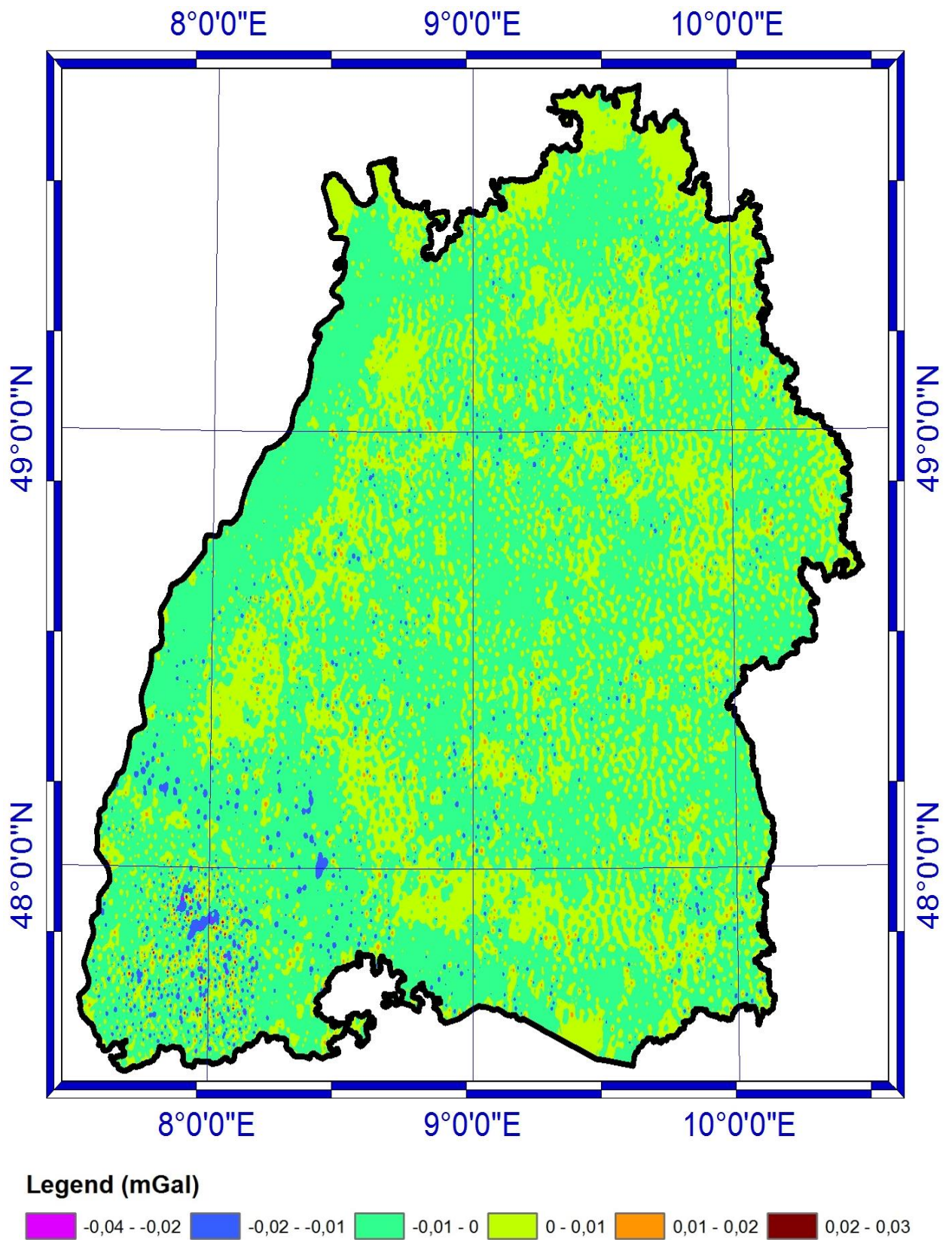


Figure (6.21): The residuals of the terrestrial gravity points in Baden-Württemberg.

To validate the ASCH model of Baden-Württemberg, 15000 topographic points distributed over the state were used as test points. The height anomalies of these points were calculated using the official height reference surface of Baden-Württemberg (DFHRS-DB) (see chapter 2.2.2). These served to validate the height anomalies predicted by the ASCH model of the integrated solution. The RMSE of the difference in height anomalies was 0.013m. The differences were less than 1 cm in the most parts of the state, but the maximum difference was less than 3cm in the south-western part of the state. This area is characterized by mountainous terrain with several deep valleys, and has the most varied topography in the state. Even the DFHRS-DB of Baden-Württemberg had residuals in the height fitting points up to 4cm in this area. Figure (6.22) and table (6.7) show the differences of the height anomalies between the DFHRS-DB and the ASCH model.

Table (6.7): The differences between the ASCH modeling and the DFHRS-DB in Baden-Württemberg.

Parameter	Value
Number of test points	14842
RMSE of the differences	1.3 cm
Maximum difference	3.1 cm
Minimum difference	-2.5 cm

The ASCH model was also compared with the German Combined Quasigeoid (GCG2011). The differences were in the range of (-6 to 5 cm) (see figure (6.23) and table (6.8)). By contrast, a comparison between the DFHRS-DB and the GCG2011 in Baden-Württemberg was applied, with differences between the two falling in the range of (-6 to 4 cm). The abstract of the results is shown in table (6.9) and figure (6.24).

Table (6.8): The differences between the ASCH modeling and the GCG2011 in Baden-Württemberg.

Parameter	Value
Number of test points	14842
RMSE of the differences	1.7 cm
Maximum difference	4.5 cm
Minimum difference	-6.4 cm

Table (6.9): The differences between the DFHRS-DB and the GCG2011 in Baden-Württemberg.

Parameter	Value
Number of test points	14842
RMSE of the differences	2.1 cm
Maximum difference	4.0 cm
Minimum difference	-6.0 cm

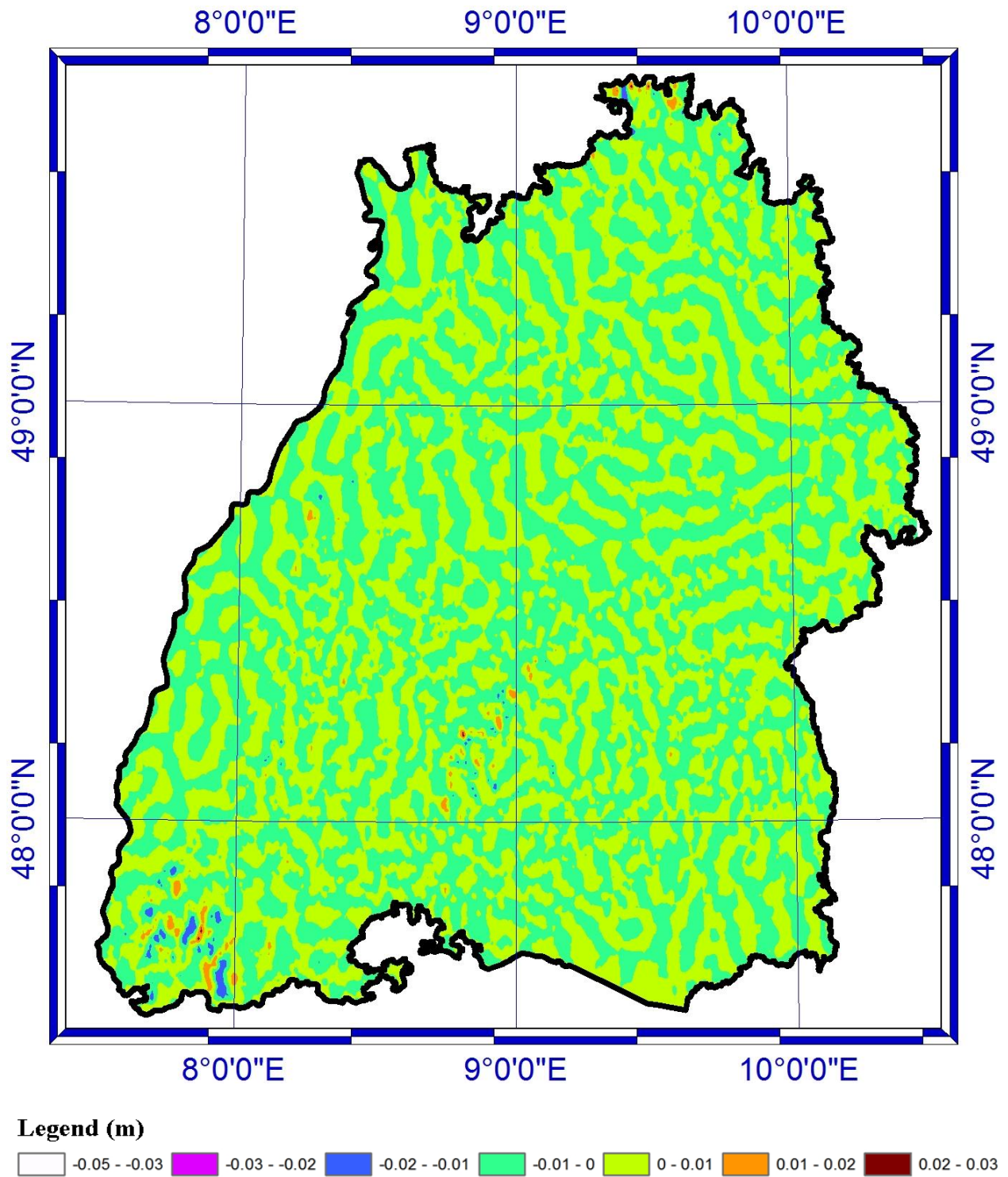


Figure (6.22): The difference between height anomalies using ASCH combined model and the 1cm-DFHRS-DB.

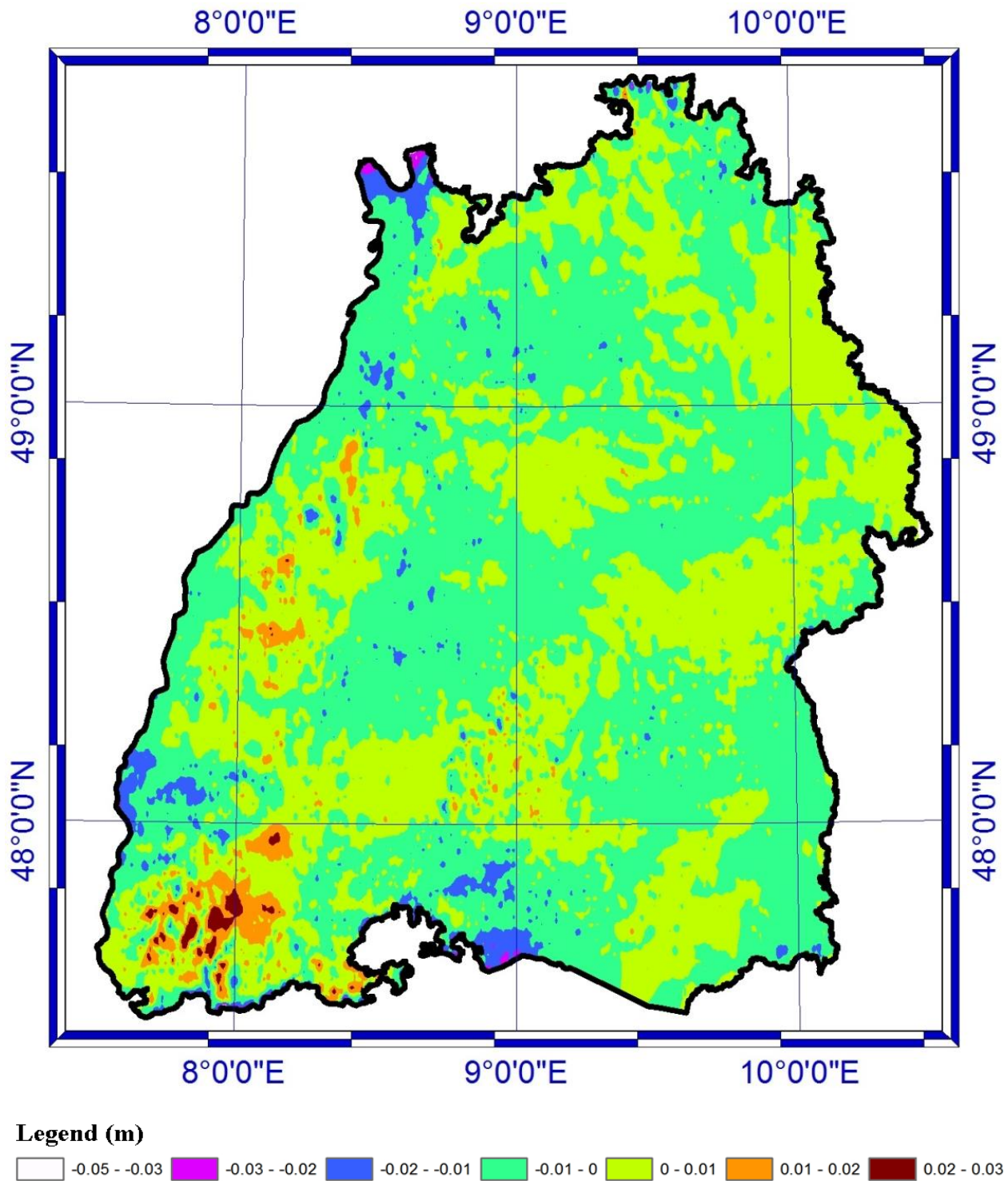


Figure (6.23): The difference between height anomalies using ASCH combined model and the GCG2011.

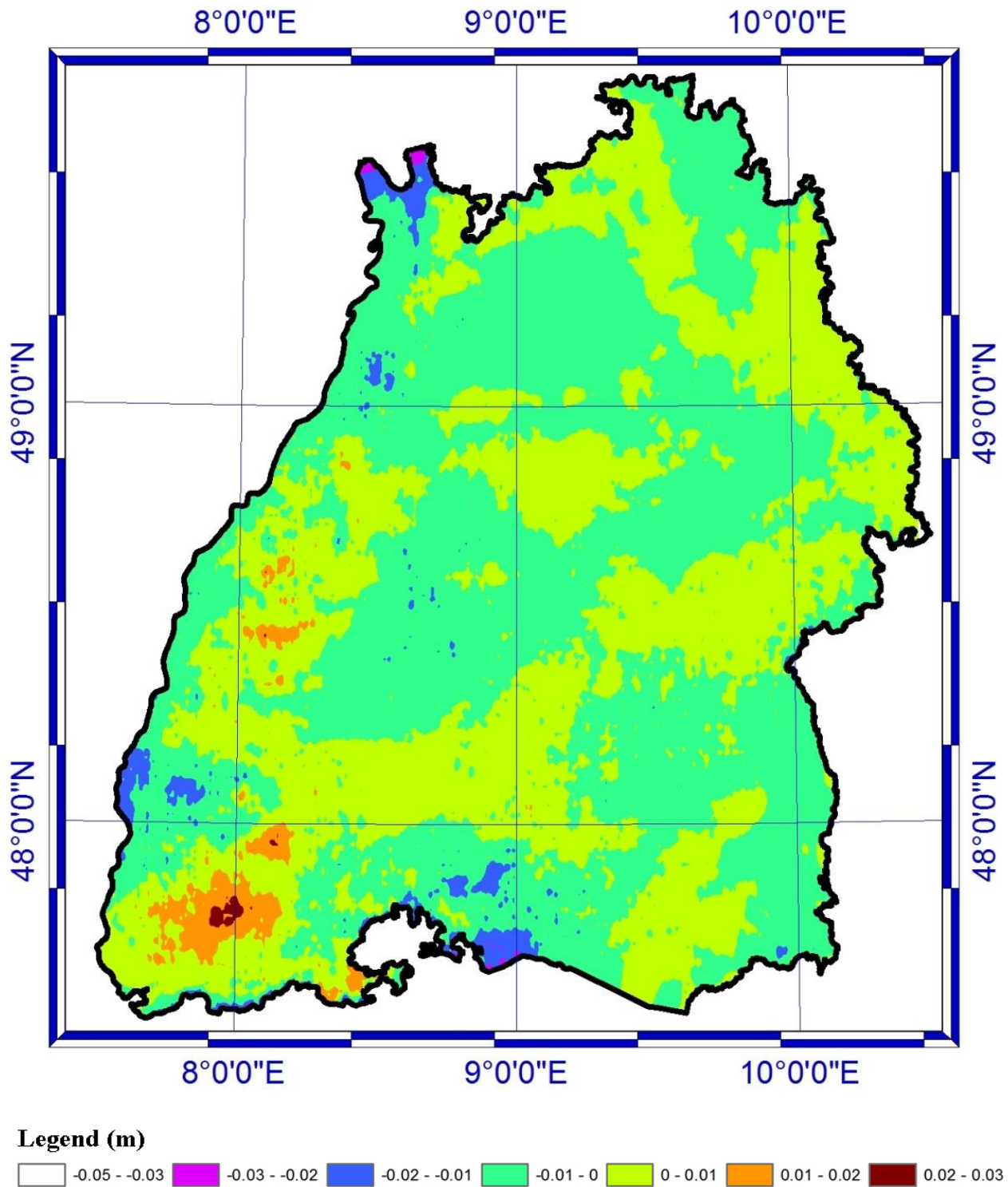


Figure (6.24): The difference between height anomalies using DFHRS-DB combined model and the GCG2011.

7. Outlook and conclusions

The objective of this thesis was to update and modify the existing SCH-modeling for local gravity and potential modeling applied in the DFHRS project at IAF of the Karlsruhe University of Applied Sciences (HS-Karlsruhe). This model was developed by Schneid (2006) and was based on the disturbing potential and related observational quantities (e.g. gravity anomalies, gravity disturbances, geoid heights, and the deflections of the vertical).

The current further development of SCH modeling of the DFHRS software is founded on the SCH introduced by Haines (1985) given in equation (3-2). They use the real degree integer order Legendre functions. The calculations of Legendre functions of real degree and integer order are introduced in chapter (3.1.2). Their calculations are iterative and not recursive compared to the normal integer degree and order Legendre functions. The implementation of SCH also requires the search for the roots of Legendre function according to boundary conditions given in equations (3-3a) and (3-3b). The calculations of the real degree Legendre functions and the search for their roots are time consuming processes. Furthermore, the related formulas are not consistently presented in geodetic literature. The use of the disturbing potential T in equation (2-57) in the calculations introduces the problem of the definitions of the reference surface as they are restricted to a specific reference ellipsoid. Also, numerical problems were found in the current version of SCH modeling in the DFHRS-software. These numerical problems appear when calculating SCH with maximum degrees and orders larger than 120. For this reason, a highly accurate solution for an area like Baden-Württemberg was applied by dividing the area to more sub-areas. This division introduces questions about the continuity along the borders and is generally insufficient due to over parameterizations. Here, a single SCH model was calculated for each sub-area separately.

In chapter (3), the different types and modifications of SCH were introduced. In addition, other types of carrier functions for modeling the potential of the Earth were briefly discussed, including ASCH. The concept of ASCH was validated so that they apply to Laplace's equation (Harmonic function) (see chapter 3.2). The ASCH harmonics have many advantages over the other types of SCH. One is that they do not need the search for the roots of Legendre function, since they can be calculated by a direct formula as given in equation (3-43). This saves times and errors due to approximations used in the different iterative algorithms or through the use of complicated algorithms to find the roots of Legendre functions of real degree and integer order are reduced. Another advantage is that Legendre functions of integer degree and order are applied, which have common and recursive formulas proved in most geodetic literatures related to the gravity field of the Earth.

A new method for mapping the global SH models to regional ASCH was presented and applied. The ASCH were used in Chapter (4) to transform the global gravity models represented by means of SH to a local area model. For example, the EGM2008 model represented by the SH of a maximum degree and order of 2190 could be modeled in the state of Baden-Württemberg by means of ASCH with a maximum degree and order of 80 as a first proof of concept. The geoid heights were compared by test points covering the entire state with a maximum difference of 5mm. To compare computer memory requirements, the EGM2008 spherical harmonic coefficients with their standard deviations to the maximum degree and order of 2190 (4 800 481 coefficients) were stored in a text file with the size of 240 MB; by contrast, the ASCH model with maximum degree and order of 80 (6561 coefficients) was stored in a text file with the size of 300KB. To implement ASCH with maximum degree and order of 80, a smaller number of

loops was needed to calculate the double summation to obtain the gravitational potential, the gravity or other related quantities using the model, saving considerable time and computer memory. For example, 15000 points geoid heights calculated using the original EGM2008 spherical harmonic coefficients by a single CPU-PC needed nearly one hour of calculation time, while the same points needed less than 5 minutes using the transformed ASCH model. The differences between the calculated height anomalies values using the original EGM2008 SH model and its transformed ASCH model were less than 5mm.

A new integrated approach, using ASCH as functional model of the Earth gravity field, was derived to implement the solution for the combination of heterogeneous data sets (e.g. terrestrial gravity data, height fitting point global gravity models). In chapter (5), the derivations of the observation equations as well the required reductions and transformations related to each set of data were presented. The results of different types of observations and the combination of different observations are explained in chapter (6). In a combined solution in the test area with maximum cap size of 0.5° , the RMSE in the height fitting points was less than 5mm and the maximum residual was 2cm. By contrast, the maximum RMSE in the terrestrial gravity observations was than 0.01 mGal with a maximum residual of 0.04 mGal (see chapter 6.5). These results prove the utility of ASCH for highly accurate gravity field modeling, Quasigeoid and Geoid computations in regional areas scalable to any size.

As the ASCH were proven for adequately modeling the potential of the Earth in an integrated solution in chapter (6.5), an ASCH model with accuracy of 1cm in the height anomalies was calculated using the combination of height fitting points and the EGM2008 in the state of Baden-Württemberg. The solution achieved 1cm accuracy using a maximum degree and order of 80. The results are shown in chapter (6.2). As the gravity data could be integrated with height fitting points and EGM2008 without encountering problems in a test area in chapter (6.5), the combined solution of the complete state of Baden-Württemberg achieved 1cm accuracy using a maximum degree and order of 300. The validation of the ASCH model in chapter (6.6) is explained in figure (6.22) and figure (2.23) by using the DFHRS-DB and the GCG2011 as reference models in the validation process.

Finally, it can be stated based on the results of the solutions shown in chapter (4) and chapter (6) that the ASCH can be properly used to model the gravity potential of the Earth and Quasigeoid and geoid computations regionally with high accuracy. Nevertheless, it is clear that the need to model gravity with high accuracy requires a significantly higher maximum degree and order when compared with the modeling of the height anomalies alone (or equivalently the potential). It must also be noted that the ASCH modeling encounters problems on the boundary, requiring application of the solution using an oversizing of the cap area with respect to the area of interest.

References

- Aledeld G. and Mayer G. (1993): The Cholesky method for interval data, *Linear Algebra and its Applications*, Vol.194 P.161-182, Elsevier Science Inc.
- Becker M. and Hehl K. (2012): *Geodäsie*, WBG-Verlag, Darmstadt, Germany.
- Breymann U. (2005): *C++ Einführung und professionelle Programmierung*, 8. Auflage, Carl Hanser Verlag, München-Wien, ISBN 3-446-40253-5.
- BKG - Bundesamt für Kartographie und Geodäsie –(2011): webpage - National Reference Systems Gravity, http://www.bkg.bund.de/nm_159878/EN/FederalOffice/Geodesy/RefSys/NatRefGrav/EN_Gravity_node.html , page visited July-2011.
- BKG - Bundesamt für Kartographie und Geodäsie –(2011): Quasi-geoid of the Federal Republic of Germany - The height reference surface of the Arbeitsgemeinschaft der Vermessungsverwaltungen der Länder (AdV), BKG, Germany.
- Chatfield A. (1997): *Fundamentals of High Accuracy Inertial Navigation*, Progress in Astronautics and Aeronautics Vol.174, American Institute of Astronautics and Aeronautics, Virginia.
- Denker H., Barriot J., Barzaghi R., Fairhead D., Forsberg R., Ihde J., Kenyeres A., Marti U., Sarrailh M. and Tziavos I. (2008): The Development of the European Gravimetric Geoid Model EGG07, *International Association of Geodesy Symposia 2008*, Volume 133, Part 2, Perugia.
- De Santis A. (1991): Translated origin Spherical Harmonic analysis, *Geophy. J. Int.* Vol.106.
- De Santis (1992): Conventional Spherical Harmonic Analysis for Regional Modeling of Geomagnetic Field, *Geophys. Res. Lett.* , Vol. 19, No. 10.
- De Santis A., Torta J. (1997): Spherical Cap Harmonics Analysis: a comment on its proper use for local gravity field representation, *Journal of Geodesy*, Vol.71, 1997.
- De Santis A., Torta J. and Falcone C. (1996): A Simple Approach to the Transformation of Spherical Harmonic models under coordinate system rotation, *Geophys. J. Int.*, Vol. 126.
- De Santis A., Torta J. and Lowes F. (1999): Spherical Cap Harmonics Revisited and their Relationship to Ordinary Spherical Harmonics, *Phys. Chem. Earth (A)*, Vol. 24, No.11-12.
- De Santis A., Chiappini M., Domonici G., Meloni A. (1997): Regional geomagnetic field modeling: the contribution of the Instituto Nazionale de Geofisica, *Annali Di Geophysica*, Vol XL, No.5.
- DFHRS, www.dfhbf.de , page visited August.2013.
- Dodson, L. P. Fortes, L. Sanchez, P. Sandoval (2001): Vertical Reference Systems, *International Association of Geodesy Symposia No. 124*, Cartagena, Colombia, 20-23.Feb.2001. Springer Verlag, Berlin, Heidelberg, NewYork. ISBN 3-540-43011-3. S. 203-208.

Fan H. (2004): Theoretical Geodesy, Royal Institute of Technology, Stockholm.

Förste C., Bruinsma S., Shako R., Marty J., Flechtner F., Abrikosov O., Dahle C., Lemoine J., Neumayer H., Biancale R., Barthelmes F., König R. and Balmino G. (2011): EIGEN-6 - A new combined global gravity field model including GOCE data from the collaboration of GFZ-Potsdam and GRGS Toulouse, EGU Assembly 2011, Vienna, Austria.

Franceschi G. And De Santis A. (1994): Ionospheric Mapping by means of Spherical Harmonic Analysis: New Developments, Advances in Space Research, Issue 15.

Franceschi G., De Santis A. and Pau S. (1994): Ionospheric Mapping by Regional Spherical Cap Harmonic Analysis: New Developments. Adv. Space res., Vol.14, No.12, Pergamon, UK.

Freeden W. (1984): Spherical spline interpolation-basic theory and computational aspects, J. of Comp. and Applied Math., Vol. 11.

GFZ-website (2012):<http://icgem.gfz-potsdam.de/ICGEM/evaluation/evaluation.html> , visited in May.2012

Ghilani C. and Wolf P. (2006): Adjustment Computations: Spatial Data Analysis, 4th edition, Jones Willey and Sons Inc., New Jersey.

Ghilani C. and Wolf P. (2008): Elementary Surveying: An Introduction to Geomatics, 12th edition, Pearson Prentice Hall, New Jersey.

Heck B., Illner M. and Jäger R. (1995): Deformationsanalyse zum Testnetz Karlsruhe auf der Basis der terrestrischen Nullmessung und aktueller GPS-Kampagnen, Festschrift für Heinz Draheim & Eugen Kuntz & Hermann Mälzer, Geodätische Institut der Uni. Karlsruhe, Germany, ASBN: 3-00-000220-0.

Haines G. (1985a): Spherical Cap Harmonic Analysis, Journal of Geophysical Research, Vol.90 No. B3.

Haines G. (1985b): Spherical Cap Harmonic Analysis of Geomagnetic Secular Variation over Canada 1960-1983, Jour. Geophys. Res., Vol.90 No. B14.

Haines G. (1988): Computer programs for Spherical Cap Harmonic Analysis of Potential and General Fields, Computer & Geosciences, Vol. 14, No. 4.

Hein G. (1986): Integrated Geodesy- State of the Art 1986 Reference Text, Mathematical and Numerical techniques in Physical Geodesy, Lecture Notes in Earth Sciences, Vol. 7, Springer-Verlag, Berlin Heidelberg.

Heiskanen W. and Moritz H. (1967): Physical Geodesy, W. H. Freeman and Company, San Francisco and London.

Hirt C., Bürki B., Somieski A. and Seeber G. (2010): Modern determination of vertical deflections using digital zenith cameras, Journal of Surveying Engineering, Vol 136 (1).

Hofmann-Wellenhof B. and Moritz H. (2005): Physical Geodesy, Springer-Verlag Wien, Austria.

Hofmann-Wellenhof B., Legat K. and Wieser M. (2003): Navigation, Springer-Verlag Wien, Austria.

Holmes S. and Featherstone W. (2002): A Unified Approach to the Clenshaw Summation and Recursive Computation of Very High Degree and Order Normalized Associated Legendre Functions, Journal of Geodesy Vol.76.

Ihde J., Mäkinen J. and Sacher M. (2007): Conventions of the European Vertical Reference System 2007, Euref Symposium 2007, London.

ICGM (2012): International Center for Global Gravity Field Models, <http://icgem.gfz-potsdam.de/ICGEM/ICGEM.html>, accessed July 2012.

Jäger R. (2010): Geodätische Infrastrukturen für GNSS-Dienste (GIPS). Festschrift zur Verabschiedung Prof. Dr. Günter Schmitt. Verlag des Karlsruhe Institute of Technology (KIT) . Karlsruhe, ISBN : 978-3-86644-576-5 .

Jäger R. and Kälber S. (2000): Konzepte und Softwareentwicklungen für aktuelle Aufgabenstellungen für GPS und Landesvermessung. DVW Mitteilungen, Landesverein Baden-Württemberg. 10/2000. ISSN 0940-2942.

Jäger R. and Schneid S. (2001): GPS-Höhenbestimmung mittels Digitaler Finite-Elemente Höhenbezugsfläche (DFHBF) - das Online-Konzept für DGPS-Positionierungsdienste. XI. Internationale Geodätische Woche in Obergurgl/Österreich, Februar 2001, Institut für Geodäsie der Universität Innsbruck, Institutsmitteilungen , Heft Nr. 19, pages: 195-200.

Jäger R. and Schneid S. (2002): Online and Post processed GPS-Heighting based on the Concept of a Digital Height Reference Surface. Contribution to IAG International Symposium on Vertical Reference Systems, February 2001, Cartagena, Columbia. In: H. Drewes, A.H.

Jäger R., Kälber S. and Ghadi Younis (2010): The New RTCM 3.1 Transformation Messages – Declaration, Generation from Reference Transformations and Implementation as a Server-Client Concept for GNSS-Services. Bulletin of Geodesy and Geomatics - BGG, issue 2-3.

Jäger R., Müller T., Saler H. and Schwäble R (2005): Klassische und robuste Ausgleichungsverfahren, Herbert Wichmann Verlag, Heidelberg.

Jäger R., Schneid S., Kälber S. and Seiler S. (2006): Precise Transformation of Classical Networks to ITRF by CoPaG and Precise Vertical Reference Surface Representation by DFHRS – General Concepts and Realisation of Databases for GIS, GNSS and Navigation Applications. Conference Proceedings, 1st International Fair of Geodesy, Cartography, Navigation and Geoinformatics. Prague, 16.03.2006 - 18.03.2006. Milan Tallich (Eds.), Czech Republic.

Jäger R., Kaminskis J., Strauhmanis J. and Younis G. (2012): Determination of Quasi-geoid as Height Component of the Geodetic Infrastructure for GNSS-Positioning Services in the Baltic States, Latvian Journal of Physics and Technical Sciences, N 3, Vol. 49, ISSN 0868 - 8257.

Jäger R., Kälber S., Spohn P., Younis G., Chiriac V., Grama V., Iacovlev A. and Nistor-Lopatenco L. (2010): Geodetic Infrastructure for GNSS Positioning Services (GIPS), 3rd GNSS Vulnerabilities and Solutions Conference, Baska - Krk Island, Croatia, 5 - 8 September 2010.

Jekeli C. (2001): Inertial Navigation Systems with Geodetic Applications, Walter de Gruyter, Berlin-New York.

Jekeli C. (2004): Spline Representations of Functions on a Sphere for Geopotential modeling, Final Technical Report, Ohio State University, USA.

Jekeli C. (2007): Potential Theory and Static Gravity Field of the Earth, Treatise on Geophysics, Volume-3 Geodesy, Elsevier B.V., Oxford, UK.

Kling T., Becker M., Euler H., Groten E. (1987): Studien zur detaillierten Geoidberechnungen, DGK, Reihe B, Heft Nr. 285.

Klees R., Tenzer R., Prutkin I., Wittwer T., (2008): a data-driven approach to local gravity field modeling using spherical radial basis functions. Journal of Geodesy, Vol. 82 (457-471)

Korte M. (1999): Kombination regionaler magnetischer Vermessungen Europas zwischen 1955 und 1995: Modellierung der geomagnetischen Säkularvariation durch Spherical Cap Harmonic Analysis zur Untersuchung möglicher Säkularvariationsanomalien. PhD. Thesis, Freien Uni. Berlin, GFZ-Scientific Technical Report.

Lang C., Pucker N. (2005): Mathematische Methoden in der Physik, 2 Auflage, Elsevier GmbH, München, Germany.

Migliaccio F, Reguzzoni M, Sansò F, Tscherning CC, Veicherts M (2010) GOCE data analysis: the space-wise approach and the first space-wise gravity field model. In: Proceedings of the ESA Living Planet Symposium, 28 June–2 July 2010, Bergen, Norway.

Müller M. (1986): Integrierte Geodäsie, IGP-Bericht Nr. 111, Institut für Geodäsie und Photogrammetrie, RTH Zürich.

Niemeier W. (2002): Ausgleichsrechnung, Walter de Gruyter, Berlin-New York.

Nool M. (1992): Block-Cholesky for parallel processing, Applied Numerical Mathematics, Vol.10 P.37-57, Elsevier Science Inc.

Nool M. (2001): Explicit parallel block Cholesky algorithms on the CRAY APP, Applied Numerical Mathematics, Vol.19 P.91-114, Elsevier Science Inc.

Okrah B. (2005): Computation of a DFHRS Database for Florida (USA) and Implementation of a Block matrix Inversion as a C++ based DLL into DFHRS Software, Master Thesis, Master of Geomatics, Hochschule Karlsruhe, Karlsruhe.

Oliver F. and Smith J. (1983): Associated Legendre Functions on the Cut, Journal of Computational Physics, Vol. 51.

Pavlis N., Holmes S., Kenyon S. and J.K. Factor (2008): An Earth Gravitational Model to Degree 2160: EGM2008, presented at the 2008 General Assembly of the European Geosciences Union, Vienna, Austria, April 13-18, 2008.

Press W., Teukolsky S., Vetterling V., Flannery B. (2002): Numerical Recipes in C++: the Art of Scientific Computing, 2nd edition, Cambridge University Press, UK.

Rapp R. (1986): Global Geopotential Solutions, Mathematical and Numerical Techniques in Physical Geodesy, Lecture Notes in Earth Sciences, Vol. 7, Springer-Verlag, Berlin-Heidelberg.

Roman D., Wang Y., Saleh J. and Li X. (2010): Geodesy, Geoids, and Vertical Datums: A Perspective from the U.S. National Geodetic Survey, FIG General Assembly 2010, Sydney, Australia.

Rothberg E. and Gupta A. (1994): An Efficient Block-Oriented Approach To Parallel Sparse Cholesky Factorization, Journal SIAM Journal on Scientific Computing, Volume 15 Issue 6, Society for Industrial and Applied Mathematics Philadelphia, PA, USA.

Schaefer U. (2003): Aspects for a block version of the interval Cholesky algorithm, J. Comput. Appl. Math., Vol. 152, combined issues 1-2.

Schiebl H. (1999): Visual C++6.0 für Einsteiger und Fortgeschrittene, Carl Hanser Verlag, München-Wien, ISBN 3-446-19548-3.

Schmidt M., Fengler M., Mayer-Gürr T., Eicker A., Kusche J., Sanchez L., Han S. (2007): Regional gravity modeling in terms of spherical base functions, Journal of Geodesy , vol. 81 (17-38).

Schneid S. (2006): Investigation of a Digital FEM Height Reference Surface as Vertical Reference Surface, PhD Thesis, University of Nottingham.

Seeber G. (2003): Satellite Geodesy, 2nd Edition, Walter de Gruyter, Berlin-New York.

Shako R., Förste C., Abrikosov O., Bruinsma S., Dahle C., Flechtner F., Neumayer H. and Marty C. (2010): High Resolution Gravity Fields by Combining GOCE, GRACE and Terrestrial Data – First Results from Real GOCE Project, Geotechnologien Science Report No. 17, Status Seminar 4 October 2010 Rheinische Friedrich-Wilhelms-Universität Bonn

Smith S. (2001): The factorability of symmetric matrices and some implications for statistical linear models, Linear Algebra and its Applications, Vol.335 P.63-80, Elsevier Science Inc.

Sneeuw N. (2006): Physical Geodesy, Lecture Notes, Institute of Geodesy, University of Stuttgart.

Thebault E. and Pique L. (2008): Applied Comparison between SCHA and R-SCHA regional modeling techniques, Geochemistry-Geophysics-Geosystems, electronic Journal of Earth Sciences., Vol. 9, Nr.1.

Thebault E., Mandeau M. and Schott J. (2006): Modeling the lithospheric magnetic field over France by means of revised Spherical Cap Harmonic Analysis (R-SCHA). Journal of Geophysical Research, Vol. 111.

Thebault E., Schott J., Mandeau M., Hoffbeck J. (2004): A new proposal for Spherical Cap Harmonics, Geophys. J. Int., Vol. 159.

Torge W. (2001): Geodesy , 3rd Edition , Walter de Gruyter , Berlin.

Torge W. and Müller J. (2012): Geodesy , 4th Edition , Walter de Gruyter , Berlin.

Torge W. und Denker H. (1999): Zur Verwendung des Europäischen Gravimetrischen Quasigeoids EGG97 in Deutschland, ZfV 124, 154-166

Tscherning C. (2001): Geoid Determination after the First Satellite Missions, Wiss. Arb. Fachr. Verm.wesen Nr. 241, University of Hannover.

Tscherning C., Rapp R., Goad C. (1983): A Comparison of Methods for computing Gravimetric Quantities from High Degree Spherical Harmonic Expansions, manuscripta geodaetica, Vol. 8.

Wahr J. (1996): Geodesy and Gravity, Samizdat Press, Colorado School of Mines , Colorado.

Wittwer T. (2009): Regional gravity field modeling with radial basis functions, NCG, Publication on Geodesy Nr 72, Delft, Holland.

Younis G, Jäger R. and Becker M. (2011): Transformation of Global Spherical Harmonic Models of the Gravity Field to a Local Adjusted Spherical Cap Harmonic Model. AJGS, Springer, Berlin / Heidelberg, DOI: 10.1007/s12517-011-0352-1.

List of Akronyms

ASCH	AdjustedSpherical Cap Harmonics
BW	State of Baden-Württemberg in Germany
DFHBF	Digitale Finite-Elemente Höhenbezugsfläche
DFHRS	Digital Finite Elements Height Reference Surface
DFHRS-DB	DFHRS database
DGNSS	Differential GNSS
EGM	Earth Gravitational Model
EIGEN	Global gravity models by GFZ-Potsdam
ETRF89	European Terrestrial Reference Frame -1989
ETRS89	European Terrestrial Reference System -1989
FFT	Fast Fourier Transform
GGM	Global Gravity Model
GNSS	Global Navigation Satellite Systems
GIS	Geographic Information Systems
GPM	Geopotential Model
GPS	Global Positioning System
HRS	Height Reference Surface
ITRF	International Terrestrial Reference Frame
LAV	Local Astronomical Vertical
LGV	Local Geodetic Vertical
PPP	Precise Point Positioning
SCH	Spherical Cap Harmonics
SH	Spherical Harmonics
SRBF	Spherical Radial Basis Functions
RTCM	Real Time Correction Message
R-SCH	Revised-Spherical Cap Harmonics
TOSCH	Translated Origin Spherical Cap Harmonics

List of Symbols

a	Semi-major axis of the ellipsoid
$a_{n,\mu}^m, b_{n,\mu}^m, c_{n,\mu}^m, d_{n,\mu}^m$	Transformation parameters between SCH and SH with the consideration of rotation between the two poles
$A_k^{m,n}$	Transformation parameters between SCH and SH without the consideration of rotation between the two poles
b	Semi-minor axis of the ellipsoid
dP_{nm}	Derivative of the Legendre function of integer degree and integer order
$dP_{n(k),m}$	Derivative of the Legendre function of real degree and integer order
g	Gravity value
\bar{g}	Gravity vector
GM	Gravitational constant of the Earth (Ellipsoid)
h	Ellipsoidal height
H	Orthometric height
H^*	Normal height
L_{\min}	Spatial resolution of the SCH/ASCH model
M, N	Ellipsoidal radius of curvature in the longitude and latitude directions
P_{nm}	Legendre function of integer degree and integer order
$P_{n(k),m}$	Legendre function of real degree and integer order
S'_{nm}, C'_{nm}	Spherical cap harmonic coefficients
$\bar{S}_{nm}, \bar{C}_{nm}$	Normalized spherical harmonic coefficients
r_1, α_1, θ_1	Modified spherical cap coordinate in the TOSCH
R_1	Modified mean radius of the cap in the TOSCH
R_s	Distance the new origin to the Earth surface in the TOSCH
s	Scale in the ASCH
T	Disturbing potential
U	Normal potential of the ellipsoid
W	Gravity potential
W_0	Reference gravity potential
x, y	Local/projected coordinates
X, Y, Z	Geocentric cartesian coordinates
α, θ, r	Spherical coordinates in the system of the cap
α, ϑ, r	scaled coordinates in the ASCH
ϕ, λ	Geographic latitude and longitude
Φ, Λ	Astronomical latitude and longitude
$\bar{\phi}, \bar{\lambda}$	Spherical latitude and longitude
$\bar{\phi}_0, \bar{\lambda}_0$	Spherical latitude and longitude of the cap center
θ_0	Maximum opening angle of the cap
w_{\min}	Minimum wavelength

Ω	Centrifugal potential of the Earth
ζ	Quasigeoid height (height Anomaly)
γ	Normal gravity of the ellipsoid
ξ	Deflection of vertical in the east-west direction
η	Deflection of vertical in north-south direction
ω	The angular velocity of the Earth around its major axis
Ψ_j	The spherical radial basis functions (SRBF)
ψ_l	The Legendre parameter related SRBF
σ_l^2	The degree variance
α_j	SRBF or Spline coefficients
σ_0^2	Apriori reference variance
$\hat{\sigma}_0^2$	Aposteriori reference variance

Matrices symbols

A	Design Matrix in the least squares solutions
C_{ll}	Covariance Matrix of the observations
$C_{\hat{x}\hat{x}}$	Covariance Matrix of the unknowns
N	Normal equations matrix
l	Matrix (Vector) of observations
L	Lower triangle matrix in Cholesky's decomposition
U	Upper triangle matrix in Cholesky's decomposition
W_{ll}	Weight matrix of the observations in the least squares solutions
\hat{x}	Matrix of unknowns in the least squares solutions

Eidesstattliche Erklärung

Ich versichere, dass ich die vorliegende Dissertation ohne fremde Hilfe und ohne Benutzung anderer als der angegebenen Quellen angefertigt habe, und dass die Arbeit in gleicher oder ähnlicher Form noch keiner anderen Prüfungsbehörde vorgelegen hat. Alle Ausführungen der Arbeit, die wörtlich oder sinngemäß übernommen wurden, sind als solche gekennzeichnet.

Darmstadt, November 2013

Curriculum Vitae

Personal Info

Surname: Younis
Given Name: Ghadi
Sex: Male
Date of Birth : 01.08.1980
Place of Birth: Deir-Ghazala – Palestine
Nationality : Palestinian

Education

- **BSc. Surveying and Geomatics Eng.** , Palestine Polytechnic University (PPU) , Palestine, 1998-2003.
 - **MSc. Geomatics**, University of Applied Science Karlsruhe, 2004-2006, **DAAD** (German Academic Exchange Service) sponsorship.
 - **PhD. Study**, Faculty of Civil Engineering and Geodesy, TU-Darmstadt. Topic “*Regional Gravity Field Modeling with Adjusted Spherical Cap Harmonics in an Integrated Approach*”, 2008-2012, **DAAD** sponsorship.
-

Professional Experience

- **Teaching assistant for Surveying and Geomatics Eng.** at PPU, Photogrammetry, Geodesy and Adjustment, 2003-2004.
 - **Teacher for Surveying and Geomatics Eng.** at PPU, Photogrammetry1, Photogrammetry2, digital Photogrammetry, Surveying, GPS, GIS, Geodesy and Adjustment, 2006-2008.
 - **External Physical Geodesy Teacher** for Master of Geomatics Students, PPU, 2009 – 2011.
 - **Research Assistant** responsible for the Digital Finite Element Height-Reference Surface (DFHRS) development at the University of Applied Sciences, Karlsruhe, 2008-2013.
-

Publications

- *Janpaule I., Jäger R., Younis G., Kaminskis J. and Zarins (2013):* DFHRS-Based Computations of Quasi-Geoid of Latvia, Geodesy and Cartography, Taylor & Francis Vol 39:(1) 11-17, ISSN 2029-6991 print / ISSN 2029-7009 online.
 - *Jäger R., Kaminskis J., Strauhmanis J. and Younis G. (2012):* Determination of Quasi-geoid as Height Component of the Geodetic Infrastructure for GNSS-Positioning Services in the Baltic States, Latvian Journal of Physics and Technical Sciences, N 3, Vol. 49, ISSN 0868 - 8257.
 - *Younis G., Jäger R., Becker M.(2011):* Transformation of Global Spherical Harmonic Models of the Gravity Field to a Local Adjusted Spherical Cap Harmonic Model. AJGS, Springer, Berlin / Heidelberg ,DOI:10.1007/s12517-011-0352-1.
-

Scholarships

-
- Jäger R., S. Kälber and Younis G. (2010): The New RTCM 3.1 Transformation Messages – Declaration, Generation from Reference Transformations and Implementation as a Server-Client Concept for GNSS-Services. Paper submitted to Bulletin of Geodesy and Geomatics. Firenze, Italy. In press.
 - Reiner Jäger , Simone Kälber , Peter Spohn, Ghadi Younis , Vasile Chiriac , Vasile Grama , Andrei Iacovlev and Livia Nistor-Lopatenco(2010) : Geodetic Infrastructure for GNSS Positioning Services (GIPS) . presentation at the 3rd GNSS Vulnerabilities and Solutions Conference, to be held in Baska, Krk Island, Croatia, 5 - 8 September 2010.
 - Ghadi Younis (2006): Further development of the L2/ L1-norm GOCA Kalman-filtering DLL and extension to the computation and visualisation of variance estimations and probability and forecasting states. MSc. Thesis at HS-Karlsruhe , Karlsruhe, Germany
 - Ghadi Younis and Mohamad Tbish (2003): Geo-map Calculator, BSc Thesis at Palestine Polytechnic University, Hebron, Palestine.
-
- 2004-2006: DAAD (German Academic Exchange Service) for the study of Master degree of Geomatics in HS-Karlsruhe.
 - 2008-2012: DAAD to complete the PhD. Studies in TU-Darmstadt.
-